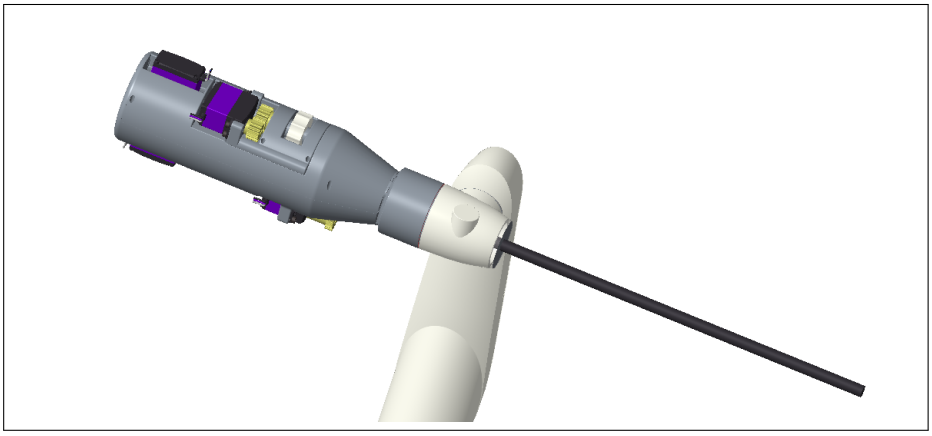
Institut für
Mechatronische Systeme
imes Leibniz Universität Hannover

Leibniz
Universität
Hannover

Actuation and Integration of a Suturing Device into the DLR MiroSurge System



Masterarbeit 907

Alexander Kirst
Matrikelnummer 3018490

Hannover, 20. Dezember 2019

Erstprüfer	Prof. Dr.-Ing. Tobias Ortmaier
Zweitprüfer	Prof. Dr.-Ing. Jörg Wallaschek
Betreuer	Moritz Schappler, M.Sc. und Dipl. Ing. Christopher Schlenk

Ich, Alexander Kirst, versichere hiermit, dass die vorliegende Arbeit selbstständig verfasst wurde, keine anderen als die angegebenen Quellen und Hilfsmittel benutzt wurden, alle Stellen der Arbeit, die wörtlich oder sinngemäß aus anderen Quellen übernommen wurden, als solche kenntlich gemacht sind und die Arbeit in gleicher oder ähnlicher Form noch keiner Prüfungsbehörde vorgelegen hat.

Hannover, 20. Dezember 2019

(Alexander Kirst)

Institut für
Mechatronische Systeme
Leibniz Universität Hannover
imes

Masterarbeit

Herr cand. mach. Alexander Kirst, Matr.-Nr. 3018490

Aktuierung und Integration eines Nahtinstrumentes in das DLR MiroSurge System

Actuation and integration of a suturing device into the DLR MiroSurge System

Allgemeines:
Das Institut für Robotik und Mechatronik des Deutschen Zentrums für Luft und Raumfahrt (DLR) hat im Jahre 2009 erstmals das DLR MiroSurge System präsentiert. Dies ist ein teleoperiertes Robotersytsem für die minimal invasive, roboterassistierte Chirurgie. Hierfür werden momentan drei Leichtbauroboter an einem Operationstisch befestigt und führen die von dem Chirurgen ausgeübten Bewegungen durch. Als Endeffektoren dienen Greifer, die der Chirurg kontrollieren kann.
Das chirurgische Nähen erfordert viel Geschick seitens des Chirurgen und ist mit den derzeit verfügbaren Robotersystemen aufgrund mangelnden haptischen Feedbacks und schlechter räumlicher Sicht komplex und langwierig durchzuführen.

Aufgabe:
Um die Vorteile eines teleoperierten Systems zu nutzen, aber gleichzeitig seine Nachteile auszugleichen, soll ein bereits existierendes, kommerziell erhältliches, abwinkelbares Nahtinstrument zuerst auf seine relevanten Eigenschaften untersucht und dann in die MiroSurge Plattform des DLR integriert werden.

Im Rahmen dieser Arbeit ergeben sich insbesondere die folgenden Aufgabenpunkte:

- Recherche über chirurgische Nahttechniken und kommerziell erhältliche Nahtinstrumente
- Auswahl eines geeigneten Nahtinstrumentes zur Integration
- Untersuchung der relevanten Eigenschaften des Nahtinstrumentes (Befestigungsmöglichkeiten, Aktuierung des Freiheitsgrade, Aktuierungskräfte etc.) und Erstellung eines CAD-Modells
- Erarbeitung der Anforderungen an eine klinisch anwendbare Schnittstelle zwischen Nahtinstrument und Robotersystem
- Auslegung und Konstruktion der aktuierten Schnittstelle
- Ansteuerung der Aktuierung über MATLAB / Simulink - Schnittstelle implementieren
- Experimentelle Evaluation der aktuierten Schnittstelle
- Dokumentation der erarbeiteten Ergebnisse und möglicher Verbesserungsmaßnahmen

Die Bearbeitungszeit beträgt 900h.
Ausgabe der Aufgabenstellung: 01.07.2019 Abgabe der Arbeit: 02.01.2019

Betreuer: M.Sc. Moritz Schappler (imes), Dipl.-Ing. Christopher Schlenk (DLR)

....
(Prof. Dr.-Ing. Tobias Ortmaier) (Alexander Kirst)

Kurzfassung

Mit dem immer größer werdenden Erfolg der roboterassistierten Chirurgie erhalten immer mehr Roboter Einzug in den Operationssaal und ermöglichen viele neue Chirurgietechniken. Neben der Ermöglichung immer neuer Operationen und der Verbesserung bestehender Praktiken muss aber auch darauf geachtet werden, dass bereits bekannte Techniken für dieses roboterassistierte Umfeld adaptiert werden. Eins der wichtigsten Verfahren der Chirurgie ist das chirurgische Nähen. Dieses bereitet der roboterassistierten Chirurgie jedoch Probleme. Es ist sehr zeitintensiv und schwierig zu automatisieren.

In dieser Arbeit wird ein Ansatz vorgestellt, das chirurgische Nähen mittels eines Nahtinstrumentes für das Robotersystem *MiroSurge* des *deutschen Zentrums für Luft- und Raumfahrt* (*DLR*) zu adaptieren. Es wird ein Adapter designed, der allerelevanten Freiheitsgrade des Nahtinstrumentes aktuiert. Neben der mechanischen Konstruktion des Adapters werden in dieser Arbeit sowohl die Motoransteuerung als auch die kinematische Modellierung vorgestellt.

Ein erster Prototyp das Adapters wird anschließend in verschiedenen Tests evaluiert und bewertet.

Der Adapter, der in dieser Arbeit vorgetellt wird, legt den Grundstein für automatisiertes minimalinvasives Nähen mit der MiroSurge Plattform.

Abstract

With the increasing success of robot-assisted surgery, more and more robots are entering the operating room and enabling many new surgical techniques. In addition to enabling more and more new operating procedures and improving existing practices, care must also be taken to adapt already known techniques to this robot-assisted environment. One of the most important surgical procedures is surgical suturing. However, this causes problems for robot-assisted surgery. It is very time-consuming and challenging to automate.
This work presents an approach for automated surgical suturing using a suturing instrument for the robotic system *MiroSurge* of the *German Aerospace Center* (*DLR*). An adapter is designed, which updates the control of all relevant degrees of freedom for the suturing instrument. In addition to the mechanical design of the adapter, both the motor control and the kinematic modelling are presented in this paper.
A prototype of the interface is then evaluated in various tests.
The adapter presented in this work lays the foundation for automated minimally invasive suturing with the *MiroSurge* platform.

Contents

1 Introduction **1**

2 State of the art **3**
2.1 Surgical Suturing . . . 3
2.1.1 Needle . . . 3
2.1.2 Thread . . . 4
2.1.3 Suture techniques . . . 5
2.1.4 Knot techniques . . . 6
2.2 Clinical sterilizability . . . 7
2.3 Minimally invasive surgery . . . 8
2.4 Suturing Devices . . . 10
2.4.1 Rotating needle suturing devices . . . 10
2.4.2 Alternating needle suturing devices . . . 11
2.5 Surgical Robotics . . . 12
2.5.1 DLR MiroSurge system . . . 14
2.5.2 Robotic systems for surgical suturing . . . 19
2.6 Summary . . . 20

3 Requirements **21**

4 Design **23**
4.1 Selection of a suturing device . . . 23
4.1.1 Research about available devices . . . 24
4.1.2 Selection of a suitable instrument . . . 26
4.1.3 Relevant properties of the suturing device . . . 26
4.2 Interface . . . 30
4.2.1 Mounting . . . 30
4.2.2 Motors . . . 31
4.2.3 Transmission . . . 31
4.2.4 Design of the actuation interface . . . 35
4.2.5 Sterilizability . . . 36
4.2.6 Commissioning . . . 37

4.3 Motor Control . . . 39
4.3.1 Servo motor . . . 39
4.3.2 Microcontroller . . . 40
4.3.3 Links and nodes . . . 41
4.4 Forward kinematic . . . 42
4.5 Inverse kinematic . . . 45
4.6 Movement mapping . . . 46
4.7 Human machine interface . . . 48
4.8 Summary . . . 51

5 Experiments and evaluation 53
5.1 Criteria of a successful integration . . . 53
5.2 Test bed for tip-positioning . . . 54
5.2.1 Test setup 1.1: Rotation . . . 55
5.2.2 Test setup 1.2: Artikulation . . . 57
5.3 Hands-on mode on the MIRO . . . 60
5.3.1 Test setup 2.1: Commissioning of the adapter . . . 60
5.3.2 Test setup 2.2: Suturing . . . 61
5.4 Summary . . . 63

6 Future work 65

7 Discussion 67

A Appendix 69

Appendix 69
A.1 Kinematic basics . . . 71
A.1.1 Homogeneous transformations . . . 71
A.1.2 Robot kinematics . . . 73
A.1.3 Summary . . . 78
A.2 List of Requirements . . . 79
A.3 Designation of the instrument parts . . . 81
A.4 Part list . . . 82
A.5 Technical drawings . . . 85
A.6 Assembly instruction . . . 86
A.7 Specification DITEX 1609S . . . 87
A.8 States of the suturing finite state machine . . . 88
A.9 HSV representaion . . . 90
A.10 Principal component analysis . . . 92

A.11 Source code of the tip-tracking 93
A.12 Source code of the test procedure 97
A.13 Source code of the 3D mouse control 100

Bibliography **107**

List of Figures

2.1 Surgical suture needles 4
2.2 Surgical suture threads 5
2.3 Different types of sutures 6
2.4 *Surgeon's knot* 6
2.5 Various approaches to reach sterility 8
2.6 Minimally invasive surgery 8
2.7 Trocarkinematics 9
2.8 Rotating needle suturing devices 11
2.9 Alternating needle suturing devices 12
2.10 Various surgical robotic systems 13
2.11 Teleoperated systems 14
2.12 *MICA* instrument 15
2.13 The *DLR MiroSurge* user interface 16
2.14 *MIRO* kinematics 17
2.15 *MiroSurge* four layer architecture 18
2.16 Robot assisted surgical suturing 20

3.1 Different configurations of the suturing instrument 21

4.1 Flowchart of the design process 23
4.2 Degrees of freedom of the *SILS Stitch* 24
4.3 Degrees of freedom of the *Endo Stitch* 25
4.4 Degrees of freedom of the *Endo 360°* 25
4.5 Degrees of freedom of the *Proxisure* 26
4.6 Positions of the handle 27
4.7 Postions of the swivelling lever 28
4.8 Testbed to evaluate required motor torques 29
4.9 Magnetic mounting adapter of the *MICA* system 30
4.10 *DITEX 1609S* 31
4.11 Gear for the rotation of the tooltip 32
4.12 Gear for the articulation of the tooltip 33
4.13 Gear for the actuation mechanism of the gripper 34
4.14 Postions of the swivelling lever 35

4.15 Gear for the swivelling mechanism 35
4.16 Workflow of packaging the adapter sterile 37
4.17 Workflow for commissioning 38
4.18 Communication structure 39
4.19 Structure of telemetry packet 40
4.20 Input schematic for inverted serial communication 41
4.21 Structure of a publish and subscribe interaction in the LN-framework 41
4.22 Schematic of the chained articulation links 42
4.23 Coordinate systems at the tool tip 43
4.24 *Spacemouse Compact* 49

5.1 Prototype of the adapter 53
5.2 Testbed for locating the tip position 54
5.3 Marker for tracking the rotation 55
5.4 Calculating the rotation angle between the markers 56
5.5 Relation between the actual and the nominal rotation angle 57
5.6 Marker for tracking the articulation 58
5.7 Calculating the articulation angle between the markers 58
5.8 Relation between the actual and the nominal articulation angle 59
5.9 Test setup with the *MIRO* 62
5.10 Performing a suture with hands-on mode 63

6.1 Disassembled suturing instrument 66

A.1 Relation between direct and inverse kinematics 74
A.2 Robot as concatenation of link fixed coordinate systems 75
A.3 *Denavit-Hartenberg* parameters of two subsequent links 76
A.4 Null space configurations of a redundant robot 78
A.5 Designation of the parts of the suturing instrument 81
A.7 Overview over all parts 84
A.8 Articulation wave 85
A.9 Dimensions of the *DITEX 1609S* 87
A.10 HSV cone to represent colors 90

List of Tables

2.1 Specification of the *MIRO* 16
2.2 *Denavit-Hartenberg* parameters of the *MIRO* 17

4.1 Distances between the coordinate systems of the adapter 44
4.2 *Denavit-Hartenberg* parameters of the interface 44
4.3 States of the variables 50

5.1 Duration of Assembling the adapter 61
5.2 Duration of disassembling the adapter 61

A.1 Listing of the part names 81
A.2 Specification of the *DITEX 1609S* 87
A.3 All states of the suturing finite state machine 89

Nomenclature

general conventions

a	scalar a
$\boldsymbol{b}$	vector b
$\boldsymbol{C}$	matrix C

latin letters

$\boldsymbol{q}$	joint angle
$\boldsymbol{t}$	displacemant vector
$\boldsymbol{T}$	homogenous transformation matrix
$\boldsymbol{R}$	rotation matrix

greek letters

$\boldsymbol{\phi}$	motor angle

coordinate systems

$(COS)_i$	coordinate system of the i-th link

1 Introduction

Suturing has always been an essential part of every surgical intervention. According to *Pschyrembel*, it is the "reunification of severed skin, soft tissues, vessels, nerves, tendons, etc." [1]. While in the Middle Ages, natural materials such as catgut or animal threads were common [2], in modern times synthetic materials such as nylon or polyester are used for suturing [3]. Also, the needle has changed a lot over time. Thus the eye needles were slowly but surely replaced by needle-thread combinations in which the thread is worked directly into the needle.

Over time, not only surgical suturing has changed, but also surgery itself: Until the 1990s, open surgery was the standard in many fields of surgery, where the complete access to the tissue to be operated on is exposed [4]. This provides much space and a good overview for the surgeon, but also results to a large trauma for the patient. With this type of surgery, sutures can be performed with ordinary needles and needle holders because the surgeon has enough space, overview and haptic feedback to perform this complex task. Since then, minimally invasive surgery has gradually gained acceptance. This surgery through small accesses or natural body orifices means significantly less trauma for the patient but brings several disadvantages for the surgeon. All his movements are scaled and inverted by the trocar kinematics, i.e. the loss of two degrees of freedom due to the local fixation of the puncture site (see Fig. 2.7). In addition to the unfavourable kinematic conditions, a significant problem with minimally invasive surgery is the limited viewing conditions of the surgeon, who can only see a section of the surgical area via a camera, which is typically an endoscope. Furthermore, there is a lack of haptic feedback, so that minimally invasive surgery cannot be performed in the same way as open surgery, because there is much friction between the instruments and the trocar.

Suture instruments simplify needle handling and enable such complex tasks to be performed even with poor visibility. However, they do not solve the problem of disadvantageous kinematics in minimally invasive surgery.

The next stage in the development of surgery is robot-assisted minimally invasive surgery, in which the surgeon is supported by suitable robot systems so that both the advantages of a human surgeon and those of a robot system are combined. While the surgeon has all the decision-making power and assessment ability, he is supported by the robot system, for example, with tremor compensation [5] or movement scaling [6]. During the operation, the surgeon no longer has to stand close to the patient and hold the instruments but can sit in a relaxed position on the console of the system. The surgeon console offers many advan-

tages for the surgeon, such as better ergonomics, more intuitive hand-eye coordination and higher precision [7]. However, since the haptic feedback and vision of such systems cannot yet compete with the environmental conditions in open surgery, minimally invasive surgical suturing is a very time-intensive process.
To combine the advantages of minimally invasive surgery with surgical suturing instruments and robot-assisted surgery, within this work, an interface for the integration of a commercially available suturing instrument into a robotic system is designed. In the future, this could significantly improve the suturing process in minimally invasive robot-assisted surgery.

In the following, firstly, the basics of surgical suturing are explained. This includes the materials (needle and thread) as well as different techniques, such as different types of sutures or knot techniques. After the basics of surgical suturing, minimally invasive surgery and conventional suturing instruments are introduced. The chapter *State of the Art* closes with the introduction of robotic assistance systems, which is discussed using the example of *DLR MIRO* and the topic of sterilizability, which is essential for many medical products. After the general requirements for the interface are stated in Chapter 3, the design of the interface is described in Chapter 4. First, the selection of a suitable suturing instrument is presented. Then the development of the interface is described by first introducing the different gears, discussing the control of the motors and calculating the mapping of the motor degrees of freedom to the end effector degrees of freedom. The forward kinematics is described using the *Denavit-Hartenberg* notation. At the end of the chapter, a concept for a human-machine-interface is presented to control the important degrees of freedom in a useful way. In the chapter *Experiments and Evaluation* the two critical aspects of the degrees of freedom are evaluated in two test series: On the one hand the accuracy of the positioning of the instrument tip and on the other hand the performance of the suturing mechanism. The work concludes with a discussion of the developed system as well as an outlook on possible improvements and possible future developments of an updated suturing instrument.

2 State of the art

To actuate a surgical suturing instrument, various aspects must be considered. In this chapter, the basics of surgical suturing are presented at first (section 2.1). This refers to materials such as needle and thread, but also to techniques for suturing and knotting. After a brief explanation of clinical sterilizability (section 2.2) and minimally invasive surgery (section 2.3), the current principles of commercially available suturing instruments are described (section 2.4). This chapter concludes with an introduction to robotic assistance systems for surgery (section 2.5). In particular, the *MiroSurge* system of the *DLR* is described, but also research systems that deal specifically with surgical suturing.

2.1 Surgical Suturing

Surgical suturing is an essential part of most operations and, in addition to skilful action and a good overview of the surgeon, it also needs technical aid. Firstly the needle and the thread have to be mentioned here. These are presented in the sections 2.1.1 and 2.1.2. In addition to these two components, needle holders in different designs depending on the surgical field are commonly used. However, they do not belong to the focus of this work, and they will not be discussed further here. High-quality, clinically sterile and purpose-adapted instruments are essential for surgical suturing, but handling them is just as important, so 2.1.3 and 2.1.4 introduce important suturing and knotting techniques.

2.1.1 Needle

The surgical needle can be defined as a "surgical suturing instrument for performing a manual suture" [1]. There is no such thing as the one right needle, but one adapted to the requirements for a specific task. Also, the needle has changed considerably over time. Whereas bones, ivory or metals such as iron, silver, copper or bronze were frequently used in the past [8], needles today are only made of stainless steel [8]. Also the reuse of the suturing needle, which was standard at that time, no longer exists. So in today's operations, disposable needles are used, which are taken out of sterile packaging and are disposed of immediately after the operation. To define the physical properties of a needle, one need not only the knowledge of the material but also the shape of the needle. There are many different shapes and designs of surgical needles. Many needles are produced round and form a segment of a full circle. Needles are produced in 1/4, 3/8, 1/2 or 5/8 circle lengths (see Fig. 2.1). In addition to

circular needles, there are straight needles, J-shaped needles and many other shapes that are required for special cases. Not only the shape of a needle defines its properties, but also its cross-section. This can be round, triangular and additionally sharp. In the past, the thread was usually attached to the needle using a hollow hole. Today it is clear that fixed combinations have become the norm. In these cases, the atraumatic suture material is particularly noteworthy: This is a combination in which the thread is not thicker than the needle and merges continuously into it, thus filling the branch canal to suppress bleeding, even in vascular sutures. For every application, the physician has to make several decisions regarding the choice of the needle. Since needle-thread combinations are common nowadays, he also has to select the type of thread.

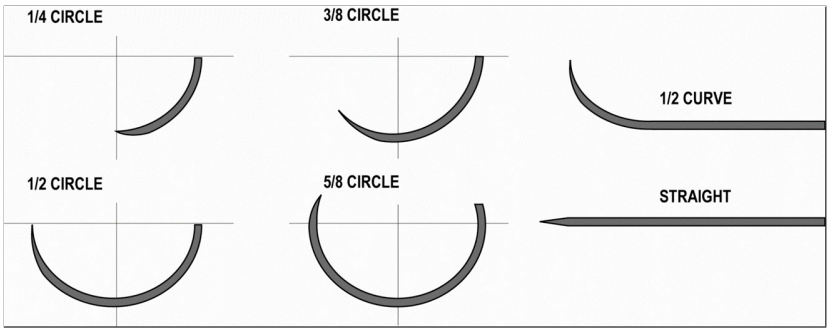


Figure 2.1: Surgical suture needles [9]

2.1.2 Thread

Surgical threads, as well as surgical needles, have changed over time.
In the past, natural materials such as natural silk or catgut were mostly used. These were then stored sterile in liquids by the metre and cut before use [10]. However, since most sterilisation procedures for threads are not reliable [10], the combination of disposable thread and needle described in 2.1.1 has become most common. Just as there are many different variations in the shape of surgical needles, the desired properties of the threads can be adjusted by various factors. The material plays an important role for threads. Surgical sutures are usually made of synthetic materials. These can be resorbable or non-resorbable. This means that they either dissolve or do not dissolve after a certain period. Resorbable sutures are advantageous, for example, in regions where the sutures cannot be removed, as the interior of organs.
Also, threads can be categorised by their thickness, or by their processing: there are monofilament threads, which consists only of one basic thread, or braided threads. Braided threads are much smoother and easier to knot, but have a sawing effect that can damage the tissue when the thread is pulled through. A mixed form of these two types is the pseudomonofila-

ment threads, which are braided but whose sawing effect is prevented by a sheathing of the braided structure. A classification of surgical threads can be seen in Fig. 2.2.

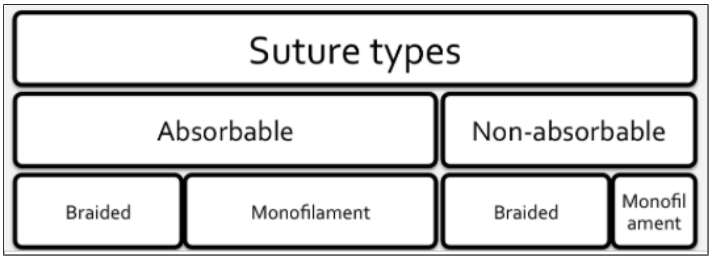
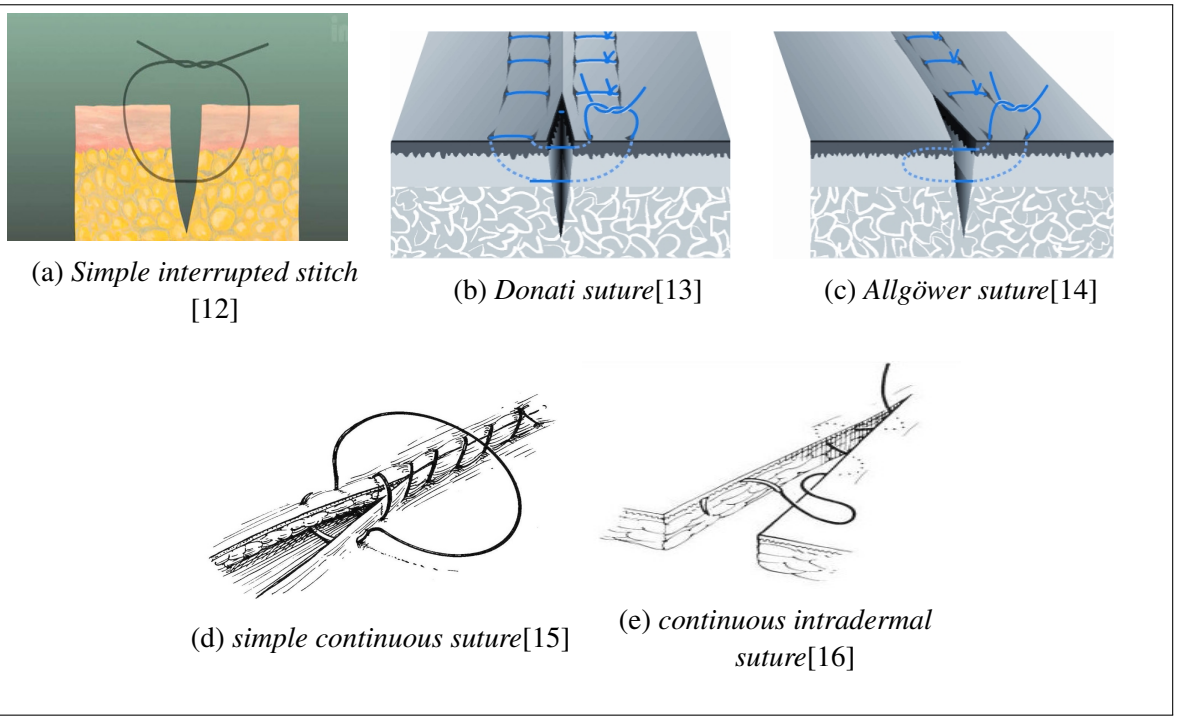


Figure 2.2: Surgical suture threads [11]

2.1.3 Suture techniques

To reunite separate tissue, the two corresponding surfaces must be brought together without tension so that they can grow together again. To achieve this, the thread is placed around the wound so that it presses both sides together. Various techniques have been developed over time to bring the tissue together optimally and to minimise the amount of scar tissue produced. The typical standard for surgical suturing is the *simple interrupted stitch* (see Fig. 2.3a). This is a discontinuous suture. The thread is drawn around the wound in a circle and closed above the wound with a *surgeon's knot* (see section 2.1.4). A punctiform wound adaptation develops. For larger wounds, therefore, several *simple interrupted stitches* must be performed.
The *Donati suture* (see Fig. 2.3b) and the *Allgöwer suture* (see Fig. 2.3c) should also be mentioned as examples for other non-permanent sutures. The *Donati suture*, for example, can also be made under tension, and the *Allgöwer suture* gets by with half the punctures of the *Donati suture*. If a wound shall be closed with only one thread, a continuous suture can be used, like the *simple continuous suture* shown in Fig. 2.3d. In this suturing technique, the thread is not inserted and removed orthogonally from the wound, but stitches are made along the wound so that the thread is present along the entire length of the wound and can bring the wound edges together. In *continuous intradermal sutures* (see Fig. 2.3d), only the stitch channels are visible at the beginning and end, and the suture runs intracutaneously between them.



(a) *Simple interrupted stitch* [12]

(b) *Donati suture*[13]

(c) *Allgöwer suture*[14]

(d) *simple continuous suture*[15]

(e) *continuous intradermal suture*[16]

Figure 2.3: Different types of sutures

2.1.4 Knot techniques

To secure a suture, the thread ends must be connected to each other or to themselves in such a way, that they no longer come loose and there is no risk of the wound opening again. The gold standard in surgery is the *surgeon's knot*. This knot is a detachment of the cross knot and allows the maintenance of the tension of the thread when the knot is knotted [17]. It is also called *wound knot* or *ligature knot*. To tie the knot, a double overhand knot is first knotted, which is completed by a single overhand knot running in opposite directions (see Fig. 2.4).

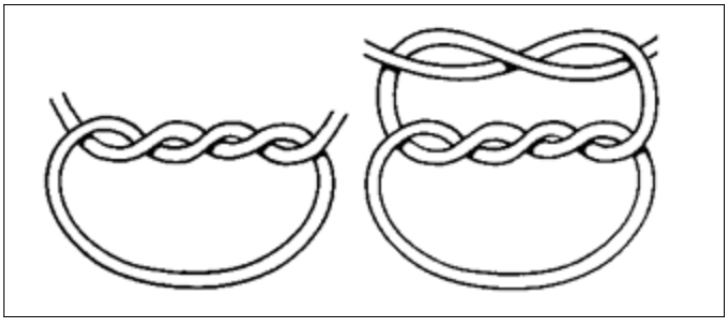


Figure 2.4: *Surgeon's knot* [18]

2.2 Clinical sterilizability

In the clinical environment, sterility is of particular importance to reduce the risk of infection. This applies not only to the staff but also to the medical instruments used during surgery. According to [1] sterilisation means the "killing or removal of all viable vegetative and permanent forms of pathogenic and apathogenic microorganisms in substances, preparations or articles". To ensure this sterility, there are many sterilisation procedures, which can be divided into many subgroups. Examples for these are chemical procedures, procedures using radiation and physical procedures [19]. In chemical procedures, the equipment is purged with gas, sometimes with the aid of a previously generated vacuum. An advantage of gas sterilisation is the feasibility of temperature-sensitive objects. A disadvantage of many gas sterilisation processes, however, is the danger of explosion, since most of the time explosive gases are used. Typical gases for this process are hydrogen peroxide, ethylene oxide or chlorine dioxide. The process that uses chlorine oxides is the gentlest, as this gas is not flammable, the process does not require a vacuum and only needs to take place at a temperature of 40°C. However, it has a long process duration.
Radiation processes such as X-ray sterilisation cause the decomposition of essential cell components. Although this process has a comparatively short duration, it can be harmful for some polymers or electronics.
Physical sterilisation can be reached, for example, by flaming, dry heat or steam. The most common sterilisation process is autoclaving, which is one of the physical sterilisation processes, reached by using steam. The object to be sterilised is placed in a high-pressure steriliser (as shown in Fig 2.5a), exposed to saturated steam at 121°C and 1 bar gauge pressure for approx. 15 - 20 minutes [1].
Another way to ensure sterility in the operating room is to cover the robot or other instruments with a sterile plastic tube, especially for devices, which cannot be sterilised in other ways. An efficient seal must be provided on the scarf so that germs or similar risks present on the robot do not penetrate from the sheath into the cleanroom atmosphere. A typical plastic sheathing for medical robots can be seen in Fig. 2.5b.



(a) Autoclave to sterilize medic instruments [20]



(b) Plastic sheathing of a robot [21]

Figure 2.5: Various approaches to reach sterility

2.3 Minimally invasive surgery

While open surgery was the standard until the 1990s, minimally invasive surgery has established itself since then. This type of surgery does not expose the entire operation area but accesses it via several small openings, which either have to be created during the operation or consist of natural orifices. The instruments are guided through these to the area of interest while the surgeon operates them from outside the body, as shown in Fig. 2.6.



Figure 2.6: Minimally invasive surgery [22]

Minimally invasive surgery has many advantages for the patient: very little tissue is separated by the small incisions, and only minor trauma occurs. This leads to considerable cosmetic advantages and, in general, to a shorter rehabilitation period [23]. While minimally invasive surgery offers many advantages for the patient, it has many disadvantages for the physician compared to open surgery.
First of all, there is the reduced visibility and the poorer overview, as there is no direct line of sight to the operation area. The view on the operation area is made possible by endoscopes. However, these only offer a small part of the scenario.
Secondly, two degrees of freedom of movement of the instruments are lost, since the trocar point determines their position in two spatial directions (see Fig. 2.7), i.e. the point of penetration into the human tissue. This leads to reduced freedom of movement of the instruments. Thirdly, there is a motion inversion, because a movement outside the body causes the tip of the instrument to move in the opposite direction. Fourthly a motion scaling occurs: Since the instruments always run through the trocar point, there is a scaling factor of the movements outside the body to those inside. This results from the different lever arm lengths of the instrument on the inside and outside of the body. In addition to poor visibility and unfavourable kinematic conditions, a further disadvantage is a reduced ability to react to complications: They are difficult to detect, and due to the limited working space it is not possible to deal with all eventualities. This means that if complications occur, the entire operation area must be uncovered and an open operation must be performed.

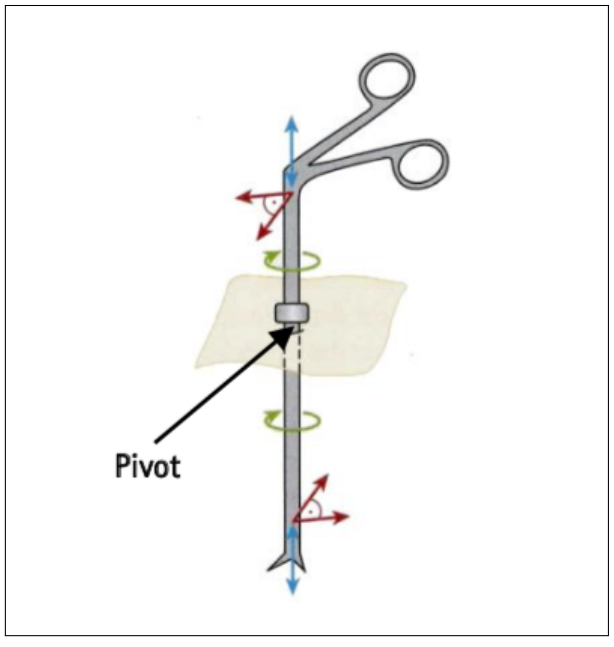


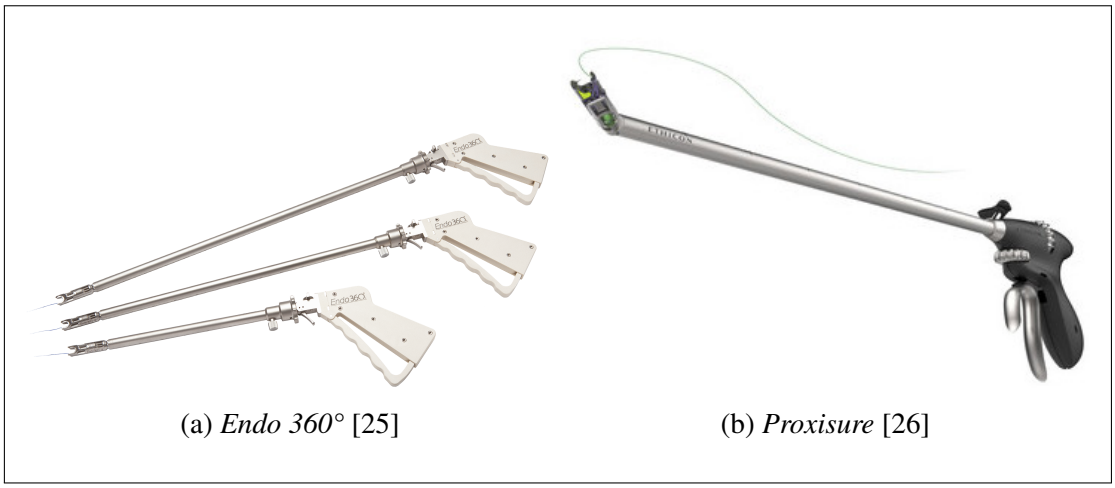
Figure 2.7: Trocarkinematics[24]

2.4 Suturing Devices

Since needle and thread handling requires high dexterity (and needle handling is usually supported by needle holders), the surgical suturing process is technically challenging, especially in minimally invasive surgery. In this scenario, the surgical area cannot be reached with conventional needle holders. The *Maryland dissector* grippers, which are typical for minimally invasive surgery, have little haptic feedback and are not ideally suited for handling surgical needles. It is difficult to achieve a defined position and orientation of the needle with the smooth or corrugated surfaces of the dissector, which does not change with movements or minor disturbances. For all these reasons, surgical suturing is a very time-intensive process in minimally invasive surgery. To compensate for the disadvantages of needle handling, suturing instruments have been developed for minimally invasive surgery, which makes it possible to manipulate the needle inside the body during an operation while controlling all the necessary degrees of freedom from outside the body. These suturing instruments use different functional principles, the most important of which will be presented in the following.

2.4.1 Rotating needle suturing devices

As described in section 2.1.1, many surgical needles have a circular shape. Therefore, many suturing instruments guide the round needle along on a circular path. The instruments using this principle have a trigger on the handle that rotates the needle at the instrument tip by 180° when actuated. The rotation of the needle can either be used to penetrate the tissue during movement or to manipulate the thread to form knots. In addition to the rotation of the needle, the tip of the instrument can usually also be rotated and angled so that during the operation there are sufficient degrees of freedom in the body to position the needle. Examples for this kind of surgical suturing instruments are the *Endo 360°* [*EndoRevolution*, Raynham, USA] (see Fig. 2.8a) and the *Proxisure* [*Ethicon*, Somerville, USA] (see Fig. 2.8b).



(a) *Endo 360°* [25] (b) *Proxisure* [26]

Figure 2.8: Rotating needle suturing devices

2.4.2 Alternating needle suturing devices

In contrast to the instruments shown in section 2.4.1, in which the needle moves on a circular path, the needle can be moved from one gripper jaw to the other and back in the devices presented in this section. This type of device has a gripper as its instrument tip. Each jaw of the gripper possesses a hole and a solvable clamp mechanism as a holder for the needle. The needle is always held at least by one jaw of the tooltip. In general, several degrees of freedom can be manipulated on the handle of these instruments: One degree of freedom closes and opens the jaws. A further mechanism, mostly designed as a toggle switch or wheel, fixes the needle in one or the other jaw, depending on the position of the switch. Thus the position of the needle in the jaws can be changed by actuating this switch. Just like the suturing instruments in 2.4.1, there are usually other degrees of freedom that allow the instrument tip to rotate or bend sideways. Examples for this suturing instrument type are the *EndoStitch* [*Medtronic*, Minneapolis, USA] (Fig. 2.9a), the *SILS Stitch* [*Covidien*, Dublin, Ireland] (Fig. 2.9b) and the *Switch* [*Mellon*, Nijmegen, Netherlands] (Fig. 2.9c). However, the *Switch* is not a device that can be used endoscopically.

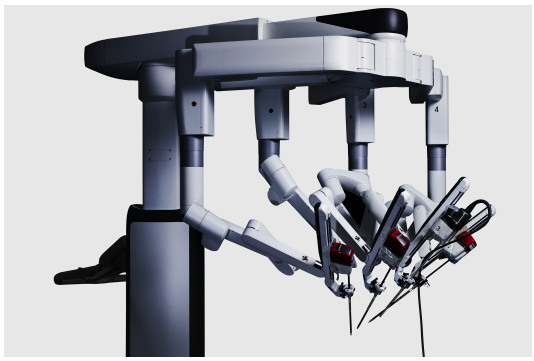


(a) *Endo Stitch* [27] (b) *SILS Stitch* [28] (c) *Switch* [29]

Figure 2.9: Alternating needle suturing devices

2.5 Surgical Robotics

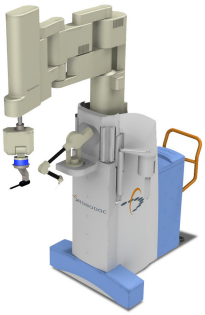
Surgical robots form besides hospital robots and rehabilitation robots a subgroup of medical robots. Surgical robots have been used clinically since the mid 1990s [30].
The aim of such robots is not to replace the medical staff, but to support them. Surgical systems can be divided in many ways. They can be classified into versatile systems (e.g. *daVinci* [*Intuitive Surgical*, Sunnyvale, USA] or *MiroSurge* by the *DLR*) and specialized systems (e.g. *ROBODOC* [*Think Surgical*, Fremont, USA] or *ARTAS* [*Restoration Robotics Inc.*, San Jose, USA]. Each of these systems is shown in Fig. 2.10.



(a) The *daVinci Xi* System [31]



(b) The *MiroSurge* System [32]



(c) The *ROBODOC* System [33]



(d) The *ARTAS* System [34]

Figure 2.10: Various surgical robotic systems

While versatile systems can be used in various areas of surgery and their versatility usually is reached by exchanging their tools, highly specialised systems are designed for a specific task and can only be used for this purpose, like the *ARTAS* system for hair transplantation or the *ROBODOC* system for hip joint surgeries. Another classification of surgical robot systems is into autonomous, mostly vision-based systems and teleoperated master-slave systems [30]. Vision-based systems mainly control themselves using a camera or other imaging systems to observe their environment and react to external influences. Master-slave systems are much more common [30]. Here the robot system is controlled by the surgeon and has none or very limited autonomy. A general structure of teleoperated systems and its signal flow is shown in Fig. 2.11. It shows the spatial separation between the operator (left) and the teleoperator (right). While the operator gets the signals in different ways like visual, haptic or audio feedback, the teleoperator can interact with the environment with actuators and sensors. There is the possibility that a closed-loop control can control each side of a teleoperated system.

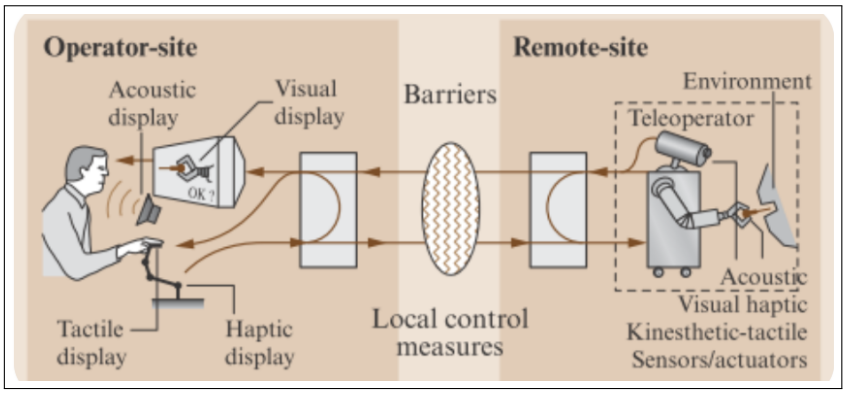


Figure 2.11: Teleoperated systems [35]

While in the first approaches of this principle no technical aids were integrated, so that the limitation of teleoperated systems lay in the human fine motor skills, reaction time and cognitive abilities [30], more and more aids are added like operation area monitoring or tremor compensation [5]. In addition to these two main types, there are, of course, also mixed forms that are controlled by the surgeon but can perform individual subtasks independently, like operation area monitoring [36]. The gold standard in minimally invasive robot-assisted surgery urology and visceral surgery is currently the *daVinci Xi* system from *Intuitive Surgical* (see Fig. 2.10a). This system has four arms to which different instruments or an endoscope can be attached, and a console, from which the surgeon can control the robot arms. In addition to the *daVinci* system, however, there are many other robot systems that are still research systems or have already been commercialised. One of these systems is the *MiroSurge*, which was developed by the *Institute of Robotics and Mechatronics* of the *German Aerospace Center* (*DLR*).

2.5.1 DLR MiroSurge system

The *MiroSurge* system (Fig. 2.10b) is a teleoperated system for minimally invasive robot-assisted surgery, which was presented to the public in 2008 [37]. It consists of up to three lightweight robot arms, called *MIRO*, that can be mounted directly on the operating table. Each arm has seven degrees of freedom, a weight of 10 kg and can carry a maximum payload of 3 kg. The robots are equipped with integrated force/torque sensors and can be used in position control as well as in torque or impedance control mode [37]. The overall control cycle has a frequency of 3 kHz [37]. Further technical data can be found in table 2.1.
Medical instruments can be attached to the lightweight robot arms using magnetic interfaces. It is possible to mount commercially available instruments with an interface, like flexible endoscopes[38], or instruments specifically designed for the *MiroSurge* system developed by the *DLR*, called *MICA* instruments. Several end effectors like scissors, grasper or needle

holder are available. A typical *MICA* instrument is shown in Fig. 2.12.



Figure 2.12: *MICA* instrument [39]

Other instruments, such as waterjet cutters are available too [40]. The *MiroSurge* system is constantly being developed further. In 2017 the robotic arm was extended with a user interface consisting of several buttons located directly on the robot and a LED ring [41].
In addition to the robot arms, the *MiroSurge* system, like the *daVinci* system, also includes a surgeon console from which the operating person can control the robots and instruments [37], as shown in Fig. 2.13.



Figure 2.13: The *DLR MiroSurge* user interface [37]

Parameter	Value
Number of joints	7
Mass	10 kg
Maximum payload	3 kg
Maximum working distance	0.76 m
Position sensors	Motor-sided, joint-sided
Cartesian speed	0.5 m/sec
Torque Sensors	Joint-sided
Safety brakes	Motor-sided
Control modes	Position, torque ans impedance
Control cycle	3 kHz

Table 2.1: Specification of the *MIRO* [37]

The mechanical dimensions of the *MIRO* robot arm, the *Denavit-Hartenberg* parameters (see section A.1.2 for further details of this notation) and joint motion ranges can be found in the Table 2.2 [42]. The coordinate systems according to *Denavit-Hartenberg* are displayed in Fig. 2.14.

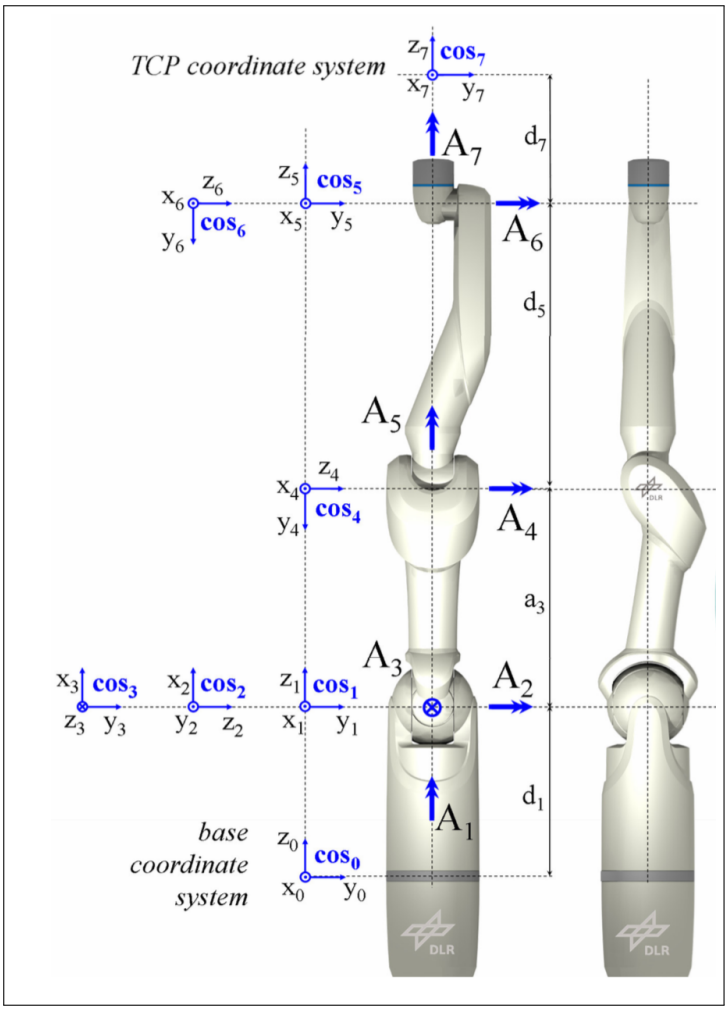


Figure 2.14: *MIRO* kinematics [42]

i	$a_{i-1}[mm]$	$\alpha_{i-1}[^\circ]$	$d_i[mm]$	$\Theta_0[^\circ]$
1	0	0	240	0
2	0	− 90	0	− 90
3	310	90	0	0
4	0	− 90	0	90
5	0	90	385	0
6	0	− 90	0	0
7	0	90	200	0

joint	*range* [°]	*software limit* [°]
1	± 172.5	± 162.5
2	± 51	± 41
3	± 51	± 41
4	− 57 / + 127	− 47 / + 117
5	± 172.5	± 162.5
6	± 172.5	± 162.5
7	± 172.5	± 162.5

Table 2.2: *Denavit-Hartenberg* parameters of the *MIRO* [42]

Communication structure of the MiroSurge System

As described in [37], the communication structure of the *MiroSurge* system must meet many requirements, such as the integration of a workflow, the processing of various control concepts and feedforward signals. It must also be very flexible to simplify prototyping. To achieve this, the structure is divided into four levels. The higher the level, the more hardware is included, but the more the details are abstracted. The first level *joint control* is responsible for the position and torque control of individual joints. The second level deals with the whole kinematic chain of a robot arm, with both kinematics and dynamics. This level is therefore responsible for the *local cartesian control*. The third level is responsible for the *bilateral teleoperation*. Here two Cartesian devices (robot arm and hand controller) are combined to create a one arm master-slave system for the teleoperation. The fourth and last level deals with *multi-arm coordination*. All robot arms and the endoscope camera are brought together here. Other third-party devices can also be integrated into this communication network. A scheme of the whole communications structure is shown in Fig. 2.15.

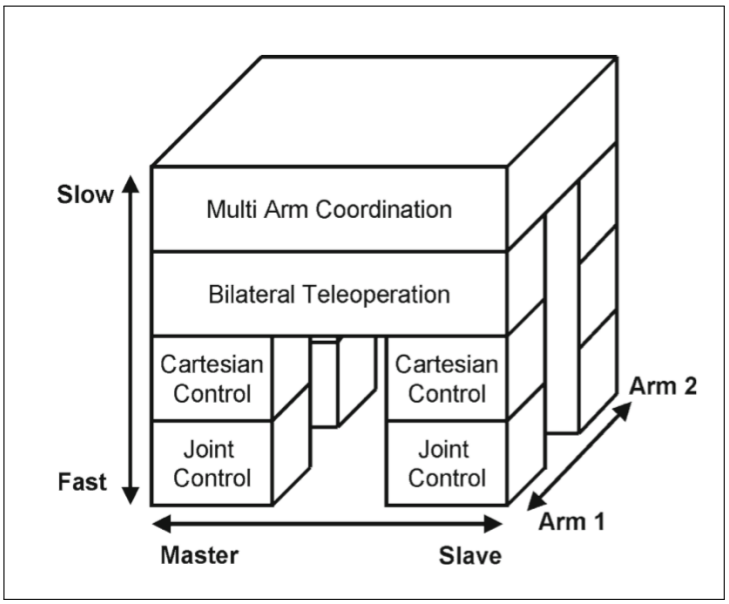
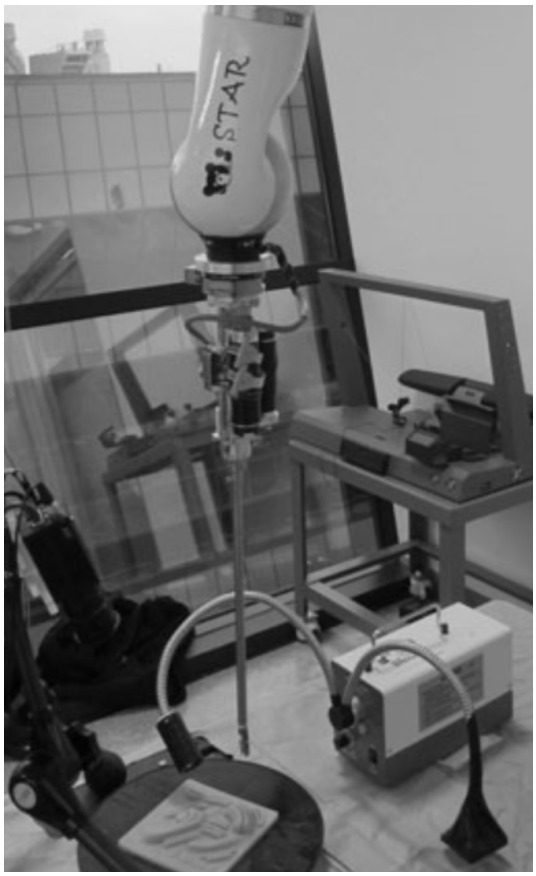


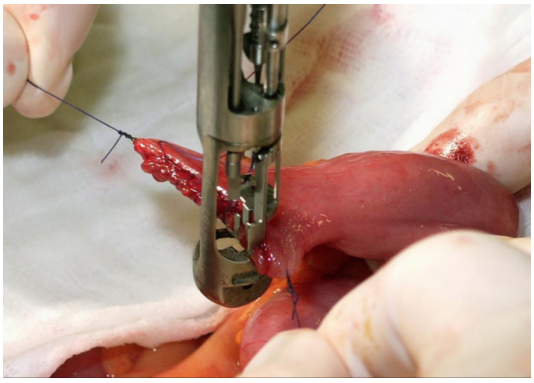
Figure 2.15: *MiroSurge* four layer architecture [37]

2.5.2 Robotic systems for surgical suturing

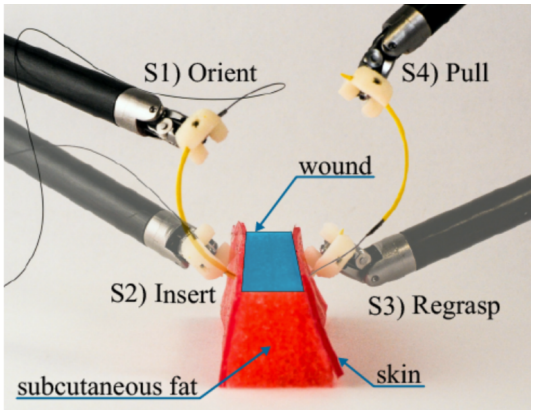
There are already various approaches to combine the surgical suturing process with robot-assisted surgery. The approaches can be divided into three groups: Firstly, existing instruments are integrated into a robot system using an adapter [43], [44], [38]. Secondly, new instruments are developed that are specially designed for surgical robots [45]. Thirdly the suturing process is performed with the standard grippers of a system, and the process is optimised through better control approaches [46]. An example of the first approach is the project *STAR* by *S. Leonhardt et al.* (see Fig. 2.16a). Here the *Endo 360°* by *EndoEvolution* already mentioned in 2.4.1 was adapted to a *KUKA LBR* [*KUKA*, Augsburg, Germany] and robot-assisted suturing was performed and compared with conventional methods. The *EndoSew* [*Karl Storz*, Tuttlingen, Germany] (see Fig. 2.16b), for example, belongs to the second type: It is a sewing-machine-like instrument specially manufactured for the *daVinci* system, which can be coupled to the *daVinci* system and can perform suturing using two additional grippers. An example of the last type, the use of conventional devices and the implementation of special control approaches, is the *SNAP* project by *S. Sen et al.*, displayed in figure 2.16c. A *daVinci* system with slightly extended standard grippers was used, and the individual steps of the suturing process were modelled on the software side. All of these approaches have advantages and disadvantages: while the *STAR* project is more accurate and faster than a manually performed suture, it is limited to planar tissue, because of the image processing used in this approach. The *EndoSew* is fast, but not completely reliable. In some cases, the sutures have to be supported with additional manual stitches. The *SNAP* system can plan and execute the sutures automatically, but the system operates at approximately 30% of the speed of a manually teleoperated suturing process. All these projects are research systems, and none of them was sold commercially or clinically.



(a) the *STAR* [43]



(b) the *EndoSew* system [45]



(c) the *SNAP* system [46]

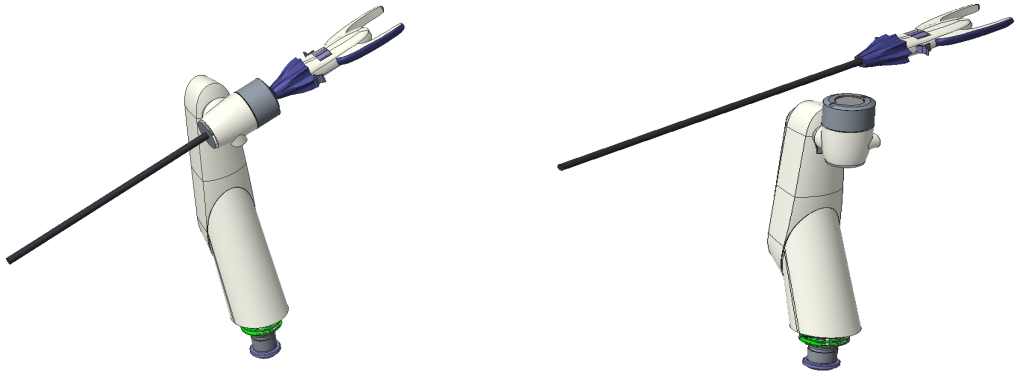
Figure 2.16: Robot assisted surgical suturing

2.6 Summary

In this chapter, the basics of surgical suturing, the current status of commercially available suturing instruments and the principle of robot-assisted surgery were discussed. These three topics are essential for the successful actuation and integration of a suturing instrument into the *DLR MiroSurge* system. From these facts, the requirements of an interface can be concluded in chapter 3.

3 Requirements

The goal of this thesis is to integrate a suitable suturing instrument into the *MiroSurge* system. The *MIRO* robot arm should be able to position the instrument and its adapter to any desired pose. For this purpose, the construction space must not be too large, and the weight must not be too high. The maximum payload of the robot arm is 3 kg. As in previous works [38], a maximum weight of 2 kg of the instrument and the adapter should allow excellent dynamic characteristics of the arm. There are two possible configurations of the instrument on the robot: Firstly, the shaft of the instrument is coincident with the hollow axis (see Fig. 3.1a). This arrangement allows the entire instrument to rotate around the last axis of the robot. However, it requires the adapter to be as small as possible so that the housing does not collide with the robot when axis 6 is moved (see Fig. 2.14). This configuration, therefore, leads to challenges when designing the adapter and, eventually, to restrictions of the working space. In a second possible configuration, the instrument and adapter are arranged perpendicular to the last axis of the robot (see Fig. 3.1b). This results in significantly more working space because the degrees of freedom of the robot can be better utilized, and a collision scenario is minimized. However, in minimally invasive surgery, the size of the workspace of the robot is less relevant. The disadvantage of this arrangement is the necessity of a further degree of freedom to rotate the instrument.



(a) Instrument pushed through the hollow axis (b) Instrument perpendicular to the hollow axis

Figure 3.1: Different configurations of the suturing instrument, as example with the *SILS Stitch*

If the suturing device is a disposable product, the exchange of the instrument should be as simple as possible and without many construction steps. In case of complications, it should also be possible to remove the instrument manually from the surgical area as quickly as possible. Since the suturing instrument, robot and adapter will be used in a clinical environment, they must also comply with the guidelines for medical devices. The instrument and the robot are already designed for this, but there are still several aspects to be considered for the adapter. As described in section 4.2.5, all products in contact with the patient being operated on must be sterile. It must be ensured that the non-sterile parts (motors, etc.) do not contaminate the sterile areas. This is particularly important when inserting the instrument into the adapter. Two different strategies can approach the sterile operation with the adapter. The first is the sterilization of the whole adapter. Since the standard of sterilization is the autoclave, the adapter should be autoclavable. For this, it should be able to withstand temperatures of over 120°C over a more extended period of time without changing its structure or physical properties. If this strategy is chosen it is important to focus on the material from which the adapter is to be made. Also, the system should be designed so that all sensitive, non-autoclavable components, such as the motors, do not come into contact with the operating area and can be quickly and easily removed from the rest of the adapter before autoclaving. The other strategy to enable the sterile operation with the adapter in the operation area is the plastic sheathing of the adapter. Therefore a concept must be developed in which the sterile instrument can be inserted in the adapter without risking the contamination of the parts of the instrument, getting in touch with the patient.

4 Design

This chapter describes the procedure for designing the interface. A flowchart of the design process is shown in Fig 4.1. First a selection of a suitable instrument (section 4.1.2) is made. Then all important and relevant properties (section 4.1.3) are analysed. An adapter is developed that meets all requirements. After the mechanical design (section 4.2) the control of the motors is discussed in more detail (section 4.3). With the knowledge of the mechanic properties und the motor control, the interface can be described kinematically, which is described in section 4.4, 4.5 and 4.6. At the end of this chapter, a way to integrate the interface in the *MiroSurge* system is presented in section 4.7

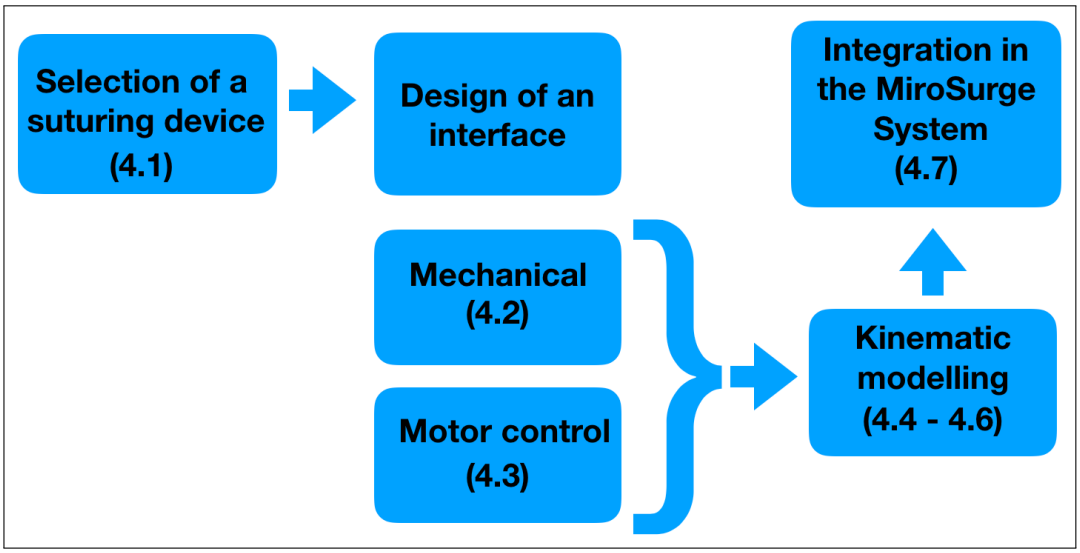


Figure 4.1: Flowchart of the design process

4.1 Selection of a suturing device

For the integration of a commercially available suturing instrument into the *MiroSurge* system, it is of great importance to select a suitable instrument. In the following different suturing instruments will be compared. After the selection of the most suitable instrument, it is analysed with regard to the degrees of freedom to be actuated, the forces/torques required for actuating the degrees of freedom and the possibility of attachment in an adapter.

4.1.1 Research about available devices

To select a suitable suturing instrument for the adaptation, various instruments were analysed and evaluated. This evaluation is limited to the instruments with the principles of the rotating needle and the alternating needle described in section 2.4. Other approaches were not considered due to high complexity or unsuitability for minimally invasive surgery. Four different instruments are briefly presented in the following, the degrees of freedom of the instruments and their suitability for adaptation are discussed.

SILS Stitch

The *SILS Stitch* by *Covidien* was introduced in 2010 [47]. An overview of each degree of freedom of this product can be seen in 4.2. The disposable product has a rotatable (yellow arrows) and deflectable (red arrows) instrument tip as well as a type of gripper that closes by actuating the handles (green arrows). In addition, there is a swivelling lever on the handle that actuates a mechanism to determine the jaw, which the needle is attached to (blue arrows). The shaft of the instrument has a diameter of 10 mm and a length of 430 mm up to the instrument tip. The overall dimensions of the instrument are 635 mm in length, 68 mm in width and 50 mm in height. The weight of this instrument is 185 g The instrument can be loaded sterile, as the corresponding needles are packed in such a way that one does not have to touch them in order to fix them in the gripper. For this fixation, there is another switch on the instrument, but it is only needed for the fixation. Thus it is not relevant during the suturing process. However, this instrument was removed from the market in 2019 and sales ceased.

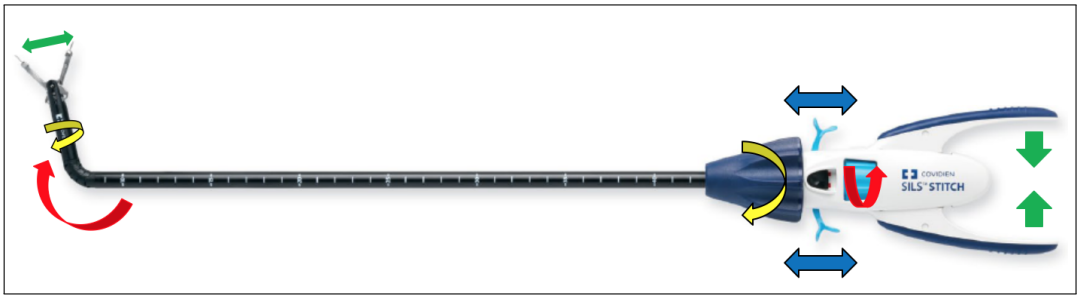


Figure 4.2: Degrees of freedom of the *SILS Stitch* [48]

Endo Stitch

Similar to the *SILS Stitch*, *Metronic's Endo Stitch* also follows the alternating needle principle. It is also a disposable product, but lighter and simpler than the *SILS Stitch*, with fewer degrees of freedom. As shown in Fig. 4.3 it has a swivelling lever to change the fixation of

the needle in the jaws (red arrows) and a push handle that opens and closes the jaws (blue arrows). The tip is rigid and can neither be angled nor rotated. The instrument also uses a 10 mm diameter shaft. It has a length from 373 mm to the tip of the instrument. The total dimensions are 550 mm in length, 67 mm in width and 29 mm in height, the weight is 105 g. The *Endo Stitch* is loaded in the same way as the *SILS Stitch* by placing the tip of the instrument in a fixture and gripping the needle.

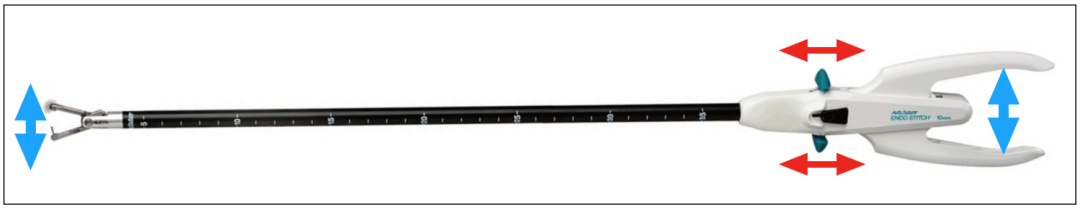


Figure 4.3: Degrees of freedom of the *Endo Stitch* [49]

Endo 360°

The *Endo 360°* from *EndoEvolution* is a reusable suturing instrument, which uses a rotating needle. In the following the degrees of freedom, as shown in Fig. 4.4 are described. In addition to the degree of freedom for triggering the mechanism (blue arrows), there are two further degrees of freedom: one for deflecting the instrument tip (green arrows) and one for rotating the entire shaft (red arrows). Due to its principle, this instrument does not have the degree of freedom for changing the fixation of the needle. In addition, the *Endo 360°* has a switch for fixing the degrees of rotation and articulation freedom. The shaft of this instrument measures 12 mm in diameter and has depending on the instrument version a length of 222 mm, 374 mm and 449 mm. However, this instrument was removed from the market in 2019 and sales ceased.

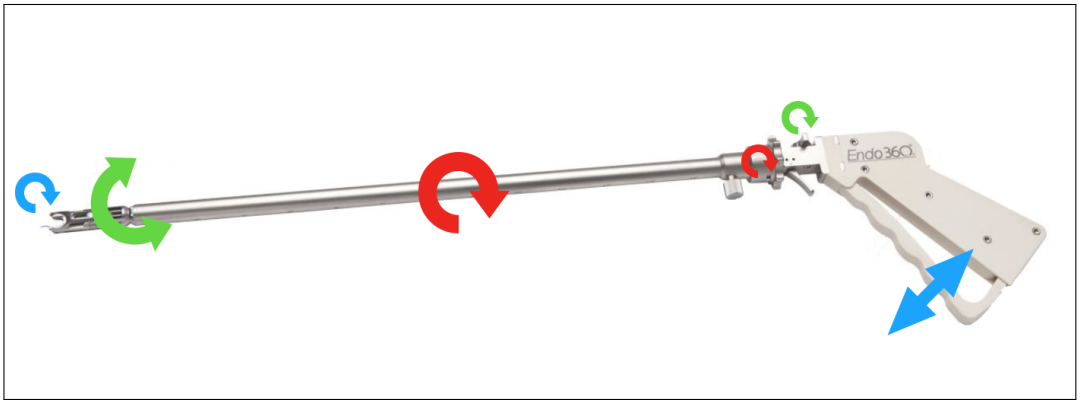


Figure 4.4: Degrees of freedom of the *Endo 360°* [50]

Proxisure

The *Ethicon Proxisure* was introduced in 2016 and is very similar to the *Endo 360°*. This instrument is a reusable suturing device with a rotating needle in the tip. The shaft of the instrument has a diameter of 12 mm and a length of 400 mm. The tip of the instrument can be rotated by 360° and angled by 45° [51]. The degrees of freedom are actuated similar to the *Endo 360°* and the product with each degree of freedom is shown in Fig. 4.5. However, this instrument was removed from the market and sales ceased.

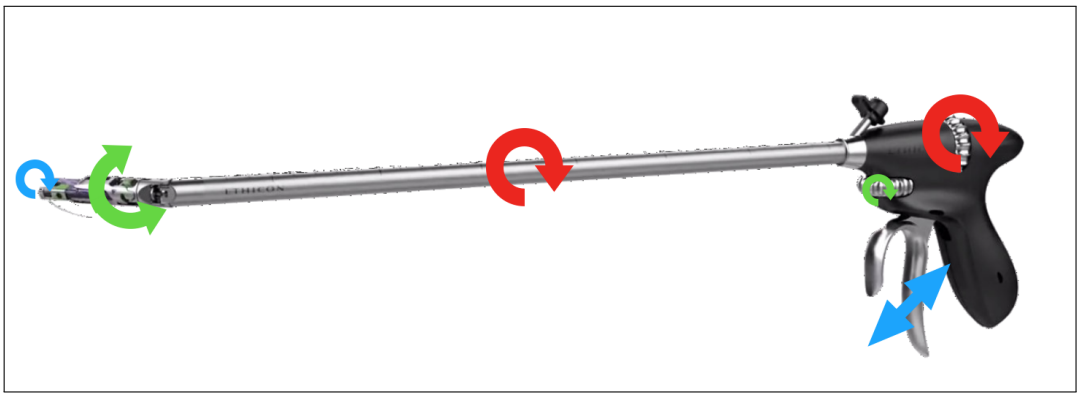


Figure 4.5: Degrees of freedom of the *Proxisure* [52]

4.1.2 Selection of a suitable instrument

A suitable suturing instrument must fulfil many properties (see appendix A.2). All four presented instruments meet most of these requirements and would be principally automatable and suitable for this work. The problem with three of the four instruments (*SILS Stitch*, *Endo 360°* and *Proxisure*) is the discontinuation of production and sales, while the lack of actuable degrees of freedom is a problem with the *Endo Stitch*. Since the *Endo Stitch* has only two actuated degrees of freedom, it was discarded. Since the hollow axis of the *MIRO* has a diameter of 11.4 mm, an instrument with a smaller diameter is desirable to allow for the use of the hollow axis. Therefore the *SILS Stitch* was chosen.

4.1.3 Relevant properties of the suturing device

After the *Covidien SILS Stitch* was chosen for the integration in the *MiroSurge* system, an analysis of all important properties such as degrees of freedom, contact areas and actuating forces was performed. The four relevant degrees of freedom are: The movable handle, which controls the closing of the grippers. In a relaxed state the two handles are 64 mm apart (Fig. 4.6a), after they have been compressed only 40 mm (Fig. 4.6b). Actuation of this degree of

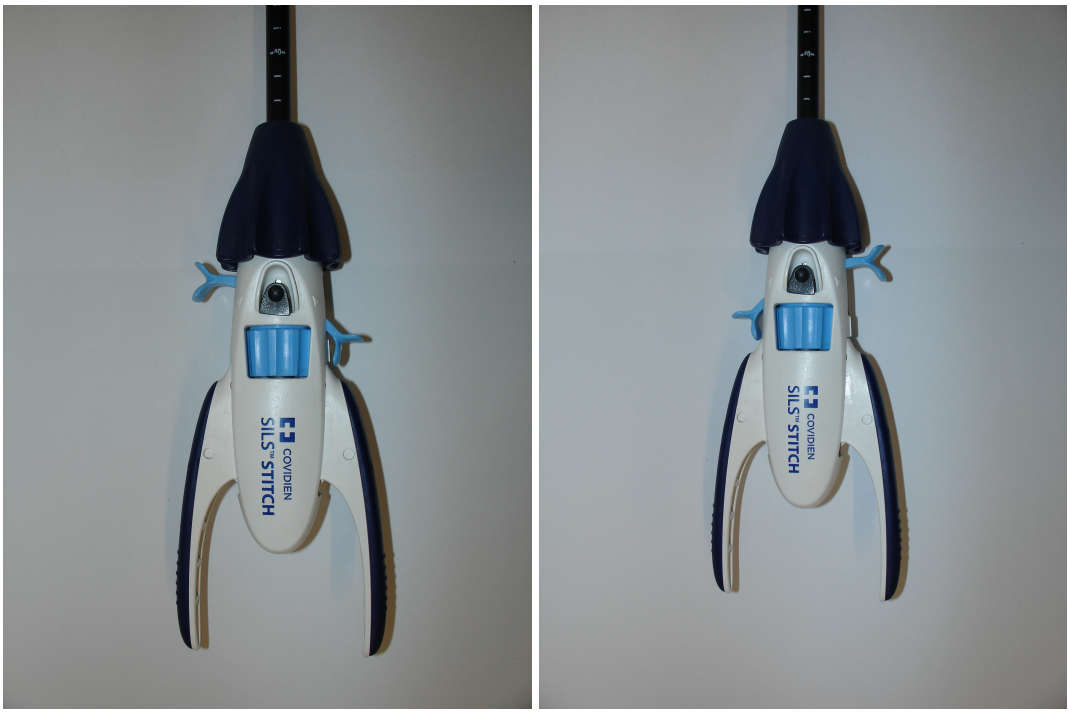
freedom must, therefore, move each handle over a distance of 12 mm.



(a) Position 1 (b) Position 2

Figure 4.6: Positions of the handle

To change the fixation of the needle in the jaws, the light blue swivelling lever must be moved from one position (Fig. 4.7a) to the other (Fig. 4.7b) when the gripper is closed, i.e. the lever must rotate around its centre by 50°.



(a) Position 1 (b) Position 2

Figure 4.7: Postions of the swivelling lever

To rotate the instrument tip the dark blue rotation gear at the beginning of the instrument shaft has to be moved. This degree of freedom has no limits and can be rotated clockwise and counterclockwise infinitely often.
The last relevant degree of freedom for actuation is the light blue gear in the centre of the instrument. This has a clearance of 270°: It must be turned around a three-quarter circle until the tip of the instrument has bent from its starting position (6° angle of the shaft axis) to its end stop (66° angle to the shaft axis).

For the selection of the motors, the force/torque required for the actuation of the degrees of freedom is relevant. Since the two degrees of freedom for the shaft rotation and the fixation of the needle are very smooth-running, a testbed was developed to determine the torque required for the other two degrees of freedom: the articulation and the closing of the handles.
For this test bed, the instrument is placed in a holder and a flexible, 3D printed gear wheel presses on the light blue articulation wheel from above. The whole testbed can be seen in Fig. 4.8a The gear wheel is connected to a shaft by form closure and can be turned by a screw (Fig. 4.8d). For the gripping mechanism, a cable adapter is mounted between the two

handles via a ball bearing. Ropes are tied to the adapter and to the handles (Fig. 4.8c). In the middle of the adapter, a screw is glued. One can exert a torque, which goes over the ropes to the grips and to pull those together.

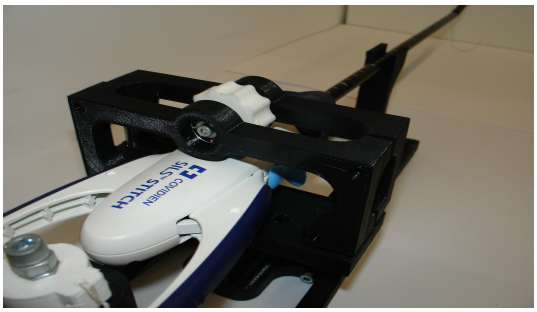


(a) Testbed

(b) Torque wrench



(c) Adapter for the handle



(d) Adapter for the articulation

Figure 4.8: Testbed to evaluate required motor torques

With the aid of a torque wrench (Fig. 4.8b), which is inserted into the screw on the shaft (Fig. 4.8d) or the rope adapter (4.8c), the required torques for actuating these degrees of freedom can be determined. The following torques were determined by measuring the torque with the torque wrench:

$$M_{Articulation} \approx 30\,cNm \tag{4.1}$$

$$M_{Handle} \approx 50\,cNm \tag{4.2}$$

Another essential property of the instrument is the size of the possible contact area to the interface. The instrument offers enough contact surfaces at its base body and at the end of the shaft to clamp it into an adapter. As mentioned in 4.1.1, the switch for the first clamping of the needle is not actuated. The needle must, therefore, be clamped in the jaws before it is installed in the adapter. However, this will not disturb the workflow.

4.2 Interface

The interface, as well as the suturing instrument, must meet some requirements (see appendix A.2). This includes aspects such as sterilizability, weight, dimensions and mountability. The following sub-sections explain which connection is required to connect the interface to the robot (section 4.2.1), which motors are used (section 4.2.2), how they actuate the degrees of freedom via a gear (section 4.2.3). Then a general description of the mechanical design of the adapter (section 4.2.4) is described and how it is ensured that the adapter can be sterilized (section 4.2.5). This section concludes with a description of the commissioning for the interface (section 4.2.6).
Since a suturing instrument with a shaft diameter of 10 mm has been selected, the shaft of the instrument can be guided through the hollow axis of the *MIRO* (see Fig. 3.1a). To ensure a sterile workflow, the disposable instrument must be placed in the adapter so that there is no risk of contamination. Also, the adapter makes it possible to insert the instrument with minimal effort.

4.2.1 Mounting

A requirement for the system is the quick mounting and dismounting of the adapter from the robot in case of complications during an operation. For this purpose, the magnetic adapters of the *MICA* instruments are very useful (see Fig. 4.9). These provide a standardized interface so that existing parts can be used. The magnetic adapter also ensures rotation of the adapter by rotating the seventh axis of the *MIRO*.



Figure 4.9: Magnetic mounting adapter of the *MICA* system

4.2.2 Motors

The servo motors *DITEX 1609S* [*Hacker Motor GmbH*, Ergolding, Germany] were used for the interface. It can be seen in Fig. 4.10 These can apply up to 113 Ncm, which is sufficient for the required torques with a safety factor of more than 2. In addition, they have good mechanical properties, and the robotics working group at *DLR* has good in-house experience with them. Further information about this motor can be found in the appendix A.7. The motor control properties are discussed in Section 4.3.1.



Figure 4.10: *DITEX 1609S* [53]

4.2.3 Transmission

Each of the degrees of freedom should be actuated using the servo motor *DITEX 1609S*. Various transmission are used for this, which are described below.

Rotation of the tooltip

To actuate the rotation of the tool tip, the servo motor must rotate the dark blue wheel at the end of the shaft. Based on a 3D model of the suturing instrument, a negative of the rotating wheel was created as an adapter. A gear with 54 teeth and a gear module of $m = 1$ and an inner diameter of 47 mm was glued onto this part. The gear holder can now be pushed over

the shaft of the instrument is then snapped on the wheel using clips. The counterpart to the gear on the gear holder has 17 teeth (gear module $m = 1$) and is pressed directly onto the motor. The gear ratio in this gear stage is therefore $i = \frac{17}{54} \approx 0.31$. The CAD model of this mechanism is shown in Fig. 4.11.

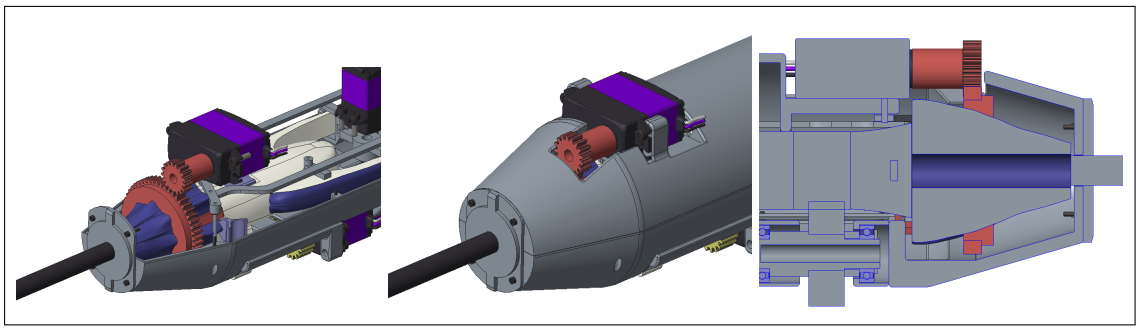


Figure 4.11: Gear for the rotation of the tooltip

Articulation of the tooltip

To bend the tip of the instrument, the light blue gear, which is located in the middle of the instrument, must be actuated. Since this gear wheel is designed for turning with the fingers, no simple counter gear wheel can be created. Therefore, a gear design printed from flexible filament is used. Due to the flexibility of the gearwheel, a positive fit results at a given contact pressure, which ensures that the light blue gearwheel of the instrument moves during rotation.
The flexible gearwheel is mounted on a shaft with a fixed/floating bearing and a gearwheel with 20 teeth on its shaft end. This gear wheel meshes with another gear wheel, which has 17 teeth and is pressed on a servo motor. The servo motor thus drives the light blue gear wheel of the instrument via two gear stages. The first gear stage has a ratio of $i = \frac{17}{20} = 0.85$. The second gear ratio, i.e. the ratio between the flexible gear and the light blue gear, is $i = 1$ since the flexible gear was designed with as many elevations as the light blue gear of the instrument. The CAD model of this mechanism is shown in Fig. 4.12.

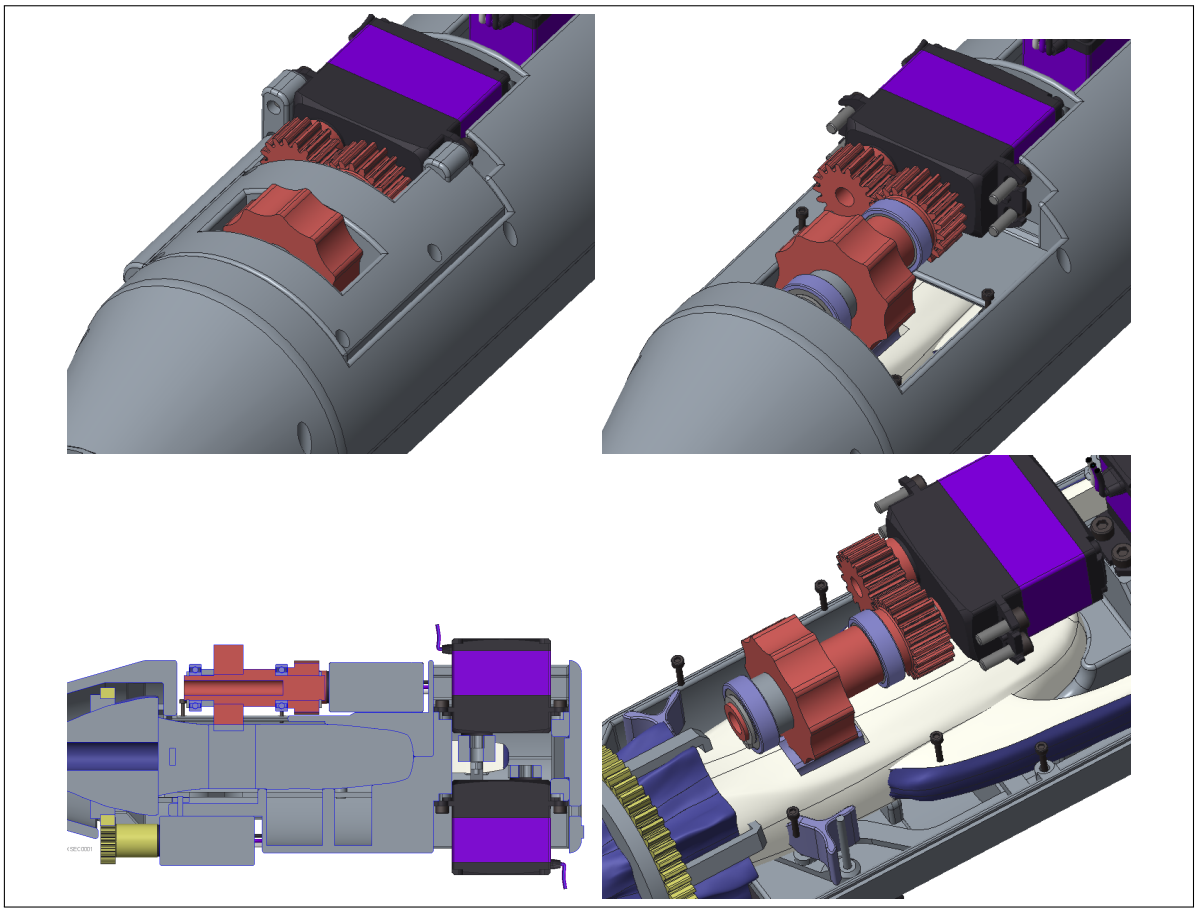


Figure 4.12: Gear for the articulation of the tooltip

Actuation mechanism of the gripper

The closing mechanism of the gripper is activated by bringing the handles together. To compress them by the rotation of the servomotor, an adapter was developed which was pressed onto the shaft of this motor. On this adapter, there are two holders for the handles of the instrument. These can be inserted into the holder, and by turning the motor, the distance of the holders is shortened. The shortening of the distance leads to a merging of the handles, which is the movement required to close the gripper of the instrument.
In this mechanism, there is no transmission, but a direct mapping of the motor angle to the condition of the gripper. There are two states of the gripper: open and closed, and each of these states is assigned a motor angle in section 4.6. The CAD model of this mechanism is shown in Fig. 4.13.

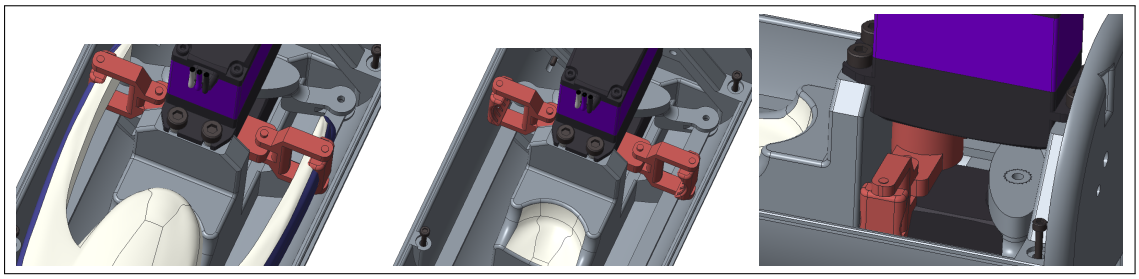
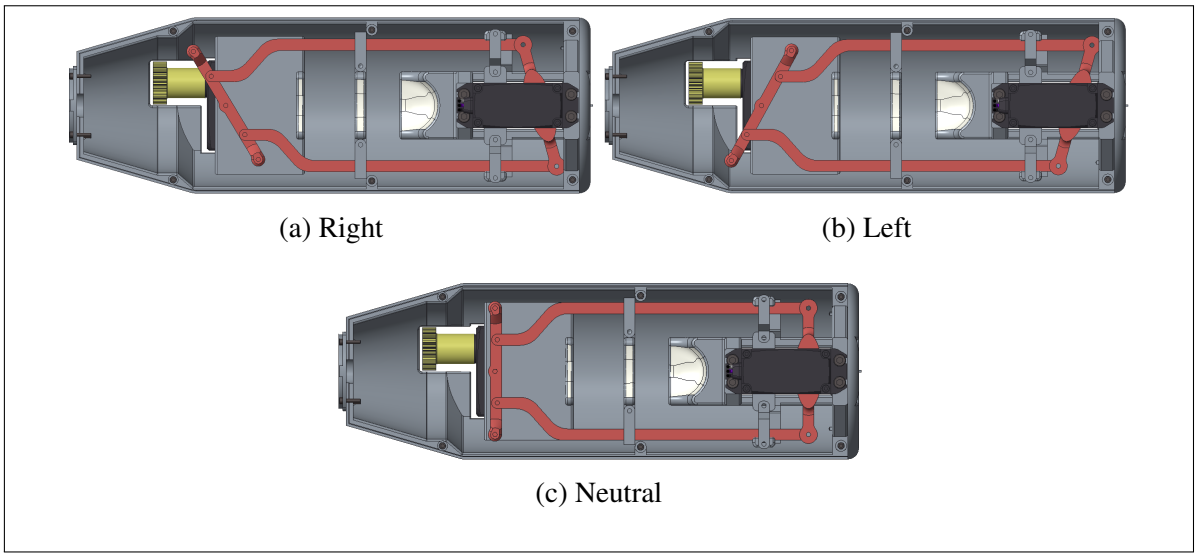


Figure 4.13: Gear for the actuation mechanism of the gripper

Swivelling lever to relock the needle

To change the position of the needle in the gripper, the light blue swivelling lever of the instrument must be turned when the gripper is closed. For this purpose, a mechanism consisting of two rods, a bracket and a motor adapter was installed on the underside of the interface. While the motor adapter was pressed onto the shaft of the servomotor, the bracket is rotatably mounted directly under the swivelling lever. The two rods were then rotatably mounted on the bracket and the motor adapter using dowel pins so that a movement of the motor causes the bracket located under the swivelling lever to rotate. Since the distance between the rod mounted on the motor adapter and the axis of rotation is larger than the distance between the rod mounting on the other bracket and its axis of rotation, there is a greater movement underneath the lever than with the motor. Long dowel pins have been pressed into the outer ends of the front bracket, which press against the swivelling lever during rotation. This pressure causes the lever to turn over and the needle fixation in the gripper to change. No gear ratio is needed here, but the angle of the swivelling lever is measured directly on the motor angles. The position of the swivelling lever is indicated in three states: Fixation of the needle right (stop of the right side of the lever - see Fig. 4.14a), fixation of the needle left (stop of the left side of the lever - see Fig. 4.14b) and neutral position (lever is in the middle - see Fig. 4.14c). The CAD model of this mechanism is shown in Fig. 4.15.



(a) Right (b) Left

(c) Neutral

Figure 4.14: Postions of the swivelling lever

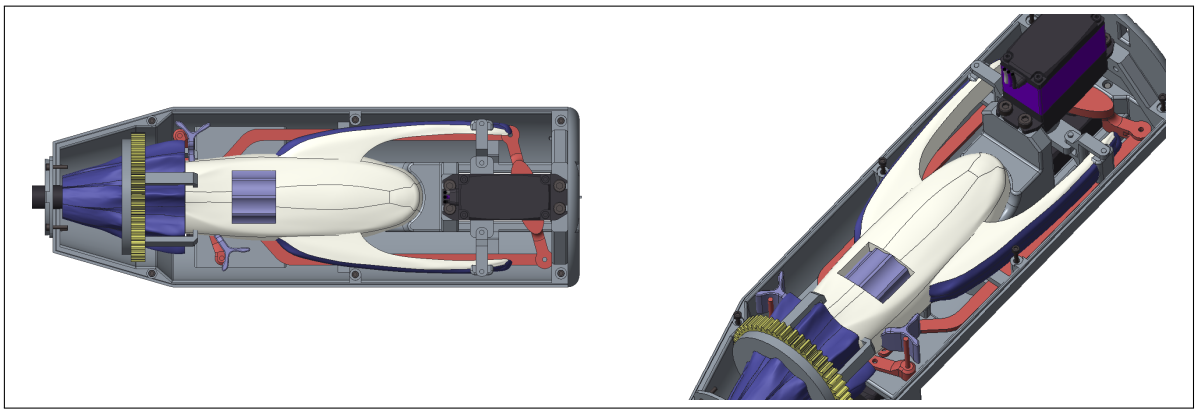


Figure 4.15: Gear for the swivelling mechanism

4.2.4 Design of the actuation interface

The interface has been designed in such a way that the instrument can be placed and fastened in the lower shell with a few simple steps. For this purpose, three of the four motors are attached to the lower shell. Only the motor, which is responsible for the deflection of the tip, is mounted together with the corresponding shaft on a specially designed component, which can be screwed to the upper shell of the interface.
To avoid disturbing cables on the surface of the interface during hands-on operation, all cables were routed in the interior of the interface and led out of the cover at the end of the adapter through recesses. On this cover, there are also screw holes to attach a circuit board

for the control of the four motors.
The interface has a height of 95.6 mm and a width of 78 mm. The length without instrument shaft is 232,4 mm and with instrument shaft 655 mm. The weight of the interface, including the suturing instrument and the centre of gravity of this assembly are also relevant for operation on the robot. The weight was determined on 815 g (1220 g with *Arduinos* and wires) by weighing. The centre of gravity of the adapter is in the division plane of the two shells, 2 mm on the right side and 103 mm behind the magnetic mounting plate.

4.2.5 Sterilizability

Since it is a mandatory requirement that the interface can be used in a clinically sterile environment, its sterilizability must be ensured, or it must be made compatible with the clinical environment by other methods. One possibility would be to sterilize the interface. For this purpose, materials would have to be selected that are autoclavable and resist disinfectant. Since the interface is to be printed in 3D, a large number of different materials are available. In addition to the tensile strength, the glass transition temperature also plays an important role. This temperature indicates the temperature at which polymers acquire a rubbery texture. For example, the interface could be printed from PEEK or PPSU, since these materials have good mechanical properties and are insensitive to temperature changes. While PEEK has a tensile strength of 90 MPa and a glass transition temperature of 142°C [54], PPSU has a tensile strength of 83 MPa and a glass transition temperature of 220°C [55]. PEEK would withstand up to 1500 cycles in an autoclave [56].
However, the design of the interface for autoclavability is difficult, since all the motors are not autoclavable. Before and after each operation, the interface would have to be completely disassembled and reassembled, because the motors have to be sterilized by another sterilisation procedure. In order to avoid this problem, the interface could be packed in a sterile tube during the operation, since only the disposable instrument, comes into contact with the patient. In this case, it must be ensured that the non-sterile components do not come into contact with the shaft of the instrument during assembly of the instrument and the interface. A possible workflow for packaging the adapter in a sterile plastic sheathing is displayed in Fig 4.16.

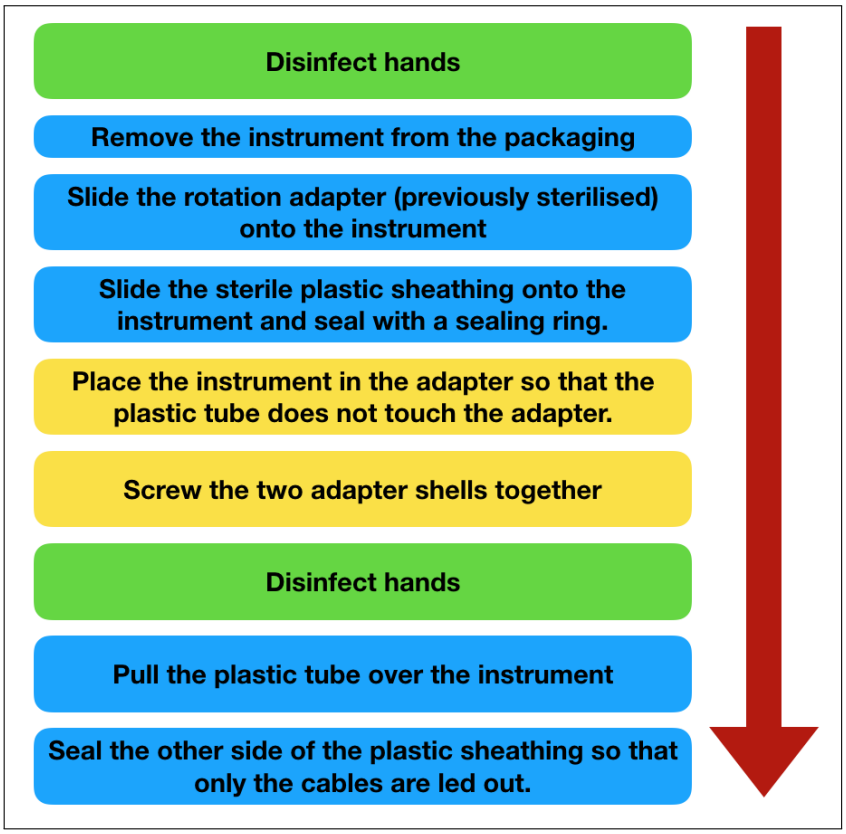


Figure 4.16: Workflow of packaging the adapter sterile

In Fig. 4.16 the steps in the blue coloured boxes are steps, that have to performed sterile, the steps in the yellow boxes are steps that are performed non-sterile and in the green boxes, the sterilisations steps are displayed.
For this sample workflow, the magnetic mounting adapter has to be modified. A two parted mounting would be favoured, because it must not slide along the whole instrument shaft.

4.2.6 Commissioning

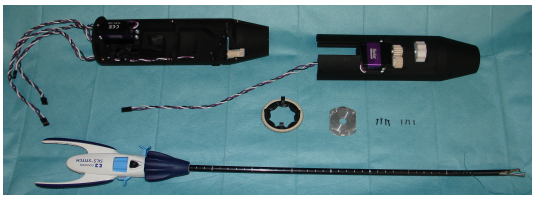
After the adapter was assembled (see appendix A.6) the adapter and the suturing instrument are ready, to be put into operation. For this, the medical staff has to unwrap the suturing instrument out of the packaging. For the commissioning the lower shell, the upper shell, the magnetic mounting, the rotation adapter, the instrument and eight M1.6 x 8 screws are needed. In Fig. 4.17a all these parts are shown. After this is done, the commissioning workflow can be divided into four substeps:

1. The rotation adapter has to be pushed over the shaft of the instrument and has to be clipped on the dark blue rotation gear of the instrument (Fig. 4.17b)

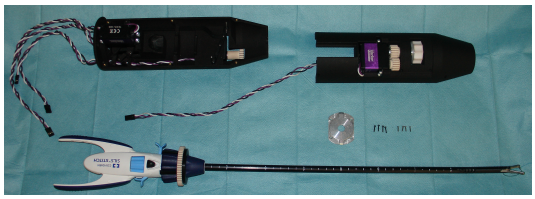
2. The instrument has to be inserted into the adapter. Therefore the two handles of the instrument are pushed in the handle holder of the adapter (Fig. 4.17c)

3. The upper shell hast to be screwed on the lower shell. Therefore the wire of the motor on the upper shell has to be put through the hole on the adapter cover and subsequently the upper shell can be pressed on the lower and can be screwed with four M1.6 x 8 screws (Fig. 4.17d)

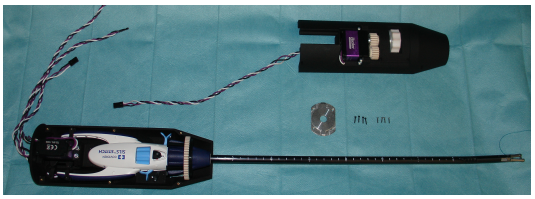
4. The magnetic mounting has to be pushed over the shaft of the instrument and then hast to be screwed with four M1.6 x 8 screws on the upper and lower shell (Fig. 4.17e)



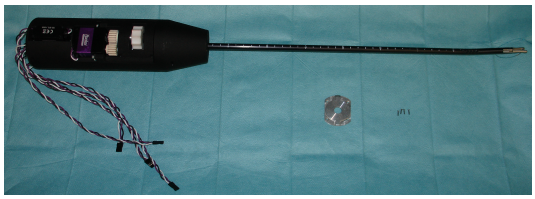
(a) All parts needed for commissioning



(b) Substep 1



(c) Substep 2



(d) Substep 3



(e) Substep 4

Figure 4.17: Workflow for commissioning

The mechanical design of the interface is finished with the discussion of the workflow for inserting a suturing instrument. A mechanical connection to the end effector of the *MIRO* was presented with the magnetic adapter. In addition, it was shown how each relevant degree of freedom of the suturing instrument could be actuated by means of a servo motor of the type *DITEX 1609S*. The general structure and mounting possibilities of the interface were

discussed. In the following, it will be dealt with the control of the motors and the kinematic modelling of the interface.

4.3 Motor Control

Besides the mechanical design of the interface, the control of the motors plays an important role for the integration into the *MiroSurge* platform. This work is based on the principles and specifications presented in [38] for the control of the *DITEX 1609S*.

To ensure the control of the motors, they must be integrated into the existing framework of the *MiroSurge* platform. This framework was implemented in *Matlab Simulink* [*MathWorks*, Natick, USA]. The structure of the communication between *Simulink* and the motor is shown in Fig. 4.18.

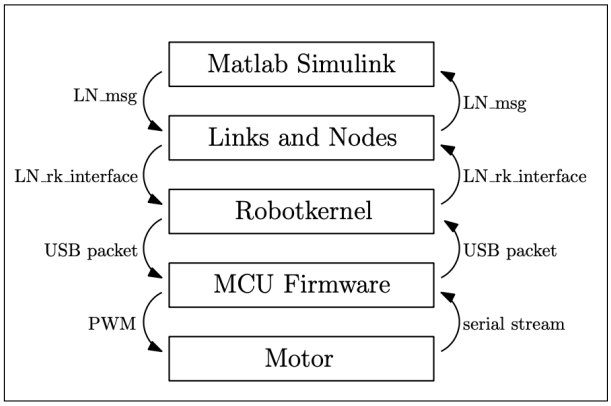


Figure 4.18: Communication structure [38]

The structure of communication consists of five levels. The lowest level is that of the motors. This is presented in section 4.3.1. In the level above, the communication of the motors via microcontrollers is provided (see section 4.3.2). The *DLR* internal robotkernel is an interface between hardware and the links and nodes framework, which is explained in section 4.3.3.

4.3.1 Servo motor

Since the servo motors *DITEX 1609S* have a standardized three-pin interface, all commands and telemetry data are sent over the same wire using pulse-width modulation (PWM). One can choose between two modes. In the first mode, individual packets are sent from the motor to its controller after each PWM pulse, and a total of 14 packets for 14 different telemetry information are sent. As a result, at a maximum pulse frequency of 125 Hz, the transmission of all information takes 112 ms. In the second mode, 11 of the 14 information are combined

and sent by one package. So information is sent much faster, in cost of the loss of the telemetry information *motor status*, *servo runtime* and *total wear-out information*. Since the loss of this data is not critical for this application, the second mode is used. The structure of a telemetry data packet can be seen in Fig. 4.19.

Byte No.	Length[Byte]	Data	Note
0	1	0x3A	Header
1	1	0x00	Status
2	1	ADDR	Address of telemetry DATA
3	1	DATA_LEN	Number of data Bytes
4	DATA_LEN	DATA	Data
4+DATA_LEN	1	CRC8	Error detecting code
4+DATA_LEN+1	1	SECURITY	Security bit

Figure 4.19: Structure of telemetry packet [38]

On the physical level, the packets are sent via RS232 protocol at TTL levels.

4.3.2 Microcontroller

To generate the PWM signal required by the motors for control, each motor is individually connected to an *Arduino Micro* [*Arduino*, Somerville, USA]. These can read the telemetry data and generate a PWM that sets the motor speed. For these *Arduinos* internal libraries were used, but also the customized USB library, which was tuned for the robotkernel. In the existing system, the hardware serial interface of the *Arduino* was used.
Since the motors need an inverted serial communication signal, in [38] an inverter circuit was designed, which inverts the output of the *Arduino*. The schematics behind it can be seen in Fig. 4.20 .

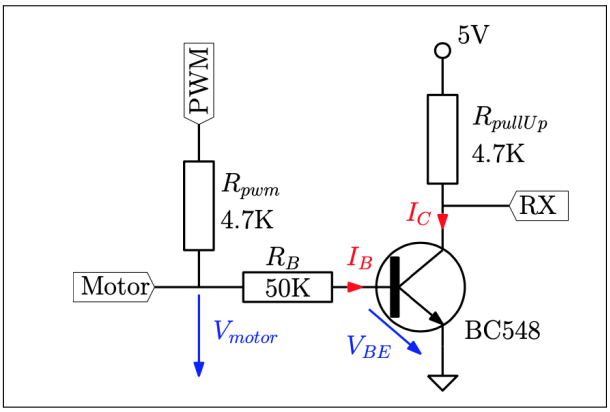


Figure 4.20: Input schematic for inverted serial communication [38]

4.3.3 Links and nodes

The *DLR* internal framework links and nodes is used to ensure the communication of the whole application. It has been developed to make it easier to deploy software into a robotic system. It facilitates communication between different processes and intercepts the different coding skills of different people. The framework allows two communications paradigms, a request-/response service and real-time signal publishing. The central component of the framework is the *ln_manager*, which provides information about all processes and communication structures. The structure of the subscribe and publish interaction in this framework can be seen in Fig. 4.21. The central component of the process of publishing and subscribing is the *ln_manager*, which provides information about all processes and communications structures. The framework manages different topics and services and enables communication between them to perform different tasks.

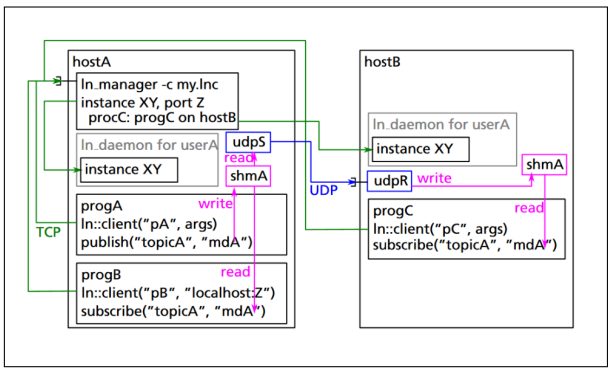


Figure 4.21: Structure of a publish and subscribe interaction in the LN-framework [57]

The integration of the motor control was achieved via the *lnrkmodule*, which allows the robot

kernel modules to run in the links and nodes framework. With this module, it is now possible to work within the frameworks with the telemetry data.

After the previous section discussed the control of the motors in detail, the connection of the mechanics with the control of the motors must now take place. These two aspects of the interface can be connected by means of kinematics. Thus the effect of a change in the motor angles on the degrees of freedom of the suturing instrument is modelled. These relations can be described by movement mapping. For modelling the interface as part of a robot, both the forward kinematics and the inverse kinematics are needed.

4.4 Forward kinematic

In order to control the suturing instrument and the interface in the *MiroSurge* system intuitively, it is essential to determine the forward kinematics of the interface and to determine the mapping of the motor degrees of freedom to the degrees of freedom of the instrument. The articulation mechanism of the instrument consists of links, that are bending the same amount when turning the articulation gear of the instrument. The structure of these links is shown in Fig. 4.22. The simplification was made, that all four articulation links were combined to one degree of freedom, called q_1.

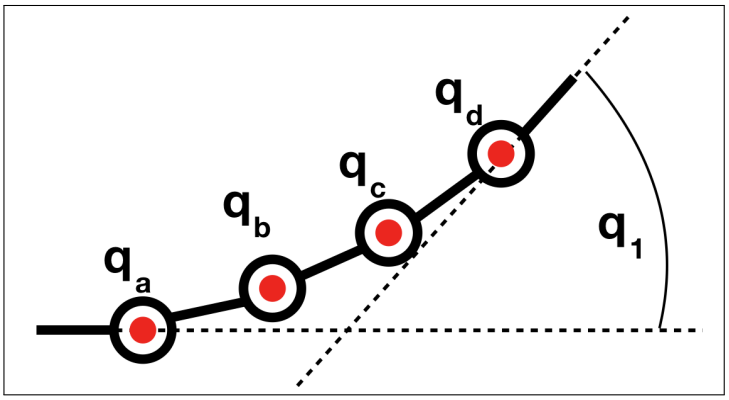
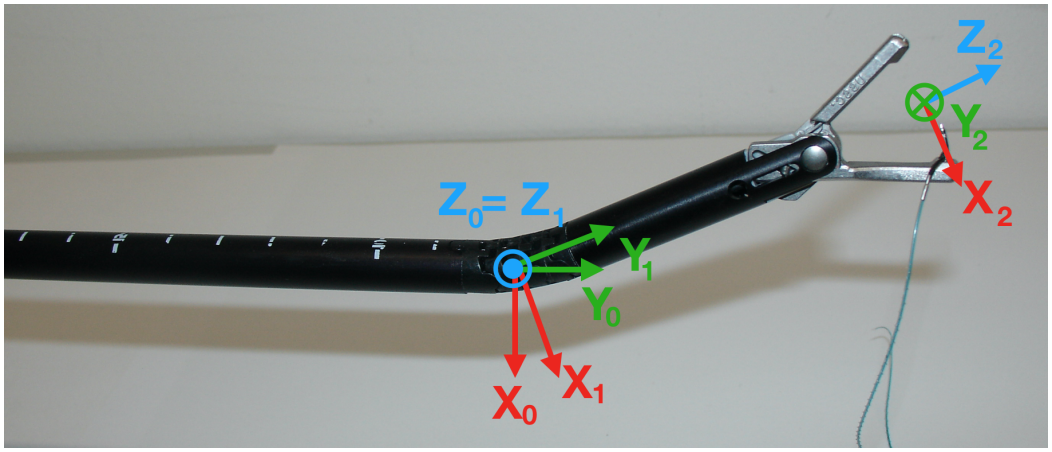


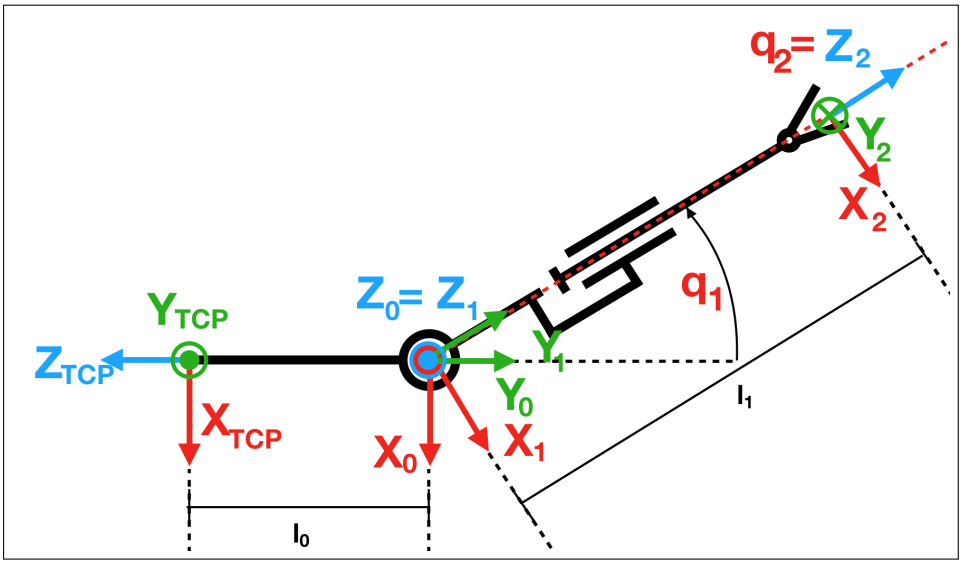
Figure 4.22: Schematic of the chained articulation links

For forward kinematics, the *Denavit-Hartenberg* parameters are determined from the interface coupling point to the tip of the instrument tool. Only two degrees of freedom of the instrument are relevant for the tip positioning because the end-effector coordinate system is placed between the two jaws of the instrument: the degree of freedom of rotation of the tip and the degree of freedom of articulation of the tip. The other two degrees of freedom are just relevant for the position of the needle, and this is neglected here. The sets of *Denavit-*

Hartenberg parameters are determined by the coordinate system configuration shown in Fig. 4.23.



(a) Postion of the coordinate systems



(b) Sketch of the tool tip with kinematic relations

Figure 4.23: Coordinate systems at the tool tip

The length l_0 ist the distance between the articulation axis Z_1 and the origin of the tool centre point coordinate system of the *MIRO*, as seen in Fig. 2.14. The length l_1 is the distance from the articulation axis Z_1 to the origin of the end effector coordinate system at the tooltip. The values for both lengths can be seen in table 4.1.

l_i	distance in mm
0	410
1	74

Table 4.1: Distances between the coordinate systems of the adapter

The transformation from the *MIRO* tool centre point coordinate system $(COS)_{TCP}$ to the coordinate system $(COS)_0$ is constant and is not depending on the articulation or rotation degree of freedom. So the homogeneous transformation matrix ${}^{0}_{TCP}\boldsymbol{T}$ can be expressed by:

$$ {}^{0}_{TCP}\boldsymbol{T} = \begin{pmatrix} 1 & 0 & 0 & 0 \\ 0 & \cos(-\frac{\pi}{2}) & -\sin(-\frac{\pi}{2}) & 0 \\ 0 & \sin(-\frac{\pi}{2}) & \cos(-\frac{\pi}{2}) & -l_0 \\ 0 & 0 & 0 & 1 \end{pmatrix} = \begin{pmatrix} 1 & 0 & 0 & 0 \\ 0 & 0 & 1 & 0 \\ 0 & -1 & 0 & -l_0 \\ 0 & 0 & 0 & 1 \end{pmatrix} \tag{4.3} $$

For the coordinate system configuration shown in Fig. 4.23 the *Denavit-Hartenberg* parameters can be seen in Tab. 4.2.

i	$a_{i-1}[mm]$	$\alpha_{i-1}[^\circ]$	$d_i[mm]$	$\Theta_i[^\circ]$
1	0	0	0	q_1
2	0	-90	l_1	q_2

Table 4.2: *Denavit-Hartenberg* parameter of the Interface

This parameter set results in the homogeneous transformation matrices ${}^{i+1}_{i}\boldsymbol{T}$ for the description of the instrument tip in the coordinate system of the end effector of the robot:

$$ {}^{1}_{0}T = \begin{pmatrix} \cos(q_1) & -\sin(q_1) & 0 & 0 \\ \sin(q_1) & \cos(q_1) & 0 & 0 \\ 0 & 0 & 1 & 0 \\ 0 & 0 & 0 & 1 \end{pmatrix} \tag{4.4} $$

$$ {}^{2}_{1}T = \begin{pmatrix} \cos(q_2) & -\sin(q_2) & 0 & 0 \\ 0 & 0 & 1 & l_1 \\ -\sin(q_2) & -\cos(q_2) & 0 & 0 \\ 0 & 0 & 0 & 1 \end{pmatrix} \tag{4.5} $$

Multiplying this results in the forward kinematc of the adapter ${}^{2}_{TCP}\boldsymbol{T}$:

$$ {}^{2}_{TCP}\boldsymbol{T} = {}^{0}_{TCP}T \cdot {}^{1}_{0}T \cdot {}^{2}_{1}T = $$

$$ \begin{pmatrix} \cos(q_1)\cos(q_2) & -\cos(q_1)\sin(q_2) & -\sin(q_1) & -\sin(q_1)l_1 \\ -\sin(q_2) & -\cos(q_2) & 0 & 0 \\ -\sin(q_1)\cos(q_2) & -\sin(q_1)\cos(q_2) & -\cos(q_1) & -\cos(q_1)l_1 - l_0 \\ 0 & 0 & 0 & 1 \end{pmatrix} \tag{4.6} $$

With the forward kinematics just determined, the position of the instrument tip in space can now be determined as a function of the joint angles of the robot and the instrument.

$$ {}^{2}_{base}\boldsymbol{T} = {}^{TCP}_{base}\boldsymbol{T} \cdot {}^{2}_{TCP}\boldsymbol{T} \tag{4.7} $$

Here the coordinate system $(COS)_2$ is the end effector system at the tooltip.

4.5 Inverse kinematic

The inverse kinematics of the kinematic chain are important for later control via the *MIRO* communication system. In this case, the joint values are calculated for a given position and orientation of the end effector:

$$ \boldsymbol{q} = \boldsymbol{g}(\boldsymbol{x}_E). \tag{4.8} $$

In the case of quite simple kinematics with only two degrees of freedom, the inverse problem (detached from the rest of the robot) can be solved geometrically. The geometric relations of the instrument can be seen in Fig. 4.23b.
In this configuration, the six degrees of freedom of the end effector can be represented as follows:

$$ {}_{(0)}\boldsymbol{x}_E = \begin{pmatrix} x_E \\ y_E \\ z_E \\ \alpha_E \\ \beta_E \\ \gamma_E \end{pmatrix} = \begin{pmatrix} l_0 + l_1\cos(q_1) \\ l_1\sin(q_1) \\ 0 \\ 0 \\ q_1 \\ q_2 \end{pmatrix} \tag{4.9} $$

To determine the joint angles $\boldsymbol{q}$ depending on the end effector degrees of freedom $\boldsymbol{x}_E$, the first and sixth lines of the equation 4.9 are converted:

$$q_1 = arccos(\frac{x_E - l_3}{l_2}) \tag{4.10}$$

$$q_2 = \gamma_E \tag{4.11}$$

Thus the inverse kinematics of the end effector was determined:

$$\boldsymbol{q} = \begin{pmatrix} q_1 \\ q_2 \end{pmatrix} = \boldsymbol{g}(\boldsymbol{x}_E) = \begin{bmatrix} arccos(x_E - l_3) \\ \gamma_E \end{bmatrix} \tag{4.12}$$

4.6 Movement mapping

In addition to the kinematics, the mapping of the motor degrees of freedom to the actual degrees of freedom of the suturing device also plays an important role. In the following, the function $\boldsymbol{f}$ is derived that represents each degree of freedom q_i of the suturing device as a function of the motor angle ϕ_i.

$$\boldsymbol{q} = \boldsymbol{f}(\boldsymbol{\phi}) \tag{4.13}$$

The rotation of the tool tip has a one to one transmission ratio to the blue rotation wheel at the shaft end. Since this wheel is driven via two gears with the transmission ratio $i_{rotation} = 0.31$, the following correlation between the angle $\phi_{rotation}$ of the motor in degrees and the rotation $q_{rotation}$ of the tool tip in degrees results:

$$q_{rotation}(\phi_{rotation}) = c + i_{rotation} \cdot \phi_{rotation} \tag{4.14}$$

If one assumes that the gripper is also in zero position when the motor is in zero position, the constant c is omitted and the mapping is simplified:

$$q_{rotation}(\phi_{rotation}) = i_{rotation} \cdot \phi_{rotation} \tag{4.15}$$

$$q_{rotation}(\phi_{rotation}) = 0.31 \cdot \phi_{rotation} \tag{4.16}$$

Since the rotation does not have an end position, there are no limits for the motor angle, so these are set in such a way that they guarantee a full rotation of the tool tip:

$$0 \leq \phi_{rotation} \leq \frac{360\circ}{i_{rotation}} \approx 1166^\circ \tag{4.17}$$

So the motor has to rotate about 3.2 revolutions to let the tooltip rotate once around itself. In the zero position, the writing "*Covidien*" on the instrument tip points straight in the top direction of the suturing device (the side, die print "*Covidien SILS Stitch"* is on). The range of $1166°$ is no problem for the servo motor, cause it can rotate more than three revolutions.

The gear for the degree of freedom for the angular deflection has two gear steps with two ratios. On the one hand the ratio between the two printed gears $i_{articulation,1} = 0.85$ and on the other hand the ratio between the flexible gear and the light blue one of the instrument $i_{articulation,2} = 1$. So there is a total ratio for this gear stage of

$$i_{articulation} = i_{articulation,1} \cdot i_{articulation,2} = 0.85 \cdot 1 = 0.85. \tag{4.18}$$

In order to bring the tool tip from its starting position (6° angle) to its stop position (66° angle), the light blue gearwheel must be rotated three quarters of a turn, 270°. Every degree that the gear wheel rotates, the tip is rotated by approximately $\frac{60°}{270°} = 0.222$. Calculated with the gear ratio, the function between the motor angle $\phi_{articulation}$ and the tip angle $q_{articulation}$ is:

$$q_{articulation}(\phi_{articulation}) = 6° + 0.222 \cdot \frac{1}{i_{articulation}} \cdot \phi_{articulation} \tag{4.19}$$

$$q_{articulation}(\phi_{articulation}) = 6° + 0.189 \cdot \phi_{articulation} \tag{4.20}$$

Since the tooltip has two extreme positions beyond which it cannot go, the angles of the motor must also be limited so that they do not bring the tooltip beyond these values.
For $q_{articulation} = 6°$ and for $q_{articulation} = 66°$ the following values result for $\phi_{articulation}$:

$$6° = 6° + 0.261 \cdot \phi_{articulation} \Leftrightarrow \phi_{articulation} = 0° \tag{4.21}$$

$$66° = 6° + 0.261 \cdot \phi_{articulation} \Leftrightarrow \phi_{articulation} \approx 230° \tag{4.22}$$

This results in the following interval for $\phi_{articulation}$:

$$0° \leq \phi_{articulation} \leq 230° \tag{4.23}$$

The motor must move from its neutral zero position by approximately 38° to trigger the closing mechanism of the gripper. Besides the closed and open position, the gripper needs the middle positions to grasp the tissue for manipulating it. This is not a fixed motor position but depends on the thickness of the tissue. These positions are interpolated between the to

fixed positions:

$$\phi_{gripper} = \begin{cases} 0°, & \text{if gripper is opened} \\ 38°, & \text{if gripper is closed} \end{cases} \tag{4.24}$$

For the last degree of freedom, i.e. the switching of the swivelling lever, only the two extreme positions and a neutral position are needed. In the neutral position, the swivelling bracket is located below the swivelling lever at 0°, and they are parallel to each other. To put the swivelling lever in one end position, that is 25° rotated from the neutral position, the motor has to rotate 15°. In the other direction, corresponding values are obtained, only with the sign reversed.
This results in the following approximately linear mapping of the motor angle $\phi_{swivelling}$ to the degree of freedom $q_{swivelling}$:

$$q_{swiveling}(\phi_{swivelling}) = m \cdot \phi_{swivelling}, \tag{4.25}$$

with $m = 1.67$. This connection is not exact for the whole trajectory, since there is play outside the touch positions. However only the following values are relevant for the function of the interface device:

$$q_{swivelling}(0) = 0° \tag{4.26}$$
$$q_{swivelling}(15°) = 25° \tag{4.27}$$
$$q_{swivelling}(-15°) = -25° \tag{4.28}$$
$$\tag{4.29}$$

The total mapping between motor angles $\boldsymbol{\phi}$ and the joint angle degree of freedom $\boldsymbol{q}$ therefore is:

$$\boldsymbol{q}(\boldsymbol{\phi}) = \begin{pmatrix} q_{rotation}(\phi_{rotation}) \\ q_{articulation}(\phi_{articulation}) \\ q_{gripper}(\phi_{gripper}) \\ q_{swiveling}(\phi_{swivelling}) \end{pmatrix} = \begin{pmatrix} 0.309 \cdot \phi_{rotation} \\ 6° + 0.261 \cdot \phi_{articulation} \\ [0, 38] \\ [-15, 0, 15] \end{pmatrix} \tag{4.30}$$

4.7 Human machine interface

In order to integrate the suturing instrument into the *MiroSurge* platform, the motors and the associated *Arduino* microcontrollers must be controlled via *DLR's* robotkernel. Within this structure, however, other human machine interfaces can also be implemented. The control

via a 3D mouse serves as a preliminary stage for the complete integration into the *MiroSurge* system, which would go beyond the scope of this work. A *Spacemouse Compact* [*3Dconnexion*, Munich, Germany], as shown in Fig 4.24, is used for this work. The *Spacemouse Compact* controls both the degree of freedom for rotation and the degree of freedom for bending freedom and triggers the suturing process.



Figure 4.24: *Spacemouse Compact* [58]

The advantage of the *Spacemouse Compact* is the intuitive control of the degrees of freedom by tilting or rotating the mouse. A finite state machine was developed to model the suturing process as soon as the trigger button on the *Spacemouse* is pressed. This requires the four state variables *motor speed of the gripper mechanism* $v_{gripper}$, *motor position of the gripper mechanism* $x_{gripper}$, *motor speed of the swivelling mechanism* $v_{swivelling}$ and *motor position of the swivelling mechanism* $x_{swivelling}$. Each of these variables has three states for modelling, as shown in table 4.3.

state	-1	0	1
$v_{gripper}$	gripper is closing	gripper doesn't move	gripper is opening
$x_{gripper}$	gripper is completely open	gripper is not completely open or closed	gripper is closed
$v_{swiveling}$	swivelling lever is moving clockwise	swivelling lever is not moving	swivelling lever is moving counterclockwise
$x_{swiveling}$	swivelling lever is in the left position	swivelling lever is not left or right	swivelling lever is on the right position

Table 4.3: States of the variables

For each combination of these four variables, it is now defined how the two motors are to be controlled. The two motor speed variable are asigned to the combination of the four state variables:

$$[v_{gripper}, v_{swiveling}] = f(v_{gripper}, x_{gripper}, v_{swiveling}, x_{swiveling}) \tag{4.31}$$

In order to determine an assignment, all possible states of the suturing process must first be broken down:

- The order for doing one suture is given. The gripping mechanism does not move, the gripper is open, the changing mechanism is stationary and is in either the left or right position.
- The gripping mechanism is just starting to close, but the gripper is still open, the changing mechanism is stationary and is in either the right or left position.
- The gripping mechanism closes, has reached the closed straight position and the changing mechanism stands still and is in either the right or left position.
- The gripping mechanism stands still, the position is closed, the changing mechanism stands still and is in either the right or left position
- The gripping mechanism stands still, the position is closed, the changing mechanism starts to move, but is still in its initial position (right or left)
- The gripping mechanism stands still, the position is closed, the changing mechanism moves, the bracket is somewhere in the middle between the two initial positions

- The gripping mechanism stands still, the position is closed, the changing mechanism moves, the bracket has reached the end position (right or left)
- The gripping mechanism stands still, the position is closed, the changing mechanism no longer moves, the bracket is in end position (right or left)
- The gripping mechanism opens, the position is closed, the changing mechanism stands still and is in the position right or left
- The gripping mechanism opens, the position is neither closed nor open, the change mechanism stands still and is in the position right or left
- The gripping mechanism opens, the position is open, the changing mechanism stands still and is in the position right or left
- The gripping mechanism stands still, the position is open, the changing mechanism stands still and is in the position right or left (opposite of the first state)

Each of these states can now be assigned a subsequent state.

By pressing the mouse button an additional variable *in_progress* is set *True*, which ensures that during the whole suturing process the finite state machine is under control and a new pressing of the mouse button has no effect. Only after completion of the suturing process the variable *in_progess* is set to *False* again so that a new suturing step can be executed. If the mechanism is blocked and one state is to long active, the suturing process should be terminated.
All possible assignments (table A.3) as well as the source code for the control (A.13) can be found in the appendix.

4.8 Summary

The suturing instrument *SILS Stich* was chosen because of its advantages over competing products for integration into the *MiroSurge* system. In the course of this chapter, a first prototype was designed mechanically, and a control concept for the servo motors used for this application was presented. After the mechanical modelling and the electronic control were discussed, the interface was modelled by means of forward kinematics, inverse kinematics and movement mapping of the motor degrees of freedom. This chapter then introduced a *Spacemouse* as human machine interface. Thus a functional and controllable prototype could be designed.

5 Experiments and evaluation

5.1 Criteria of a successful integration

Successful integration of the suturing instrument includes two aspects: On one hand, the tip must be positioned precisely to ensure that the suturing instrument can be used sensibly on the robot. For this, the two degrees of freedom of rotation and articulation are essential, because these two have a direct influence on the position of the instrument tip in relation to the robot base (compare section 4.4). On the other hand, the actuated instrument must be able to create sutures and to deal with tissue resistance. For this, the interaction of the two degrees of freedom for the grip actuation and for changing the locking mechanism is essential.
With the functional prototype described in section 4 both indicators of success can be measured and the advantages of robot-assisted suturing can be demonstrated. Therefore a complete adapter was built, as shown in Fig 5.1.

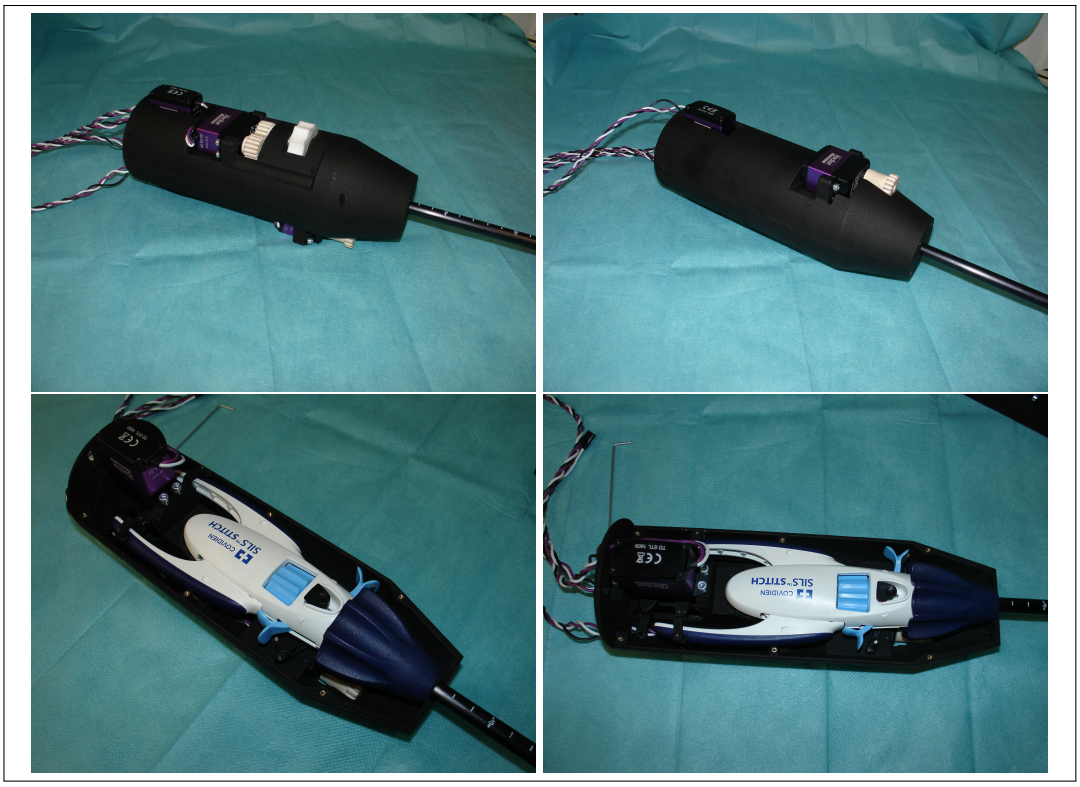
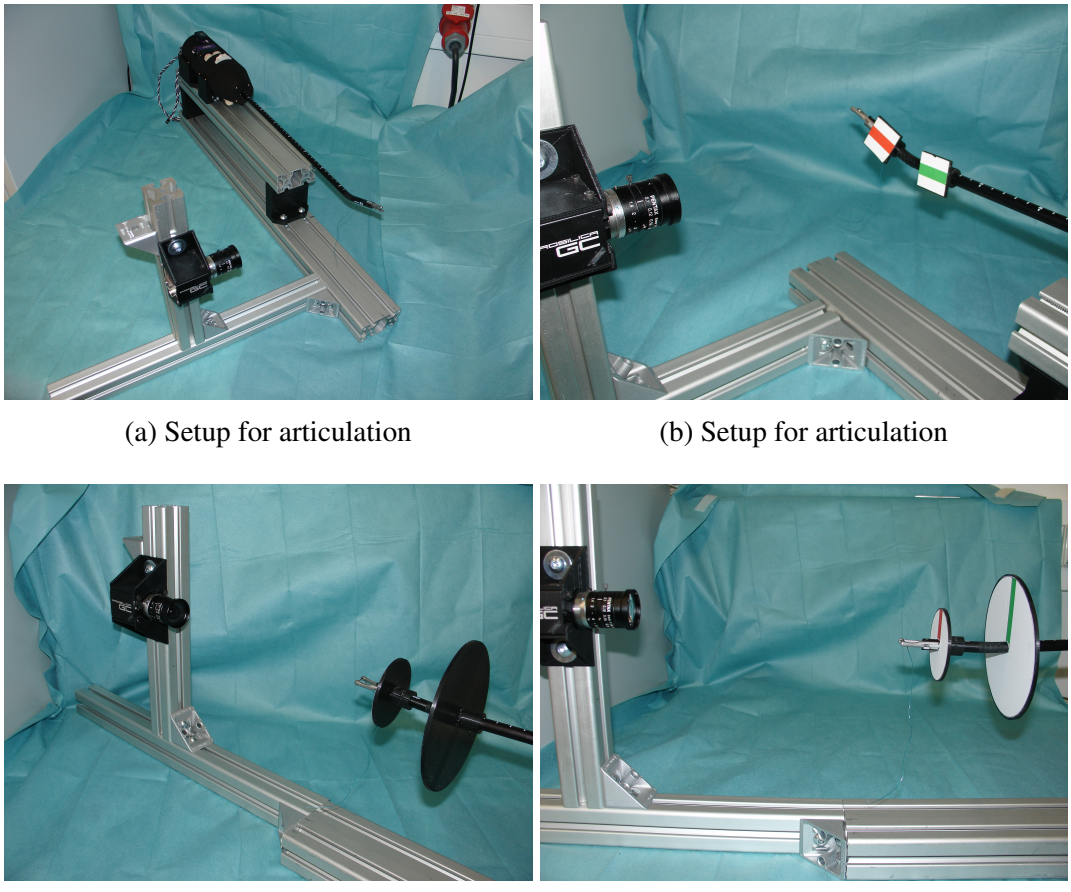


Figure 5.1: Prototype of the adapter

In the following, these two indicators for successful integration of the instrument are considered and evaluated in two different test setups.

5.2 Test bed for tip-positioning

For the positioning of the instrument tip, a testbed was set up on which the instrument and the adapter were clamped. A camera was rigidly connected to the mounting of the interface, and its camera lens was aligned so that the camera could see the tip from the required angle to measure either the rotation (see Fig. 5.2c and 5.2d) or the articulation (see Fig. 5.2a and 5.2b) of the instrument. For each of the two degrees of freedom, the experimental setup was slightly modified, see subsection 5.2.1 and 5.2.2 for more details.



(a) Setup for articulation

(b) Setup for articulation

(c) Setup for rotation

(d) Setup for rotation

Figure 5.2: Testbed for locating the tip position

5.2.1 Test setup 1.1: Rotation

In order to measure the rotation of the instrument tip, the camera was aligned with the axis of the instrument tip so that it looks at the instrument frontally. The articulation angle of the instrument is kept constant at 6° during the entire experiment. A clamp with a marker was placed on each of the two moving parts of the shaft. The markers are coloured stripes which can be segmented by means of image processing.

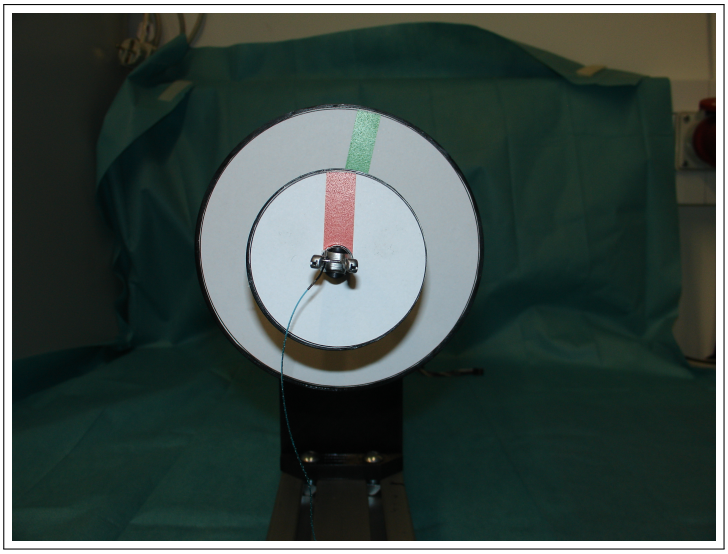
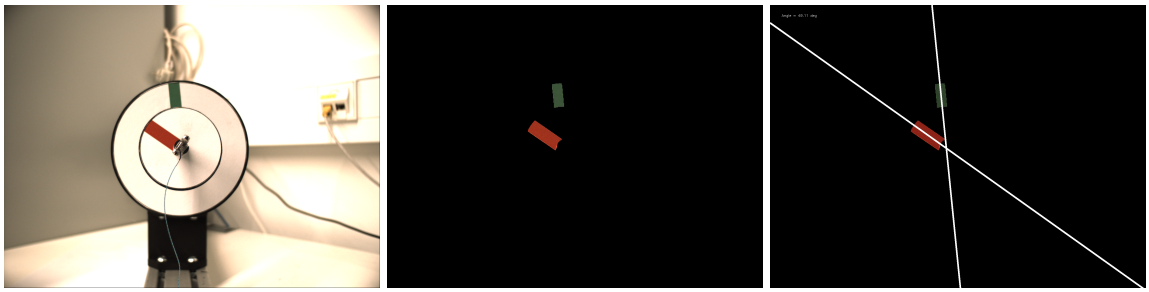


Figure 5.3: Marker for tracking the rotation

Data processing

In each image taken by the camera, the two differently coloured markers are visible. The colour image of the camera is first transformed into the HSV space. The HSV space does not assign values for red, green and blue to pixels, as the RGB space does, but the colours are described by the three components hue (h), saturation (s) and value (v). In this colourspace, pixels in a certain colour range can easily and robustly be segmented much easier via the value h. For more details about the HSV space see appendix A.9. To select the marker in HSV space, all pixels in the red colour spectrum are selected once and all pixels in the green colour spectrum once. After the point clouds of the coloured pixels have been segmented, a principal component analysis is used to determine the two principal axes. Subsequently, the angle between the two largest principal axes was calculated (see section A.10), as this indicates the rotation of the two markers in relation to each other. The source code for the image processing can be found in appendix A.11.



(a) raw image of the marker (b) segmentated pointclouds (c) principal axes of the markers

Figure 5.4: Calculating the rotation angle between the markers

Implementation

For the execution of the experiment, certain angles for the rotation of the tip were chosen which the motor should run into. Since the working range of the rotation covers 360°, the complete working area was traversed in 2° steps, in the aggregate 160 steps. In order to detect hysteresis and backlash, after the movement from 0° to 360° the complete movement was carried out backwards. In the second part of this experiment, the motor, therefore, moved in 2° steps in the working range from 360° to 0°. In order to test the reproducibility of the degree of freedom of the rotation, the described measurement was carried out five times. The instrument was then removed and reinstalled, and a further five runs were measured. The actual angle was determined by the procedure presented in section 5.2.1, the nominal angle by the movement mapping presented in section 4.6. The source code for this measurement series can be found in A.12.

Evaluation

The nominal and actual angles were now plotted against each other to show the behaviour of this degree of freedom. The results can be seen in Fig. 5.5. The blue line is the bisector of the angle and represents a perfect mapping between the nominal angle and the measured angle. The first five measurements are shown in green; the measurements after removal and reinstallation are shown in red.

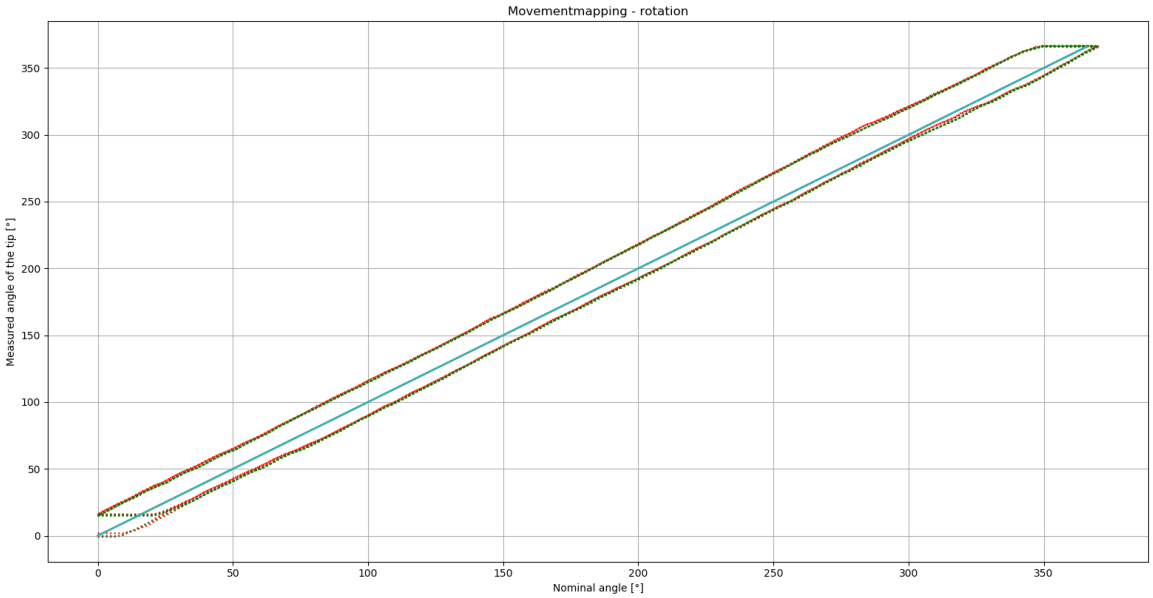


Figure 5.5: Relation between the actual and the rotation nominal angle

It can be seen that the behaviour of the control of this degree of freedom is linear, but has a hysteresis. While in the first part of the experiment the measured position is about 8° below the bisector of the angle and thus below the desired value, the measured value on the way back of the movement is about 16° above it. The deviation from the desired position is up to 25°, depending on the direction from which it is approached. However, this has remained constant over all experiments and even after removal and reinstallation of the instrument, the same behaviour was obtained.

5.2.2 Test setup 1.2: Artikulation

The second test setup is very similarly structured. Only the camera is positioned so that it does not look at the instrument tip from the front but from the side. So it can take pictures in which the angle of articulation can be measured. For the measurement of the articulation, also other markers are needed. They have been modified so that they can be tracked from the new camera position, see figure 5.6. During the whole experiment, the angle of rotation remains constant at 0°.

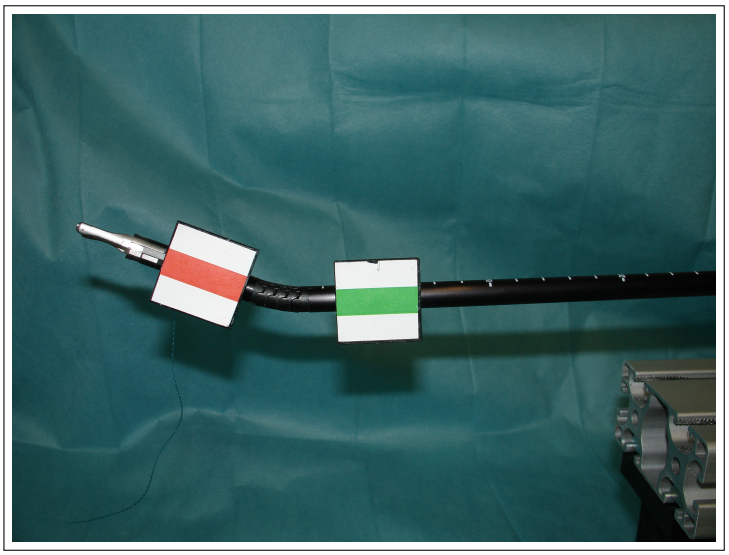
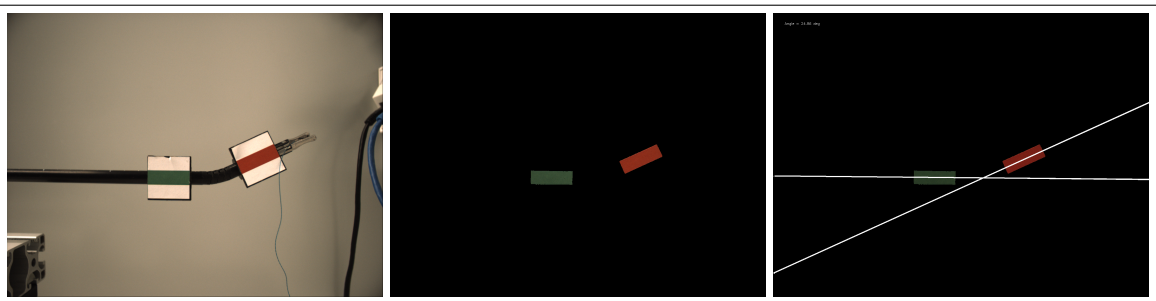


Figure 5.6: Marker for tracking the articulation

Data processing

The data processing of this test is identical to the procedure described in section 5.2.1.



(a) raw image of the marker (b) segmentated pointclouds (c) principal axes of the markers

Figure 5.7: Calculating the articulation angle between the markers

Implementation

In this test series, the motor responsible for articulation is controlled and not the motor responsible for the rotation of the instrument tip. The behaviour is to be measured over the entire working area, so the articulation goes from 6° to 66°. In order to completely cover the entire range of motion of the degree of freedom and also to check for hysteresis or backlash, the entire range of motion is traversed in 0.4° steps and then retracted again. The whole measurement was repeated five times. The instrument was then removed from the adapter,

reinstalled and measured five additional times to check whether the movement behaviour is reproducible. The actual angle was determined by the procedure presented in section 5.2.1, the nominal angle by the movement mapping presented in section 4.6. The source code for this measurement series can be found in A.12.

Evaluation

The nominal and measured angles were now plotted against each other to show the behaviour of this degree of freedom. The results can be seen in Fig. 5.8. The blue line is the bisector of the angle and represents a perfect mapping between the motor angle and the measured angle. The first five measurements are shown in green; the measurements after removal and reinstallation are shown in red.

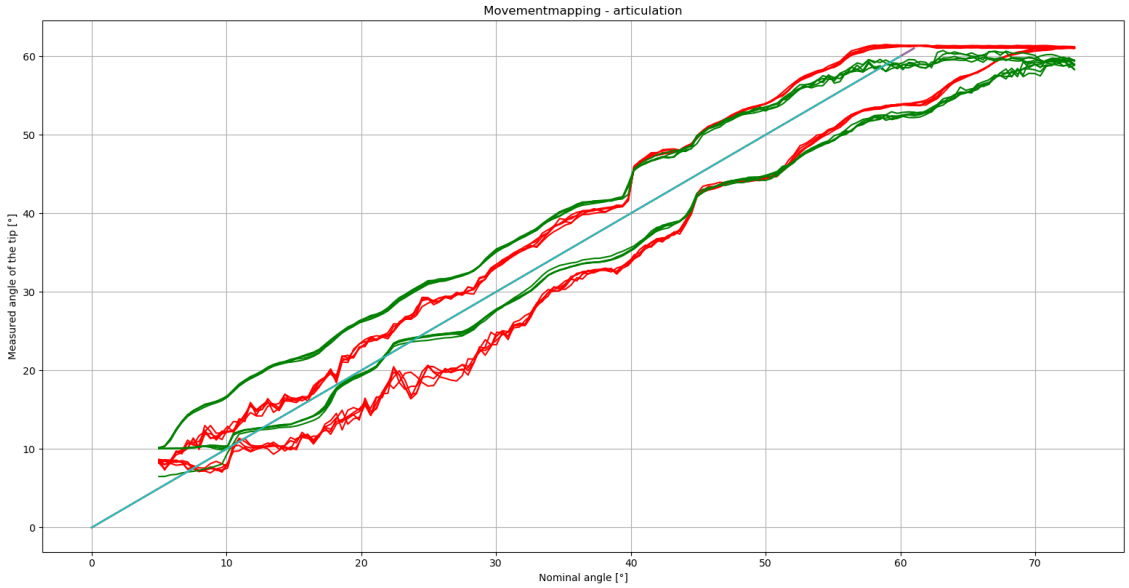


Figure 5.8: Relation between the actual and the nominal articulation angle

In Fig. 5.8, several results can be clearly seen: On the one hand, a hysteresis is recognizable. While increasing the articulation, the measured angle is about 6° below the angle bisector, while on the way back, the measured angle is about 6° above the angle bisector. The deviation of the controlled angle can, therefore, be 12°, depending on the direction from which the position is approached. In addition to the hysteresis, non-linear behaviour can also be detected. Plateaus are formed which are interrupted by sections of a steep gradient. These are caused by the elastic form closure of the articulation gear. The third phenomenon that can be seen in the diagram is the discrepancy of the measured values after the removal and installation of the instrument. While the five measurements before and after disassembly

and reassembly show similar behaviour, the measurements differ between the groups. This phenomenon is caused by the position of the two articulation gears in relation to each other when the instrument is installed.
With a lever arm of 74 mm (see Fig. 4.1) and an angular inaccuracy of about 6°, the position accuracy would, therefore, be about 8 mm.

5.3 Hands-on mode on the MIRO

In the second test, the workflow of use of the tool should be simulated, and the usability of the adapter should be checked. For this again, two partial tests are accomplished. The first part deals with the commissioning of the adapter. In the second part, the hands-on mode of the adapter shall be tested at the *MIRO*, as well as suturing.

5.3.1 Test setup 2.1: Commissioning of the adapter

The commissioning of the adapter is the process from unpacking the suturing instrument from the packaging to mounting the adapter on the *MIRO*. This would be carried out by the medical staff during operation and is always necessary if a suturing instrument is to be used or changed.

Implementation

As explained in 4.2.6, several assembly steps must be carried out for commissioning. Commissioning can be divided into four steps:

1. Attachment of the rotation adapter to the suturing instrument
2. Inserting the suturing instrument in the lower shell of the housing
3. Screw the upper shell of the housing onto the lower shell of the housing
4. Screw the magnetic mounting on both shells

In order to assess the feasibility of the process with regard to the time of commissioning in the operation scenario, the suturing instrument was built into the adapter five times and removed again. The times for each substep were measured and averaged.

Evaluation

Both the assembling of the adapter and the disassembling were performed five times and the times of the intermediate steps were measured and averaged.

substep	Duration [s]					Mean duration	Standard deviation [s]
1	7	6	5	5	6	5.8	0.75
2	9	8	14	6	7	8.8	2.79
3	73	80	61	63	69	69.2	6.88
4	59	75	63	64	51	62.4	7.79
all	148	169	143	138	133	146.2	12.45

Table 5.1: Duration of Assembling the adapter

substep	Duration [s]					Mean duration [s]	Standard deviation [s]
1	5	4	4	4	4	4.2	0.4
2	6	4	6	5	4	5	0.89
3	71	41	44	41	42	47.8	11.65
4	31	27	29	24	31	38.4	2.65
all	113	76	83	84	81	87.4	14.18

Table 5.2: Duration of disassembling the adapter

As shown in the table 5.1 and 5.2, the most time-consuming steps are screwing the two halves of the housing together and screw the magnetic adapter. For faster commissioning, these two steps would have to be optimized, while the other two steps are of little importance.
One possible optimization of the third step would be to switch from screws to quick-release fasteners. The fourth step would be completely omitted if instead of the *MICA* magnet mounting a modified variant was used which consists of two parts and could already be screwed onto the housing halves during the assembly (see appendix A.6) of the adapter and not during every commissioning.

5.3.2 Test setup 2.2: Suturing

In addition to the easy and fast commissioning of the interface, suturing is essential for a surgical suturing instrument. To be able to evaluate this process qualitatively, a test setup with the *MiroSurge* system was set up. This will be used as an example to test the usability of the adapter. The aim of this experiment is no quantitative key features, but the qualitative impression of the performer.

Test setup

First, the weight and the position of the centre of gravity were entered into the control of the *MIRO*, then the adapter was attached to the robot by means of the magnetic mounting.

An artificial tissue sample was positioned on the operating table so that the suturing process could be tested.

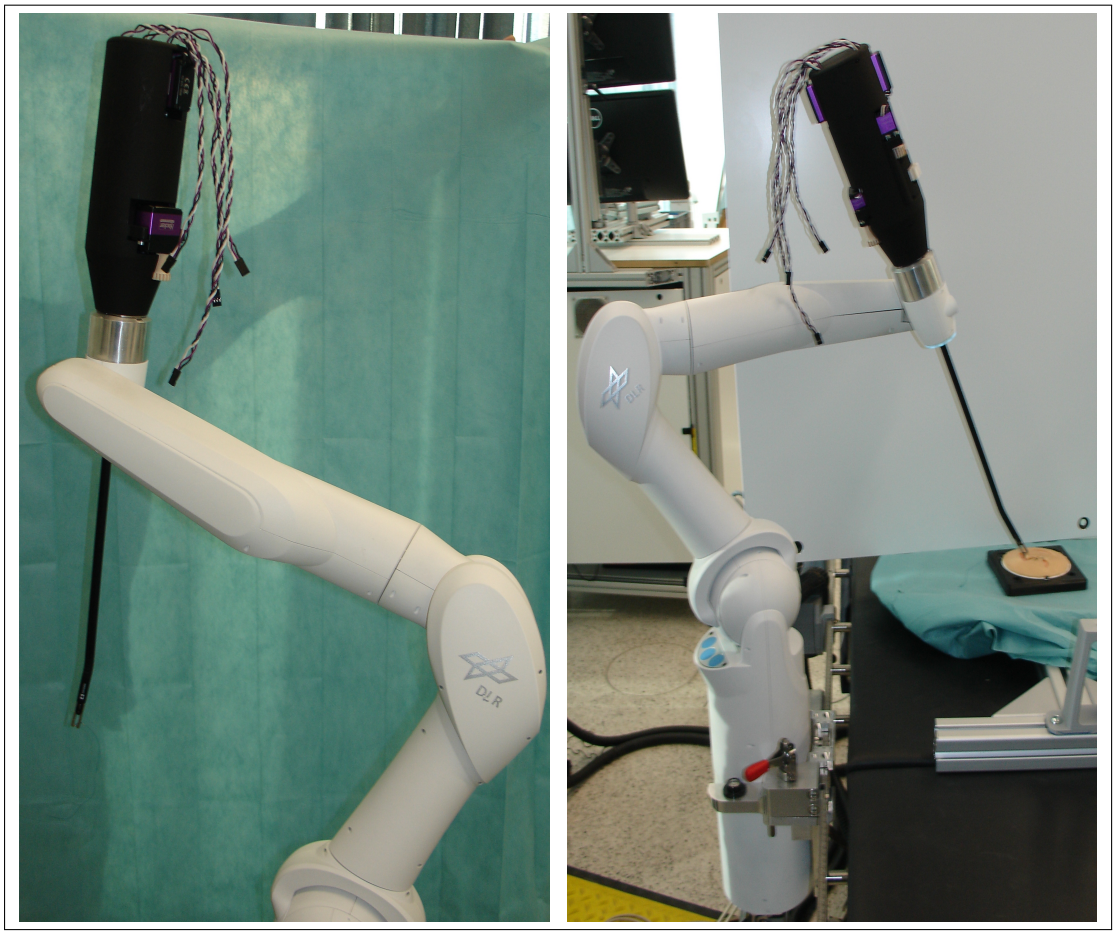


Figure 5.9: Test setup with the *MIRO*

Implementation

In gravitational compensation mode, the robot together with the adapter and suturing instrument, could be operated stably in hands-on mode. Now the *Spacemouse* presented in section 4.7 was used to perform various stitches on the tissue sample. For this purpose, the robot, together with the adapter, was brought into a position by hand so that the tissue is in the middle of the gripper. The positions of the gripper can be seen in Fig. 5.10.

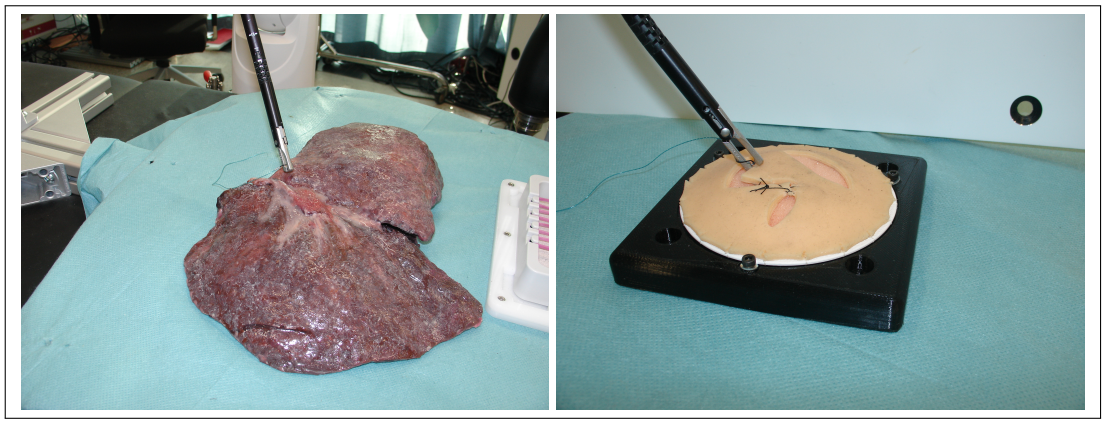


Figure 5.10: Performing a suture with hands-on mode

Evaluation

The suturing tests with the adapter were not successful. By triggering the process via the *Spacemouse*, the suturing process was not reliably controlled, so that the needle did not change its position in the gripper. This was because the handle holder pulling the handles inwards to actuate the gripper mechanism could not always apply enough friction to keep the handles closed. So the handle holder partially slipped and the handle opened again before the swivelling mechanism could change the needle. This led to a very unreliable execution of the suturing process.
In order to successfully actuate this mechanism, the design of the handle holder should be changed so that either significantly more friction occurs and the handles remains closed, or a form closure connection should be designed.
Even though this test was not successful, it showed that the principle could work if these facts are optimized.

5.4 Summary

In this chapter, several attempts were made to evaluate different aspects of the adapter of a suturing instrument. The position precision and repeatability of the two degrees of freedom for the rotation and articulation of the instrument tip were tested. In addition, the workflow was tested by a time evaluation of the commissioning process and by suturing tests. While the first three tests were successful and pointed to a possible integration into the *MiroSurge* system and an operation scenario, the last test, the execution of the suturing process on artificial tissue, showed the weaknesses of the prototype.

6 Future work

In this thesis, a functional interface of a suturing instrument for the *MIRO* was developed. Since this was however, only the first iteration stage of a development process, there are many possibilities to improve it further. As mentioned in 5.4 the interface is functional, but not yet very well-developed. To fix this, a further iteration stage of the prototype has to be done, which eliminates the weaknesses of the current adapter. The handle holders have to be improved to exert more friction or enables form closure. Additionally, the whole adapter should be a little bigger so that the jaws can be opened completely in a relaxed state, and thicker tissue can be sutured. Furthermore, as already mentioned at the end of chapter 3, a device for fixing a plastic cover for the interface should be planned, or a solution should be found in which the motors are not firmly screwed together, but can be released quickly and easily from the adapter shells. Another improvement, which was not critical for the proof of concept, but is important for the ergonomics of the application in the operating scenario, is the modification of the connection between the two halves of the housing. These are currently screwed together with four M 1.6 x 8 screws. This is a secure connection, but not optimal for mounting and commissioning the device. For this purpose, a quick-release fastener should be designed which can be closed and opened in a few simple steps and without additional tools.

In addition to the further mechanical development of the adapter, the instrument must also be completely integrated into the *MiroSuge* system. At present, the control of the degrees of freedom is separated from the control of the robot but runs via the same communication structure. The degrees of freedom of the instrument can be controlled via a *Spacemouse Compact*, while the robot is controlled via the control panel. All instrument degrees of freedom should also be controlled via the control console so that the interface can be controlled as a fully integrated instrument of the *MIRO*.

If the interface is mechanically more well-developed and wholly integrated into the *MiroSurge* communication structure, further attempts will be made to evaluate the quality of the integration. In addition to positional accuracy, it is important to be able to evaluate the suturing process itself quantitatively. For example, the time of a robot-assisted suturing process could be compared with that of a minimally invasive suturing process. In addition, these tests should be carried out by trained medical personal who already have experience in the field of minimally invasive suturing and can therefore also make statements about the improved

ergonomics. These test series should also be larger, contain more tests and thus provide validated statements about the suturing process that are not so strongly influenced by individual persons or scenarios.

Another way to advance the development of minimally invasive, robot-assisted suturing is the complete development of a stand-alone device that enables suturing. For this purpose, commercially available suturing instruments should be completely dispensed. This would have the advantage that the degrees of freedom, which were designed to be quickly and easily controlled by hand, can be much smaller and more precisely actuated via other mechanisms. As in Fig. 6.1 shown, the suturing instrument was taken apart completely to understand the mechanisms of the instrument. It is noticeable that, for example, the closing mechanism (number 4 in the figure), which is triggered by the compression of the handles, could be controlled internally by a comparatively small contraction of a spring. Similarly, the replacement of the light blue articulation gear by an involute toothed gear would result in significantly more precession and significantly fewer hysteresis (number 3 in the figure). The actuation of the swivelling mechanism could be replaced by push the two rods back and forwards (number 1 in the figure).
Should the path be taken that an instrument should be completely redesigned, however, possibilities of sterilization would have to be found for this, since this concept does not work with disposal products.

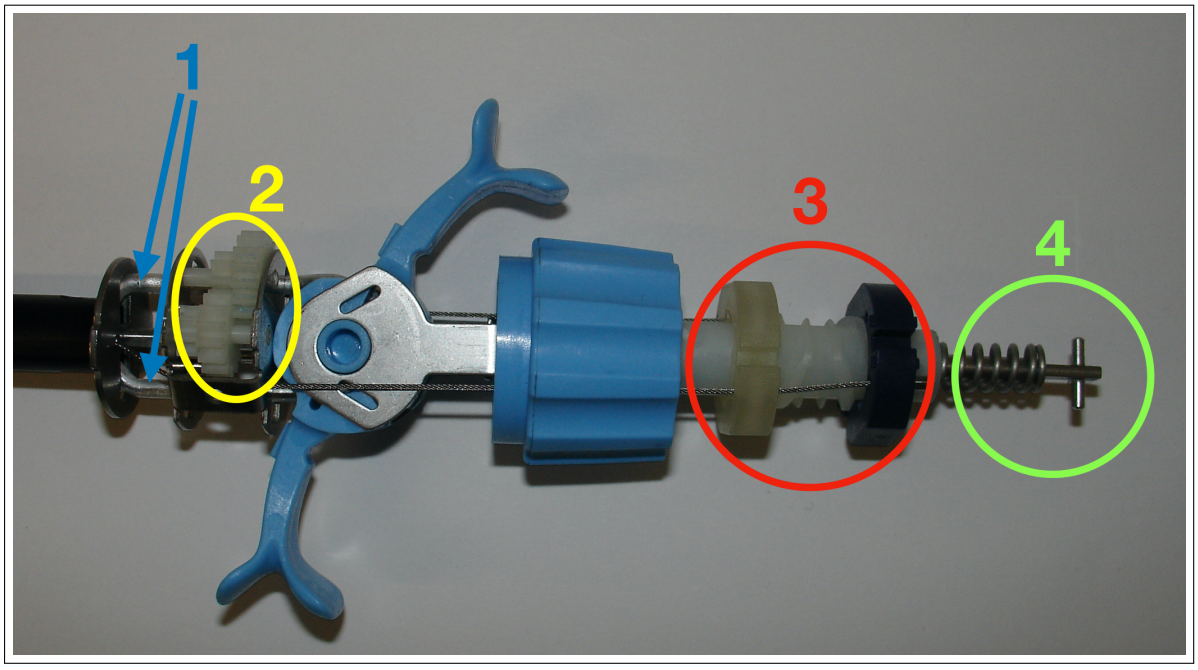


Figure 6.1: Disassembled suturing instrument

7 Discussion

With the success of robot-assisted surgery in surgery, many surgical techniques were improved and optimized for surgical robots. However, the process of automatic surgical suturing is still extremely time-consuming and cumbersome to perform with assistant robotics. To improve this, this work presents an adapter that integrates a commercially available medical suturing instrument into the surgical robot platform *MiroSurge*. As mentioned in chapter 3 and appendix A.2, both the adapter and the selected suturing instrument must fulfil various requirements. In this thesis, it was tried to fulfil as many of these requirements as possible or to present concepts how these can be fulfilled in later iterations.
Thus all requirements to the size and the maximum weight were fulfilled.
The presented adapter fulfil the requirement that all relevant degrees of freedom have been actuated. However, the suturing process, as described in 5.3.2, does not work reliably, because the handles of the instrument sometimes slip along the handle holders. The degrees of freedom for articulation and rotation of the instrument tip were also tested, with the result that hysteresis can be detected in their control.
Another requirement that the adapter must meet is sterility during surgery. This has not yet been achieved with the first prototype, but the work presents concepts on how this can be achieved in another iteration of the prototype (see 4.2.5). The sterility can be achieved by packaging of the adapter in the plastic sheathing.
The workflow in the use of the adapter and the suturing instrument was simulated and checked for applicability.
Overall, the concept of adapting a suturing instrument to the *MiroSurge* system has been successfully proven, and many suggestions for future improvements were made for further development of the adapter. In the future, it will be possible to create a fully functional adapter that significantly simplifies and accelerates automatic suturing in minimally invasive, robot-assisted surgery by applying the sterility concept and improving the guidance of the handles by the handle holders.

A Appendix

List of contents - appendix

A.1 Kinematic basics **71**
A.1.1 Homogeneous transformations 71
A.1.2 Robot kinematics 73
A.1.3 Summary 78
A.2 List of Requirements **79**
A.3 Designation of the instrument parts **81**
A.4 Part list **82**
A.5 Technical drawings **85**
A.6 Assembly instruction **86**
A.7 Specification DITEX 1609S **87**
A.8 States of the suturing finite state machine **88**
A.9 HSV representaion **90**
A.10 Principal component analysis **92**
A.11 Source code of the tip-tracking **93**
A.12 Source code of the test procedure **97**
A.13 Source code of the 3D mouse control **100**

A.1 Kinematic basics

Besides the knowledge of the technical and medical fundamentals, mathematical fundamentals are of great importance if a functional interface is not only to be designed but also modelled and integrated into a robot system. In the following, the homogeneous transformations will be discussed first to change from one coordinate system to another, which is essential to describe points in body-fixed systems. After this topic has been presented separately from the robot context, the area of application in this context will be discussed. Robot kinematics, in general, will be introduced, forward kinematics and inverse kinematics. Furthermore, the notation, according to *Denavit-Hartenberg*, which is very common in robotics for describing the transformation between successive joints, is presented. According to the general principles of robotic kinematics, reference is made to the particular case of redundancy, since it occupies an outstanding position, especially like medical robots such as the *MIRO*.

A.1.1 Homogeneous transformations

The following section is based on the explanations from [59] about homogeneous transformations.
In order to describe the pose, i.e. the orientation and the position of an object in space six different degrees of freedom are required:

- three degrees of freedom describing the position (e.g. X- ,Y- ,Z-position in cartesian coordinates),
- three degrees of freedom for orientation (e.g. three Cardan angles).

In order to define an object exactly by means of these six degrees of freedom and its position as orientation, the object must be a rigid body. Rigid bodies are characterized by the fact that they do not allow any deformation and have infinitely high stiffness. As a result, two body-fixed points on a rigid body always have the same relation to each other. If this is the case, the transformation of one body into another can be unambiguously defined by a rigid-body transformation. For the relative transformation between two bodies, also six degrees of freedom are required since distortions play no role. The rigid-body transformation can be described as a combination of elementary rotation and translation. Rotations can be described by a combination of elementary rotations around the axes of the coordinate system. The rotation matrices for the rotation around the different axes of a coordinate system look as follows:

$$\boldsymbol{R}_x(\alpha) = \begin{pmatrix} 1 & 0 & 0 \\ 0 & \cos(\alpha) & -\sin(\alpha) \\ 0 & \sin(\alpha) & \cos(\alpha) \end{pmatrix} \tag{A.1}$$

$$\boldsymbol{R}_y(\beta) = \begin{pmatrix} \cos(\beta) & 0 & \sin(\beta) \\ 0 & 1 & 0 \\ -\sin(\beta) & 0 & \cos(\beta) \end{pmatrix} \tag{A.2}$$

$$\boldsymbol{R}_z(\gamma) = \begin{pmatrix} \cos(\gamma) & -\sin(\gamma) & 0 \\ \sin(\gamma) & \cos(\gamma) & 0 \\ 0 & 0 & 1 \end{pmatrix}. \tag{A.3}$$

In order to be able to describe any rotation of a body, elementary rotations can be combined with each other. There are different conventions and possibilities for this combination. One of the best known is, for example, the cardan rotation, which is composed of the elementary rotations as follows:

$$\boldsymbol{R}_{CARD}(\alpha, \beta, \gamma) = \boldsymbol{R}_x(\alpha) \cdot \boldsymbol{R}_y(\beta) \cdot \boldsymbol{R}_z(\gamma) = \tag{A.4}$$

$$\begin{pmatrix} \mathrm{c}_\beta \mathrm{c}_\gamma & -\mathrm{c}_\beta \mathrm{s}_\gamma & \mathrm{s}_\beta \\ \mathrm{c}_\alpha \mathrm{s}_\gamma + \mathrm{s}_\alpha \mathrm{s}_\beta \mathrm{c}_\gamma & \mathrm{c}_\alpha \mathrm{c}_\gamma - \mathrm{s}_\alpha \mathrm{s}_\beta \mathrm{s}_\gamma & -\mathrm{s}_\alpha \mathrm{c}_\beta \\ \mathrm{s}_\alpha \mathrm{s}_\gamma - \mathrm{c}_\alpha \mathrm{s}_\beta \mathrm{c}_\gamma & \mathrm{s}_\alpha \mathrm{c}_\gamma + \mathrm{c}_\alpha \mathrm{s}_\beta \mathrm{s}_\gamma & \mathrm{c}_\alpha \mathrm{c}_\beta \end{pmatrix}, \tag{A.5}$$

with the abbreviations $\mathrm{s}_i = \sin(i), \mathrm{c}_i = \cos(i)$, and $i = \alpha, \beta, \gamma$.

In various other areas of the economy, other conventions have established themselves in addition to the Cardan angle convention to express arbitrary rotations. For example, the Euler angle convention or the aviation convention is used particularly in aerospace engineering. However, these are not used in this paper and are only mentioned for the sake of completeness:

$$\boldsymbol{R}_{Euler,AC}(\gamma, \beta, \alpha) = \boldsymbol{R}_z(\gamma) \cdot \boldsymbol{R}_y(\beta) \cdot \boldsymbol{R}_x(\alpha). \tag{A.6}$$

For the sake of completeness, it should be mentioned here that there are also other possibilities to perform and describe rigid body transformations - such as the axis-angle representation or the representation using quaternions, which is very common in robotics, but which have no relevance for this work.

As already mentioned, rigid-body transformations always consist of a rotation and a translation. While matrices usually describe the rotation, the translation is described as the displacement of the origin in the direction of the X-, Y-, Z- axes of the base coordinate system. Thus a rigid body transformation results from the multiplication of the coordinates with a rotation matrix and subsequent addition of the displacement vector:

$$\boldsymbol{x'} = \boldsymbol{R} \cdot \boldsymbol{x} + \boldsymbol{t}. \tag{A.7}$$

In order to realize these arithmetic operations (the multiplication with the rotation matrix $\boldsymbol{R}$ and the addition of the translation vector $\boldsymbol{t}$) in one arithmetic step, a homogeneous extension is introduced. Location vectors are now represented by

$$\boldsymbol{x} = (x, y, z, 1)^T \tag{A.8}$$

and direction vectors through

$$\boldsymbol{r} = (x, y, z, 0)^T. \tag{A.9}$$

The rigid body transformation of a spatial vector $\boldsymbol{x}$ can thus be described by the multiplication of the homogeneous transformation matrix $\boldsymbol{T}$ with the spatial vector $\boldsymbol{x}$:

$$\boldsymbol{x'} = \boldsymbol{T}\boldsymbol{x} = \left(\begin{array}{c|c} \boldsymbol{R}_{3\times3} & \boldsymbol{t}_{3\times1} \\ \hline \boldsymbol{0}_{1\times3} & 1 \end{array}\right) \begin{pmatrix} x \\ y \\ z \\ 1 \end{pmatrix}. \tag{A.10}$$

With this representation of a homogeneous transformation, it is now possible to describe changes in the coordinate systems with an operation that has six degrees of freedom as presented in formula A.10.

A.1.2 Robot kinematics

To model a robot kinematically, the relation between joint angles $\boldsymbol{q}$ and end effector degrees of freedom must be known. Kinematically, robots are a series of articulated links. They can either be arranged as open kinematic chains (serial kinematics) or as closed kinematic chains (parallel-kinematics). Mixed forms are possible too. For this work, only serial chains are relevant, because such a chain can model the *MIRO* robot and the interface. The relation of the joint angles and the end effector degrees of freedom can be described in two ways: The forward kinematics expresses the end effector degrees of freedom as a function of the joint angles. The inverse kinematics determines the joint angles for given end effector degrees of freedom. The representation of the robots by their joint angles is called joint space, while the end effector coordinates represent the task space, as seen in Fig. A.1 .

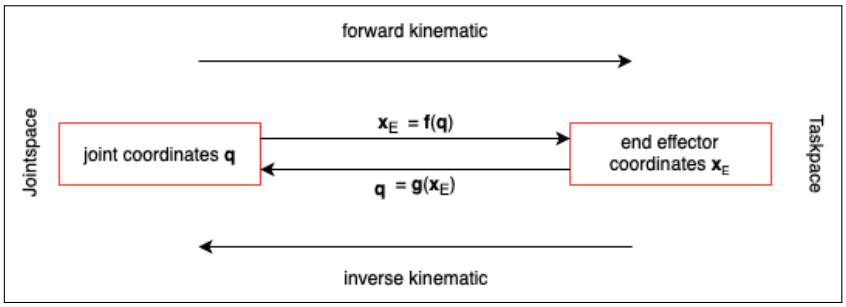


Figure A.1: Relation between direct and inverse kinematics [60]

As described in [61], the forward kinematics can be described by

$$\boldsymbol{x}_e = \boldsymbol{f}(\boldsymbol{q}) \tag{A.11}$$

Here $\boldsymbol{q}$ is the vector of the joint angles:

$$\boldsymbol{q} = \begin{pmatrix} q_1 \\ q_2 \\ \vdots \\ q_n \end{pmatrix} \tag{A.12}$$

and $\boldsymbol{x}_e$ the vector of the end effector coordinates:

$$\boldsymbol{x}_e = \begin{pmatrix} x_1 \\ x_2 \\ \vdots \\ x_m \end{pmatrix} \tag{A.13}$$

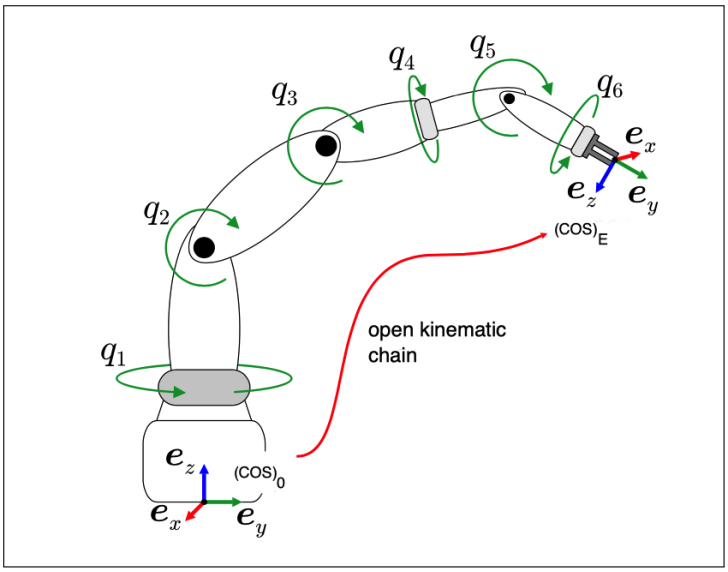


Figure A.2: Robot as concatenation of link fixed coordinate systems [60]

To describe robot kinematics using the formula A.11 for the forward kinematic, fixed coordinate systems are placed in each robot joint (or in special cases outside the joint). Between these, the transformation matrix $\boldsymbol{T}$ is determined, which depends on the degree of joint freedom q_i. Since the robot is modelled as a series of joints, as shown in Fig. A.2, the dependence of the end effector coordinates from the joint angles can be determined by multiplying the individual transformation matrices:

$$\boldsymbol{x}_e = \prod_{i=1}^{n} {}^{i}_{i-1}\boldsymbol{T}(q_i) \cdot \boldsymbol{x}_0 \tag{A.14}$$

A useful notation of homogeneous transformation matrices is the *Denavit-Hartenberg* notation presented in Section A.1.2. This notation offers a set of four parameters to calculate the homogeneous transformation matrix $\boldsymbol{T}$.

The problem of inverse kinematics, i.e. the representation of joint angles as a function of end effector degrees of freedom

$$\boldsymbol{q} = \boldsymbol{g}(\boldsymbol{x}_e) \tag{A.15}$$

is more complex and not always analytically solvable. In special cases or for simple kinematics it can be determined analytically or geometrically. For more complex kinematics, however, this problem must be solved numerically.

Denavit-Hartenberg notation

To model a robot arm, a fixed coordinate system is placed in each robot link. This coordinate system rotates with the rotation of the joint and enables the description of this link in space. Since each link has such a coordinate system, from the robot base to the end effector, the position of the end effector can be described via a transformation chain over the individual links. In this thesis the *Denavit-Hartenberg* notation according to *Yoshikawa* [62] and *Craig* [63] is used. This means that the coordinate systems are put into the links according to specific systematics, and the transformation into the next following system is described by the four parameters a_{i-1}, α_{i-1}, d_i and δ_i. The positions of the coordinate systems of two arbitrary, coupled links are shown in Fig. A.3.

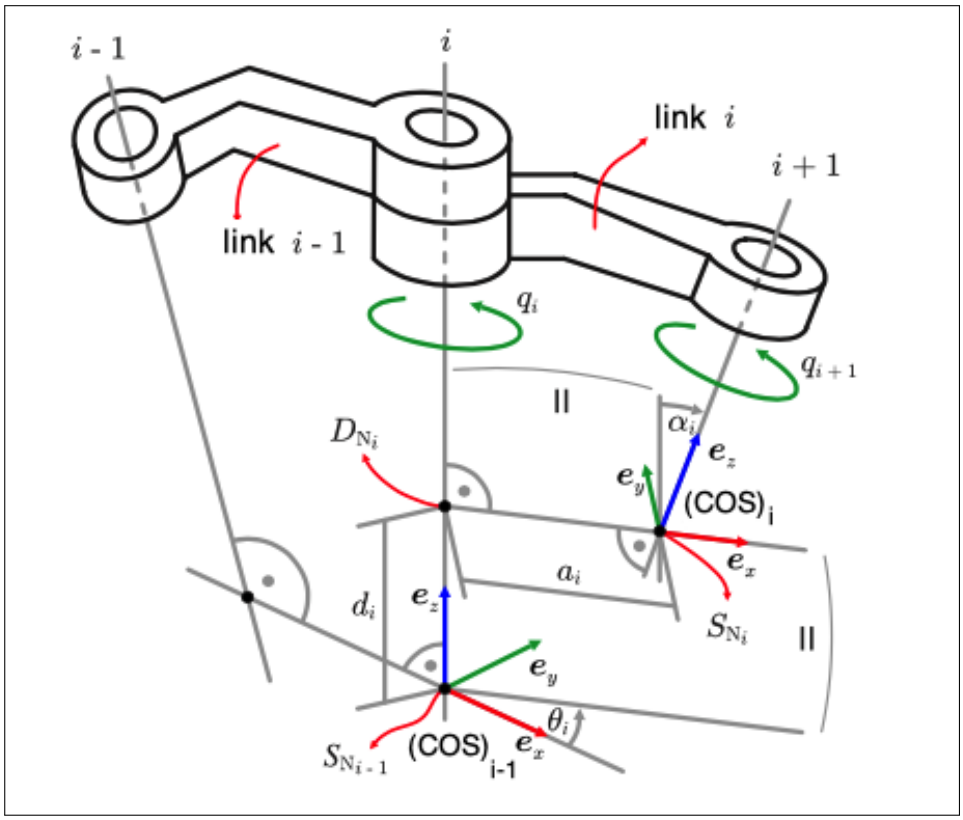


Figure A.3: *Denavit-Hartenberg* parameters of two subsequent links [60]

To determine the four *Denavit-Hartenberg* parameters for each joint, firstly, a fixed coordinate system must be set for each joint. The Z_i axis of the i-th coordinate system always lies on the i-th joint axis. The origin of the coordinate system lies on the point of least distance to the $i+1$-th joint axis. The X_i axis points towards the $i+1$ axis. The Y_i axis is now derived from the right-hand convention. As shown in figure A.3, four parameters are required for the transformation from the coordinate system $(COS)_i$ to the coordinate system $(COS)_{i+1}$.

To move from the i-th coordinate system to the $i+1$-th, four steps must be performed. The first step is to move the coordinate system along the X_i axis, the distance a_i from Z_i to Z_{i+1}. Then the X_i axis is rotated until the Z_i axis is superimposed with the Z_{i+1} axis, this rotation is described with the parameter α_i. The third step of the transformation consists in moving the coordinate system along the Z_i axis until the origins of the two coordinate systems lie on top of each other, this distance is called d_i. For purely rotational joints (as will be the case in this work), these three parameters are fixed and are also called link parameters. The last parameter, the so-called joint parameter, is the angle δ_i. The coordinate system is rotated around the Z_{i-} axis until all axes of the new and old coordinate systems are congruent. In summary, the following four parameters result:

1. a_{i-1} : Crossing distance, translation in the direction of the previous X-axis x_{i-1}
2. α_{i-1} : Crossing angle, rotation around the previous X-axis x_{i-1}
3. d_i : Axis distance, translation in the direction of the previous joint axis Z_{i-1}
4. δ_i : Axis angle, rotation around the previous joint axis Z_{i-1}

The exact rules, especially for special cases, on how to define the coordinate systems and how to determine the parameter sets can be found in [62] and [63].
The following matrix results for the homogeneous transformation matrix depending on the four *Denavit-Hartenberg* parameters:

$$
{}^{i}_{i-1}T = \begin{pmatrix} \cos(\theta_i) & -\sin(\theta_i) & 0 & a_{i-1} \\ \sin(\theta_i)\cos(\alpha_{i-1}) & \cos(\theta_i)\cos(\alpha_{i-1}) & -\sin(\alpha_{i-1}) & -\sin(\alpha_{i-1})d_i \\ \sin(\theta_i)\sin(\alpha_{i-1}) & \cos(\theta i)\sin(\alpha_{i-1}) & \cos(\alpha_{i-1}) & \cos(\alpha_{i-1})d_i \\ 0 & 0 & 0 & 1 \end{pmatrix} \tag{A.16}
$$

Redundancy

Kinematic redundancy is a phenomenon where the dimension of the joint angle vector is higher than the dimension of the end effector coordinates:

$$
\dim(\boldsymbol{q}) > \dim(\boldsymbol{x}_e) \tag{A.17}
$$

As a result, there is no clear configuration of joint angles for a given end-effector pose (see Fig. A.4). The robot can, therefore, change its joint angles while the end effector remains stationary - these are so-called null space movements.

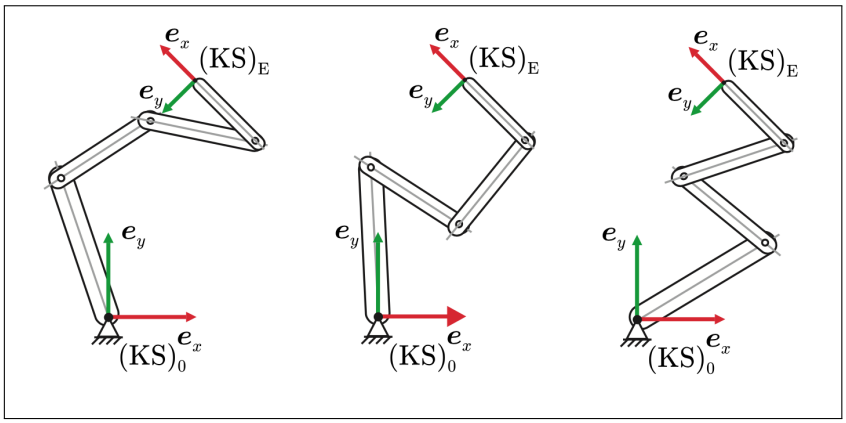


Figure A.4: Null space configurations of a redundant robot [60]

Redundancy does not affect the solvability of the forward kinematics but results in several solutions for the inverse kinematics. As an example, Fig. A.4 shows three different configurations for the same end-effector position of a redundant robot.

The *MIRO* robot arm has seven degrees of freedom. This means, since the end effector has only three degrees of translational freedom and three degrees of rotational freedom, the robot is kinematically redundant. It has one more degree of freedom than would be necessary for positioning the end effector. Nullspace movements are of great importance in a clinical environment, as they allow the robot arm to be repositioned without moving the end effector, which can already be located in the surgical area and used by the surgeon.

A.1.3 Summary

In this section, the most essential kinematic principles for robot modelling were explained, such as forward kinematics, inverse kinematics, *Denavit-Hartenberg* notation and redundancy. These topics are of great importance for the integration of the interface to the *MIRO* and allow the description of the kinematic relationships of the interface.

A.2 List of Requirements

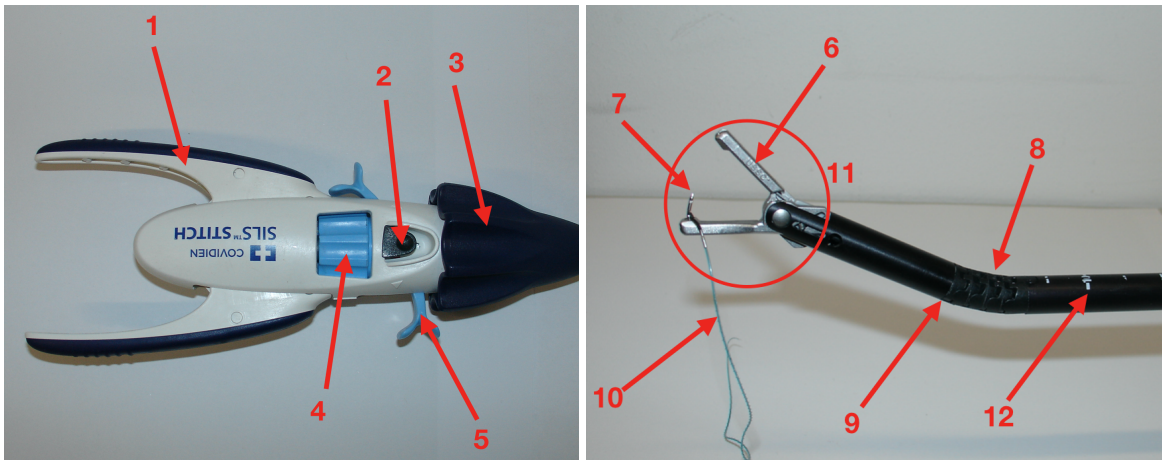
Legend Requiremnt implementation

fixed requirement	F	complied	c.	partly complied	p.c.
wish requirement	W	not complied	n.c.	not applicatable	n.a.

Item No.	F/W	Requirement	Values / Data	Suturing Instrument	Adapter
1	**Geometry and dimensions**				
1.1	**W**	Shaft diameter compatible with *MIRO* hollow axis	Shaft diameter $\leq$ 10 mm	c.	
1.2	**W**	Compactness in order not to limit the working space of the robot too much		c.	c.
1.3	**W**	Maximum dimensions	Depends on the arrangement - the usual *MICA* instrument: 60 mm in diameter and 220 mm in length		p.c.
2	**Weight**				
2.1	**F**	Maximum weight	$< 3\,kg$	c.	c.
2.2	**W**	Desired weight	$< 2\,kg$	c.	c.
3	**Kinematics**				
3.1	**F**	Actuability of the degrees of freedom		c.	
3.2	**F**	Deflectability of the tool-tip		c.	
3.3	**W**	Little play in the degrees of freedom		p.c.	
3.4	**W**	Little hysteresis in the degrees of freedom		n.c.	
4	**Strain & Forces**				
4.1	**F**	Forces to be exerted	Has to penetrate tissue		p.c. (incon-sistent)
5	**Energy**				
6	**Materials, auxiliary materials**				
6.1	**W**	Material must be autoclavable	For the first prototype not necessarily		n.c.

Item No.	F/W	Requirement	Values / Data	Suturing Instrument	Adapter
6.2	**W**	High stiffness			c.
6.3	**W**	3D printed parts			c.
7	**Ergonomics**				
7.1	**W**	Adaptable for different instruments			n.c.
8	**Fabrication**				
8.1	**W**	Production must not take too long			c.
9	**Monitoring**				
9.1	**F**	Tapability of actuator data	Speeds, velocities, current, voltage, temperature		c.
9.2	**F**	Integration into the *MIRO* communication network			p.c.
10	**Assembly and disassembly**				
10.1	**W**	Actuatability without conversion of the instrument		c.	c.
10.2	**W**	Fast and simple assembly			p.c.
10.3	**F**	Connectivity to the *MIRO*			c.
10.4	**F**	Use existing magnetic holder - either concentric to shaft or perpendicular			c.
11	**Transportation**				
11.1	**F**	Easy assembly, disassembly and transport			c.
12	**Use**				
12.1	**W**	Little preparation effort before use		c.	p.c.
12.2	**F**	Fast removal in case of complications			c.
13	**Maintenance and service**				
13.1	**F**	Sterile operation		n.c.	n.c.
13.2	**W**	Autoclavability	constant material properties till 120-150°C, 1-3 bar	n.c.	n.c.
13.3	**W**	(spatial) Separation of the parts to be sterilized from the others			p.c.
14	**Recycling**				
14.1	**W**	Reusability		n.c.	
14.2	**F**	Reusability			c.
15	**Expenses**				
15.1	**W**	Commercially available		p.c.	

A.3 Designation of the instrument parts



(a) Naming on the instrument body

(b) Naming on the instrument tool tip

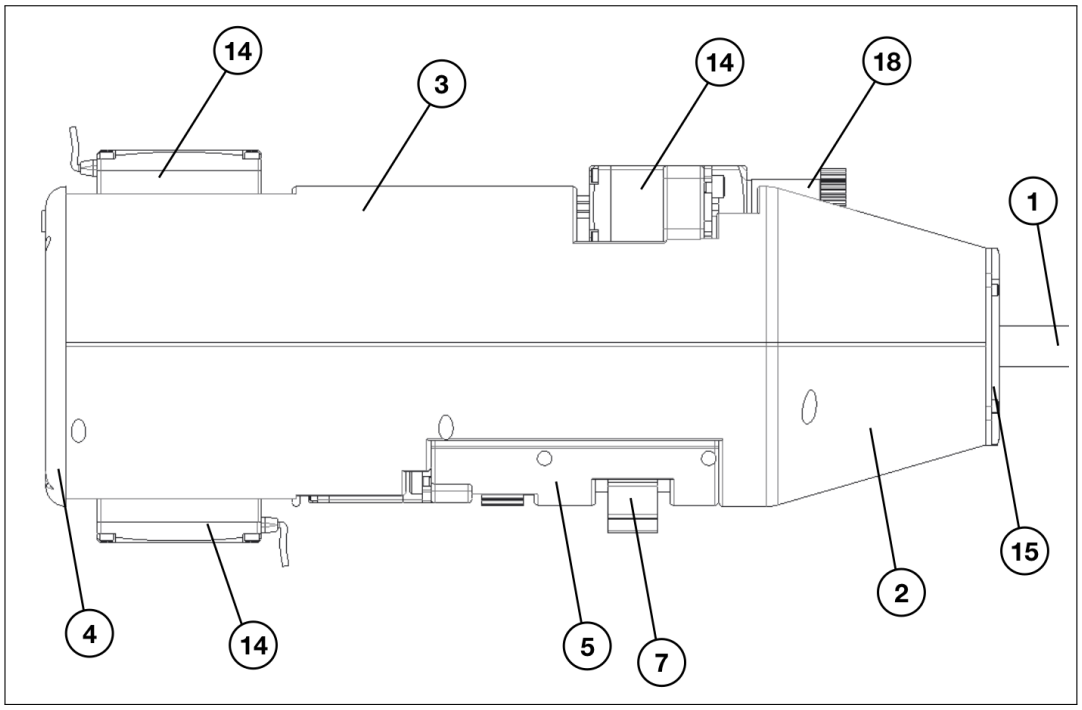
Figure A.5: Designation of the parts of the suturing instrument

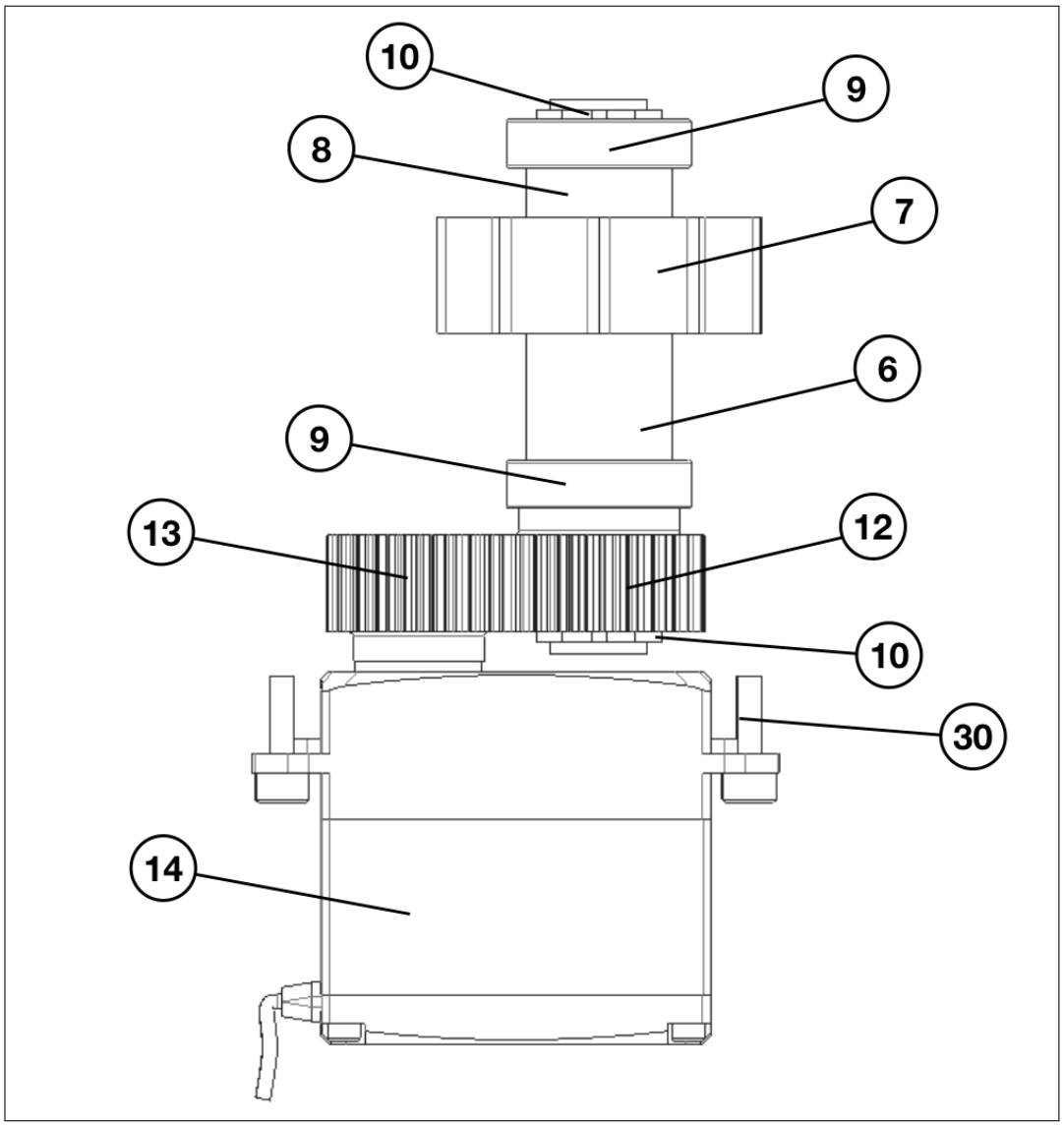
Number	Designation
1	Handle
2	Loading mechanism for the needle
3	Dark blue rotation gear
4	Dight blue articulation gear
5	Swivelling lever
6	Jaw
7	Needle
8	Articulation link
9	Rotation link
10	Thread
11	Gripper
12	Shaft

Table A.1: Listing of the part names

A.4 Part list

Part No.	Name	Description	Unit	Quantity
1	*SILS Stich*	Suturing Instrument	EA	1
2	upper shell		EA	1
3	lower shell		EA	1
4	cover		EA	1
5	wave holder		EA	1
6	articulation wave		EA	1
7	flexible articulation gear		EA	1
8	spacer sleeve		EA	1
9	ball bearing	RK_618_10x19x5	EA	2
10	retaining ring	DIN 471 10x1	EA	2
11	key	DIN 6886 - A - 3x3x10	EA	1
12	articulation gear	for the wave (Part No. 6)	EA	1
13	articulation gear	for the motor	EA	1
14	*DITEX 1609S*	servo motor	EA	4
15	magnetic mounting adapter		EA	1
16	rotation adapter		EA	1
17	rotation gear	for the adapter (Part No. 17)	EA	1
18	rotation gear	for the motor	EA	1
19	motor adapter	handle	EA	1
20	handle link		EA	2
21	handle holder		EA	2
22	motor adapter	swivelling mechanism	EA	2
23	handle bar		EA	2
24	swivel bracket		EA	1
25	safety clip	for handle bars (Part No. 23)	EA	2
26	dowl pin	diameter 2mm, length 25mm	EA	2
27	dowl pin	diameter 2mm, length 13mm	EA	2
28	dowl pin	diameter 2mm, length 8mm	EA	3
29	dowl pin	diameter 2mm, length 5mm	EA	6
30	screw	DIN 912 M3 x 10	EA	14
31	screw	DIN 912 M1,6 x 8	EA	18
32	screw	DIN 965 M1.6 x 8	EA	4


14
3
14
18
1
4
14
5
7
2
15


10
9
8
7
6
9
13
12
10
30
14

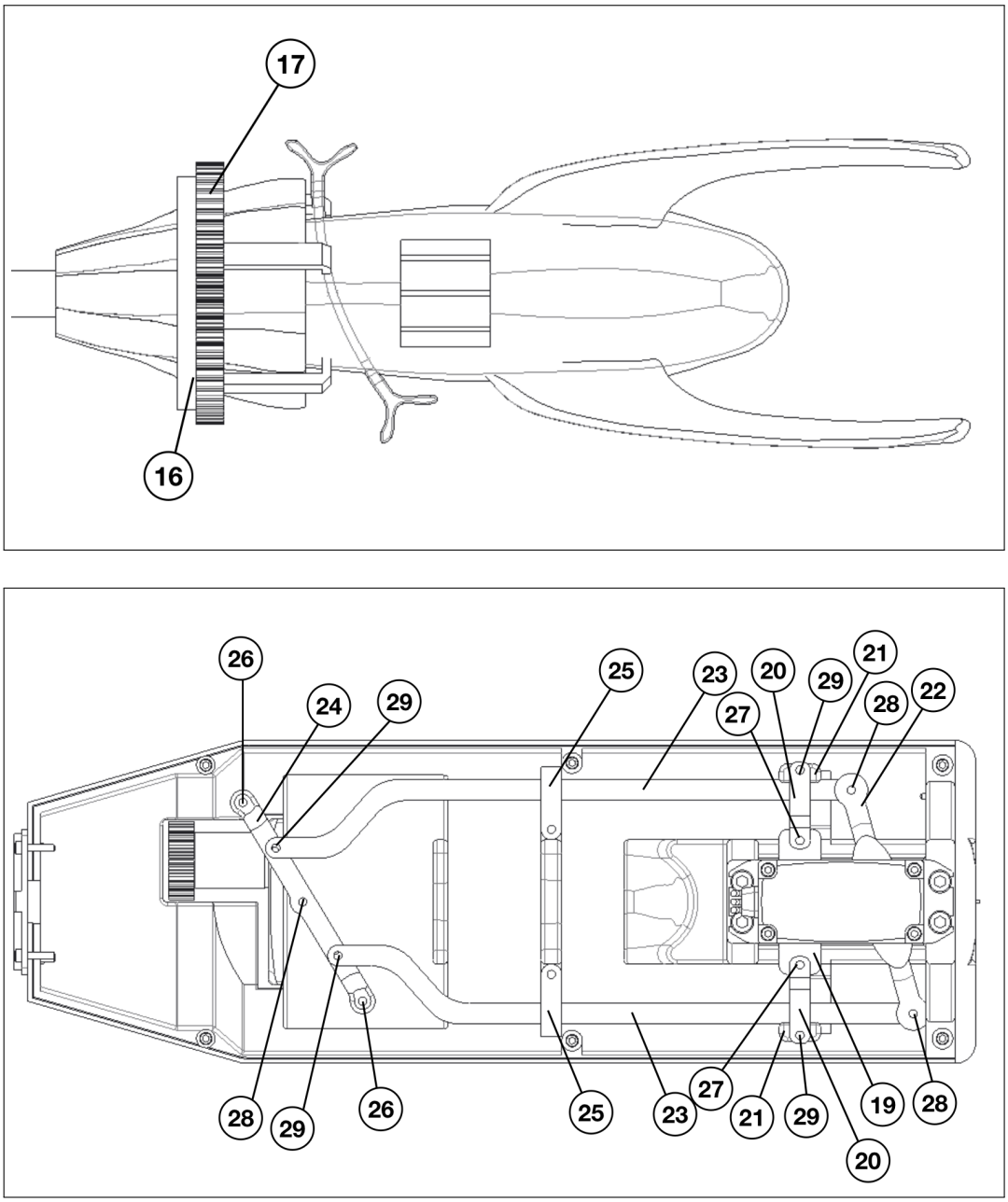


Figure A.7: Overview over all parts

A.5 Technical drawings

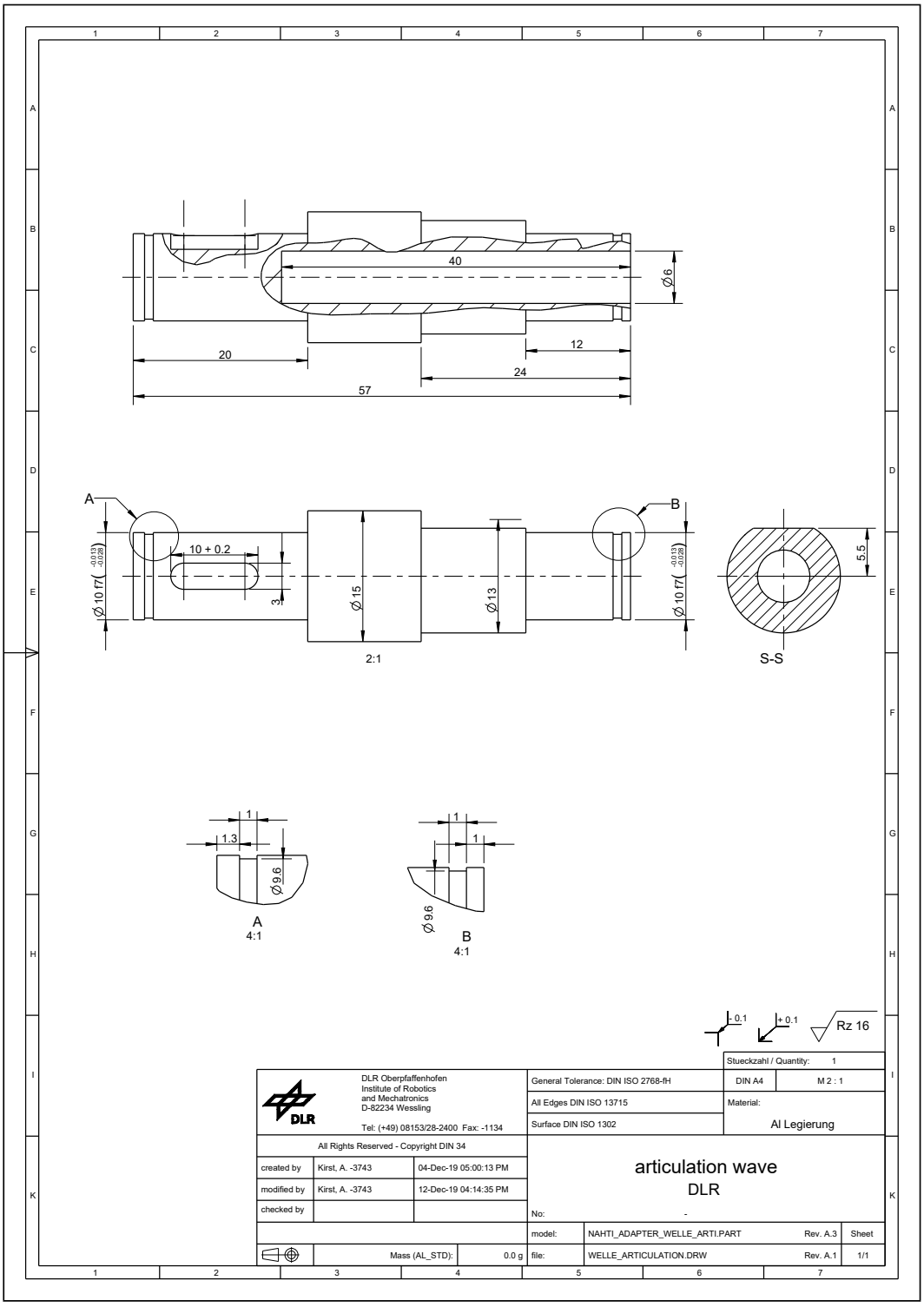


Figure A.8: Articulation wave

A.6 Assembly instruction

To mount the adapter, all threaded inserts must first be pressed into the holes provided for this purpose.
Then the motor, which is responsible for the swivelling lever, can be inserted from below into the lower shell and fastened with four M3 x 10 screws. Now the mechanism for turning the swivelling lever can be assembled. To do this, place the two rods in the motor adapter for the swivelling mechanism and fix them with dowel pins Ø2 x 8. The other sides of the rods are placed on the dowel pins Ø2 x 5, which have been pressed into the swivel bracket before. In addition, the long dowel pins Ø2 x 25 for turning the lever are pressed into this bracket, which should turn the lever. A further dowel pin Ø2 x 8 is pressed into the designated position in the lower shell, which serves as the centre of rotation of the swivel bracket. Now the whole construction can be put into the shell: at the front place the bracket is placed on the dowel pin, and at the motor, the motor adapter is pressed onto the shaft of the motor.
To mount the motor responsible for the locking mechanism of the handles, the motor adapter is first attached to it: For this purpose, it is pressed onto the motor. In the following, the handle links can be attached to the motor adapter with dowel pins Ø2x13. Now the handle holder can be attached to the handle links with dowl pins Ø2 x 5. The motor responsible for the closing mechanism of the gripper together with the motor adapter can be mounted by screwing it tight with four M3 x 10 screws in the holding over the other motor.
Finally, the motor for rotating the instrument tip is attached to the underside of the lower shell. The gear wheel is pressed onto its axis, and the motor is screwed to the housing shell with two M3 x 10 screws. The cable of this motor must be led through the recess in the shell to the inside and then to the rear. Now the cover of the adapter can be fastened with four M1.6 x 8 screws to the lower shell. It is important that the three wires of the motors, screwed on the lower shell, are also routed through the holes in the cover.
The wave is now mounted in the handle holder, which is provided for this purpose. First, the ball bearing must be glued in the front hole of the wave holder. Then the second bearing, a key and the articulation gearwheel are pushed onto the drive side of the wave. This side is fixed with a retaining ring. Now the wave can be pushed through the floating bearing side of the wave holder. It's important that the wave is also pushed through the flexible gear wheel and the spacer sleeve, which are located in the opening between the two bearing seats. It can then be pushed through the fixed bearing and secured with a second retaining ring. On the last motor, articulation gearwheel has to be pressed. The motor now can be screwed to the wave holder using four M3 x 10 screws. The whole shaft holder can now be screwed onto the upper shell.
The last gear wheel is glued onto the adapter ring for the dark blue rotation wheel of the instrument.

A.7 Specification DITEX 1609S

Name	DITEX TD1609S
Art-Nr.	50001609
Type	Standard
Length	40 mm
Width	20 mm
Heigth	37 mm
Weight	63 g
Torque @ 6.0 V	113 Ncm
Speed @ 6.0 V	0.111 sec/60°
Torque @ 7.4 V	132 Ncm
Speed @ 7.4V	0.1 sec/60°
Torque @ 8.4 V	162 Ncm
Speed @ 8.4 V	0.08 sec/60°
Gear	Metal
Bearing	Ball-bearing
Case	Alu / plastic
Output drive	25-teeth Spline
Use	Airplane
received input voltage	6.0 – 8.4 V
max. input voltage	10.0 V

Table A.2: Specification of the *DITEX 1609S* [64]

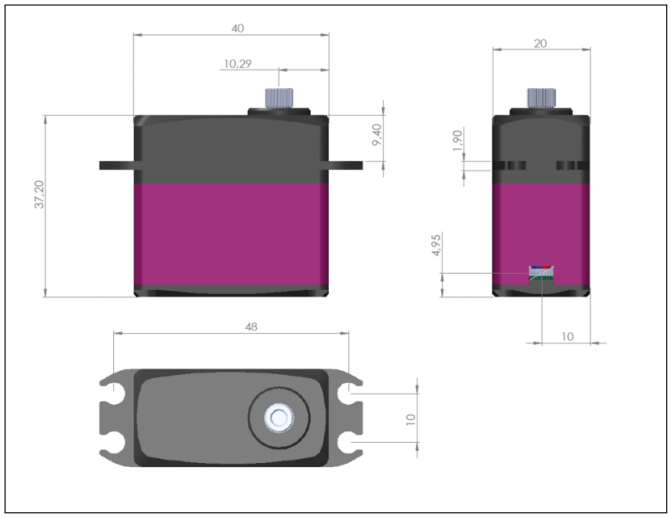


Figure A.9: Dimensions of the *DITEX 1609S* [64]

A.8 States of the suturing finite state machine

$V_{Gripper}$	$P_{Gripper}$	$V_{Switching}$	$P_{Switching}$	next $V_{Gripper}$	next $V_{Switching}$	next $in_progress$
-1	-1	-1	-1	not possible		
-1	-1	-1	0	not possible		
-1	-1	-1	1	not possible		
-1	-1	0	-1	0	0	$False$
-1	-1	0	0	not possible		
-1	-1	0	1	0	0	$False$
-1	-1	1	-1	not possible		
-1	-1	1	0	not possible		
-1	-1	1	1	not possible		
-1	0	-1	-1	not possible		
-1	0	-1	0	not possible		
-1	0	-1	1	not possible		
-1	0	0	-1	-1	0	$False$
-1	0	0	0	not possible		
-1	0	0	1	-1	0	$False$
-1	0	1	-1	not possible		
-1	0	1	0	not possible		
-1	0	1	1	not possible		
-1	1	-1	-1	not possible		
-1	1	-1	0	not possible		
-1	1	-1	1	not possible		
-1	1	0	-1	0	0	$False$
-1	1	0	0	not possible		
-1	1	0	1	0	0	$False$
-1	1	1	-1	not possible		
-1	1	1	0	not possible		
-1	1	1	1	not possible		
0	-1	-1	-1	not possible		
0	-1	-1	0	not possible		
0	-1	-1	1	not possible		
0	-1	0	-1	-1	0	$False$
0	-1	0	0	not possible		
0	-1	0	1	-1	0	$False$
0	-1	1	-1	not possible		
0	-1	1	0	not possible		
0	-1	1	1	not possible		

0	0	-1	-1	not possible		
0	0	-1	0	not possible		
0	0	-1	1	not possible		
0	0	0	-1	not possible		
0	0	0	0	not possible		
0	0	0	1	not possible		
0	0	1	-1	not possible		
0	0	1	0	not possible		
0	0	1	1	not possible		
0	1	-1	-1	0	-1	$False$
0	1	-1	0	0	-1	$False$
0	1	-1	1	0	0	$False$
0	1	0	-1	0	-1	$False$
0	1	0	0	not possible		
0	1	0	1	0	1	$False$
0	1	1	-1	0	1	$False$
0	1	1	0	0	1	$False$
0	1	1	1	0	0	$False$
1	-1	-1	-1	not possible		
1	-1	-1	0	not possible		
1	-1	-1	1	not possible		
1	-1	0	-1	0	0	$True$
1	-1	0	0	not possible		
1	-1	0	1	0	0	$True$
1	-1	1	-1	not possible		
1	-1	1	0	not possible		
1	-1	1	1	not possible		
1	0	-1	-1	not possible		
1	0	-1	0	not possible		
1	0	-1	1	not possible		
1	0	0	-1	1	0	$False$
1	0	0	0	not possible		
1	0	0	1	1	0	$False$
1	0	1	-1	not possible		
1	0	1	0	not possible		
1	0	1	1	not possible		
1	1	-1	-1	not possible		
1	1	-1	0	not possible		
1	1	-1	1	not possible		
1	1	0	-1	1	0	$False$
1	1	0	0	not possible		
1	1	0	1	1	0	$False$
1	1	1	-1	not possible		
1	1	1	0	not possible		
1	1	1	1	not possible		

Table A.3: All states of the suturing finite state machine

A.9 HSV representaion

Beside the representation of the color space via the components *red*, *green* and *blue* (RGB) the representation of a color via the three components *hue*, *saturation* and *value* is common - especially for segmenting specific colors. In this, a combination of these three components is assigned to each colour. *Hue* indicates the colour value and is described by an angle in the colour circle (red is at 0°, green at 120° and blue at 240°). The saturation of the colour is indicated by the component *saturation*, if it is 0, it is neutral grey, and if it is completely saturated, it is the pure colour. The brightness of the colour is described by *value*, and goes over an interval from 0 to 1 and becomes black at 0. The space that is spanned here is not a cube as in the RGB representation, but a cone is formed. Along the rotation axis the *value* is displayed, the distance to this corresponds to the *saturation*. Like the *value* it corresponds to an interval from 0 to 1. The angle around the axis is assigned a colour value of the colour circle and is in an interval from 0° to 360°. The colour space is shown in Fig. A.10.

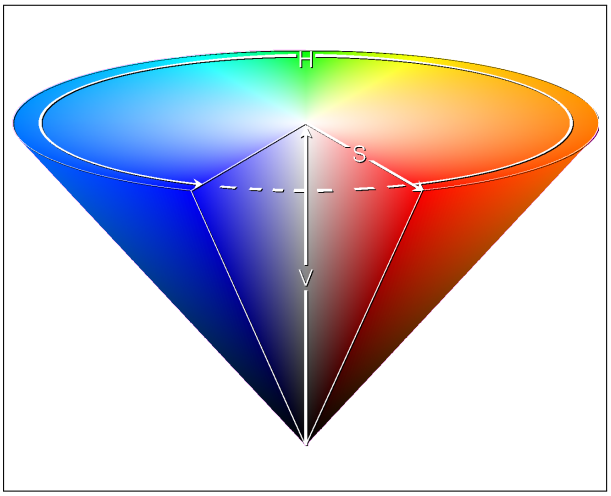


Figure A.10: HSV cone to represent colors

The conversion of a color represented in the RGB color space into the HSV space can be described by the following formulas [65]:

$$V \leftarrow max(R, G, B) \tag{A.18}$$

$$S \leftarrow \begin{cases} \frac{V - min(R,G,B)}{V}, & \text{if } V \neq 0 \\ 0, & \text{otherwise} \end{cases} \tag{A.19}$$

$$H \leftarrow \begin{cases} \frac{60(G-B)}{V-min(R,G,B)}, & \text{if } V = R \\ 120 + \frac{60(B-R)}{V-min(R,G,B)}, & \text{if } V = G \\ 240 + \frac{60(R-G)}{V-min(R,G,B)}, & \text{if } V = B \end{cases} \tag{A.20}$$

The values generated in this way, which lie in the interval from 0 to 1 or from 0° to 360°, must now be scaled for the data type used. For this work, each image channel was saved with 8 bits. This results in [65]:

$$V \leftarrow 255 \cdot V \tag{A.21}$$

$$S \leftarrow 255 \cdot S \tag{A.22}$$

$$H \leftarrow \frac{H}{2} \tag{A.23}$$

A.10 Principal component analysis

In the principal component analysis, the covariance of a set of different correlated variables is reproduced by less uncorrelated variables. This can be used in image processing to determine the two main directions of a point cloud of image coordinates.
To calculate the two principal components, various calculation steps must be carried out. First, the matrix of the image coordinates must be centred. The image coordinates are available in a matrix P of the dimension $m \times 2$, where the first column has the x-coordinates of the points and the second column the y-coordinates. For centring, the mean value of the corresponding column is subtracted from each value. The components of the centered point matrix can be determined as follows:

$$M_{k,j} = P_{k,j} - \frac{1}{m} \sum_{i} P_{i,j} \tag{A.24}$$

The main axes can now be determined by the eigenvalues and eigenvectors of the covariance matrix C of the centered point matrix. The elements of the covariance matrix can be represented as follows:

$$C = \begin{bmatrix} \text{Var}(C_1) & \text{Cov}(C_1, C_2) \\ \text{Cov}(C_2, C_1) & \text{Var}(C_2) \end{bmatrix} \tag{A.25}$$

Here, C_i describes the i-th column of the matrix. The covariance of two vectors can be expressed by the following formal:

$$\text{Cov}(C_i, C_j) = \frac{\sum_{k=1}^{m} (C_{k,i} - \bar{C_i})(C_{k,j} - \bar{C_j})}{m-1} \tag{A.26}$$

with

$$\bar{C_i} = \frac{1}{m} \sum_{k} C_{k,i} \tag{A.27}$$

The variance of a vector is expressed by:

$$\text{Var}(C_i) = \text{Cov}(C_i, C_i) = \frac{\sum_{k=1}^{m} (C_{k,i} - \bar{C_i})(C_{k,i} - \bar{C_i})}{m-1} \tag{A.28}$$

The eigenvectors of this matrix now indicate the direction of the two main axes and the corresponding eigenvalues indicate the size of the eigenvectors.

A.11 Source code of the tip-tracking

```
#!/usr/bin/python

import thread
import time
import sys
import pdb
import cv2
import timeit
from math import cos, sin, asin, pi, atan
import numpy as np
from matplotlib import pyplot as plt

import links_and_nodes as ln

from pysn.stream import InChannel
import numpy as np


class Image_Processor:
    def __init__(self):


        self.sn_image_channel = InChannel.create("cameras")

        self.svc = clnt.get_service_provider("angle from img", "
            angle_service")
        self.svc.set_handler(self.img_process)
        self.svc.do_register()
        self.imMain = np.array([])
        self.imAngle = np.array([])

        self.angle = None


    def segmentateImage(self,img_rgb, color="red"):

        hsv = cv2.cvtColor(img_rgb, cv2.COLOR_RGB2HSV)
        if color == "red":
            mask = cv2.inRange(hsv,(0,20,70),(10,255,255))
        else:
            mask = cv2.inRange(hsv, (40, 30, 60), (70, 255,255))

        kernel = np.ones((5,5),np.uint8)
```

```
43          mask = cv2.morphologyEx(mask,cv2.MORPH_OPEN,kernel,iterations
                =1)
44          return mask
45
46      def getPointCloud(self,masked_img):
47
48          pc = []
49
50          coords = np.where(masked_img == 255)
51          pc = list(zip(coords[0],coords[1]))
52
53          return pc
54
55
56
57      def PCA(self,pc):
58          pc = np.array(pc)
59          #print(pc.shape)
60          M = np.mean(pc.T, axis=1)
61          C = pc - M
62          V = np.cov(C.T)
63          values, vectors = np.linalg.eig(V)
64          return (vectors, values, M)
65
66      def getHighstPricipleComponent(self, vectors, values):
67          pos = np.argmax(values)
68          highestVector = vectors[pos]
69          if highestVector[0] < 0:
70              return (-1 * highestVector[0], -1 * highestVector[1])
71          else:
72              return (highestVector[0], highestVector[1])
73
74      def getAngleBetweenVec(self, vec1, vec2):
75          angle = np.arctan2(vec1[1], vec1[0]) - np.arctan2(vec2[1],
                vec2[0])
76          angle = angle * 360 / (2 * np.pi)
77          #angle = 180 - angle
78          return angle
79
80
81      def img_process (self, req, req_data, resp_data):
82          img = self.sn_image_channel.read(InChannel.BLOCKING_WAIT)
83          if(img.field0.data==None):
84              print ('image does not exist')
85              quit()
86
```

```
87          img = img.field0.copy()
88          redblob = self.segmentateImage(img, "red")
89          greenblob = self.segmentateImage(img, "green")
90
91          pc_green = self.getPointCloud(greenblob)
92          pc_red = self.getPointCloud(redblob)
93
94          vec_red, val_red, m_red = self.PCA(pc_red)
95          vec_green, val_green, m_green = self.PCA(pc_green)
96
97          direc_red = self.getHighstPricipleComponent(vec_red, val_red)
98          direc_green = self.getHighstPricipleComponent(vec_green,
                val_green)
99
100         self.angle = round(self.getAngleBetweenVec(direc_red,
                direc_green),2)
101
102         mask = cv2.bitwise_or(greenblob, redblob)
103
104         t = cv2.bitwise_and(img,img,mask=mask)
105         t = cv2.cvtColor(t, cv2.COLOR_RGB2BGR)
106         new_t = cv2.line(t, (int(m_red[1] - direc_red[1]*2000), int(
                m_red[0] + direc_red[0] * 2000)), (int(m_red[1]+ direc_red
                [1]*2000), int(m_red[0] - direc_red[0] * 2000)),
                (255,255,255), 1)
107         new_tt = cv2.line(new_t, (int(m_green[1] - direc_green
                [1]*2000), int(m_green[0] + direc_green[0] * 2000)), (int(
                m_green[1]+ direc_green[1]*2000), int(m_green[0] -
                direc_green[0] * 2000)), (255,255,255), 1)
108         new_ttt = cv2.putText(new_tt, "Angle = {} deg".format(self.
                angle), (50,50), cv2.FONT_HERSHEY_SIMPLEX, 0.5,
                (255,255,255), 1)
109         print("Angle: {}".format(self.angle))
110         self.imMain = cv2.cvtColor(img, cv2.COLOR_RGB2BGR)
111         self.imGray = t
112         resp_data.angle = self.angle
113         req.respond()
114
115
116     def __del__(self):
117         self.sn_image_channel.close()
118         cv2.destroyAllWindows()
119
120
121 if __name__== "__main__":
122
```

```
123     clnt = ln.client("Image Processor", sys.argv)
124     ip = Image_Processor()
125     cv2.namedWindow("main",cv2.WINDOW_NORMAL)
126     cv2.namedWindow("gray",cv2.WINDOW_NORMAL)
127     cv2.resizeWindow('main', (500,400))
128     cv2.resizeWindow('gray', (500,400))
129
130     while True:
131         if clnt.wait_for_service_requests():
132             clnt.handle_service_requests()
133             try:
134                 cv2.imshow('main',ip.imMain)
135                 cv2.imshow('gray',ip.imGray)
136                 cv2.waitKey(1)
137                 pass
138             except:
139                 print 'image not ready'
```

A.12 Source code of the test procedure

```
import sys
import links_and_nodes as ln
import key_value_wrapper
import time
import numpy as np
import matplotlib.pyplot as plt

clnt = ln.client("test notebook", sys.argv)

port1 = clnt.subscribe("endo_telemetry", "gen/lnrk/micros/
    telemetry_71040b92fc2881f3f3c211ab59d2d0c7_wohc")
svc_arti = clnt.get_service('micros.articulation.set_commands','gen/
    lnrk/micros/sensor_micro/set_commands')
svc_rot =  clnt.get_service('micros.rotation.set_commands','gen/lnrk/
    micros/sensor_micro/set_commands')
cnt = 1

def command_pos(service, position, count):
    service.req.cmd_cnt = count % 255
    service.req.command = 1
    service.req.value = position
    service.call_gobject()

    if service.resp.error_message_len:
        raise Exception(service.resp.error_message)

svc3 = clnt.get_service('angle from img','gen/angle_service')

cnt = 1

#testscript for measuring the angle of articulation

for test in [1,2,3,4,5]:
    value = 8000
    back = False

    command_pos(svc_arti, 8200, cnt)
    cnt += 1
    time.sleep(5)

    data = []

    while value > 7999:
```

```
41
42          command_pos(svc_arti, value, cnt)
43          moving = True
44
45
46          while moving:
47              pkt = port1.read(True).articulation
48              if pkt.velocity == 0.0:
49                  moving = False
50          sleep(0.5)
51
52          angles = []
53
54          for i in range(1,11):
55              svc3.call_gobject()
56              angle_median.append(svc3.resp.angle)
57
58          pkt = port1.read(True).articulation
59
60          data.append([np.median(angles), value])
61
62          cnt = cnt + 1
63
64          if back == False:
65              value += 50
66          else:
67              value -= 50
68
69          if value > 16000:
70              back = True
71              value -= 100
72
73      data = np.array(data)
74      np.savetxt('angles_arti_{}.csv'.format(test), data, delimiter=','
            )
75
76  #testscript for measuring the angle of rotation
77
78  cnt = 1
79
80  for test in [1,2,3,4,5]:
81      value = 8200
82      back = False
83
84      command_pos(svc_rot, 8000, cnt)
85      cnt += 1
```

```
86      time.sleep(5)
87
88      data = []
89
90      while value > 7999:
91
92          command_pos(svc_rot, value, cnt)
93          moving = True
94
95          while moving:
96              pkt = port1.read(True).rotation
97              if pkt.velocity == 0.0:
98                  moving = False
99          sleep(0.5)
100
101         angles = []
102
103         for i in range(1,11):
104             svc3.call_gobject()
105
106             angles.append(svc3.resp.angle)
107
108         pkt = port1.read(True).rotation
109
110         data.append([np.median(angles), value])
111
112         cnt = cnt + 1
113
114         if back == False:
115             value += 500
116         else:
117             value -= 500
118
119         if value > 16000:
120             back = True
121             value -= 1000
122
123     data = np.array(data)
124     np.savetxt('angles_rot_{}.csv'.format(test), data, delimiter=',')
```

A.13 Source code of the 3D mouse control

```
#!/usr/bin/python

## space mouse control
import time
import sys
import links_and_nodes as ln
import key_value_wrapper
import time
import numpy as np

def command_pos(service, position, count):
    service.req.cmd_cnt = count % 255
    service.req.command = 1
    service.req.value = position
    service.call_gobject()

    if service.resp.error_message_len:
        raise Exception(service.resp.error_message)

def check_minmax(value):
    if value < 8192:
        return 8192
    if value > 16384:
        return 16384
    else:
        return value

def suturing(handle_velo, handle, swivelling_velo, swivelling):

    print("hv: {}, h: {}, sv: {}, s: {}".format(handle_velo,handle,
        swivelling_velo,swivelling))

    statemachine = {"-1-10-1": [0,0,True],
                    "-1-101": [0,0,True],
                    "-100-1": [-1,0,True],
                    "-1001": [-1,0,True],
                    "-110-1": [0,0,True],
                    "-1101": [0,0,True],
                    "0-10-1": [-1,0,True],
                    "0-101": [-1,0,True],
                    "01-1-1": [0,-1,True],
                    "01-10": [0,-1,True],
                    "01-11": [0,0,True],
```

```
                    "010-1": [0,-1,True],
                    "0101": [0,1,True],
                    "011-1": [0,1,True],
                    "0110": [0,1,True],
                    "0111": [0,0,True],
                    "1-10-1": [0,0,False],
                    "1-101": [0,0,False],
                    "100-1": [1,0,True],
                    "1001": [1,0,True],
                    "110-1": [1,0,True],
                    "1101": [1,0,True],
                    }

    if handle < 8700:
        handle = 1
    elif 8700 <= handle < 14500:
        handle = 0
    else:
        handle = -1

    if handle_velo < 0:
        handle_velo = -1
    elif handle_velo == 0:
        handle_velo = 0
    else:
        handle_velo = 1

    if swivelling < 8500:
        swivelling = -1
    elif 8500 <= swivelling < 14500:
        swivelling = 0
    else:
        swivelling = 1

    if swivelling_velo < 0:
        swivelling_velo = -1
    elif swivelling_velo == 0:
        swivelling_velo = 0
    else:
        swivelling_velo = 1

    print("{} {} {} {}".format(handle_velo,handle,swivelling_velo,
        swivelling))

    try:
        return statemachine["{}{}{}{}".format(handle_velo,handle,
```

```
            swivelling_velo,swivelling)]
88      except:
89          return [0,0,False]
90
91  if __name__== "__main__":
92
93      mode = "statemachine" #select statemachine mode
94      #mode = "manual"
95
96      clnt = ln.client("test notebook", sys.argv)
97
98      port1 = clnt.subscribe("endo_telemetry", "gen/lnrk/micros/
            telemetry_71040b92fc2881f3f3c211ab59d2d0c7_wohc")
99      svc_handle = clnt.get_service('micros.handle.set_commands','gen/
            lnrk/micros/sensor_micro/set_commands')
100     svc_rot = clnt.get_service('micros.rotation.set_commands','gen/
            lnrk/micros/sensor_micro/set_commands')
101     svc_swiv =  clnt.get_service('micros.swivelling.set_commands','
            gen/lnrk/micros/sensor_micro/set_commands')
102     svc_arti = clnt.get_service('micros.articulation.set_commands','
            gen/lnrk/micros/sensor_micro/set_commands')
103
104     space_mouse = clnt.subscribe("spacemouse.measurements", "
            spacemouse/measurements", rate=-1)
105
106     rot_velo = 0.0
107     arti_velo = 0.0
108     handle_velo = 0.0
109     swivelling_velo = 0.0
110     cnt = 3
111
112     time_old = time.time();
113
114     in_progress = False
115
116     print(port1.read(True).rotation.angle)
117     print(port1.read(True).articulation.angle)
118     print(port1.read(True).handle.angle)
119     print(port1.read(True).swivelling.angle)
120
121     command_pos(svc_rot,13000,cnt)
122     command_pos(svc_arti,13000, cnt)
123     command_pos(svc_handle, 16300, cnt)
124     command_pos(svc_swiv, 16300, cnt)
125     time.sleep(2)
126     cnt = 4
```

```
127
128     while True:
129
130         #provide current position so no rapit movements occurs
131         rotation = 11999.96+port1.read(True).rotation.angle*6.6777
132
133         articulation = 11990.208+port1.read(True).articulation.angle
                *30.759
134
135         handle =  12006.23 + port1.read(True).handle.angle * 200.246
136
137         swivelling =  12048.289 + port1.read(True).swivelling.angle *
                241.6418
138
139         swivelling_new = swivelling
140
141         pkt = space_mouse.read(False)
142
143         if in_progress:
144
145             if mode == "manual":
146                 command_pos(svc_handle,int(8200),cnt)
147                 time.sleep(3)
148                 cnt += 1
149                 if swivelling > 12000:
150                     command_pos(svc_swiv, int(8200),cnt)
151                     cnt += 1
152                 else:
153                     command_pos(svc_swiv,int(16300), cnt)
154                     cnt += 1
155                     time.sleep(3)
156                     command_pos(svc_handle, int(16300), cnt)
157                     time.sleep(3)
158                     cnt += 1
159                 in_progress = False
160             elif mode == "statemachine":
161                 handle_velo, swivelling_velo, in_progress = suturing(
                        handle_velo, handle, swivelling_velo, swivelling)
162
163         else:
164             print(swivelling)
165             if swivelling > 15500:
166                 swivelling_new = 14500
167             elif swivelling < 9000:
168                 swivelling_new = 10000
169             else:
```

```
170                 pass
171
172         if pkt:
173             if pkt.buttons[0] == 1:
174                 in_progress = True
175
176             rot_velo = pkt.axes[5]
177             arti_velo = pkt.axes[3]
178
179
180         time_new = time.time()
181         d_time = time_new-time_old
182
183         rotation_new = rotation + 50 * rot_velo * d_time
184         articulation_new = articulation + 50 * arti_velo * d_time
185         handle_new = handle + 40 * handle_velo
186         swivelling_new = swivelling + 4000 * swivelling_velo
187
188         time_old = time_new
189
190         rotation_new = check_minmax(rotation_new)
191         articulation_new = check_minmax(articulation_new)
192         handle_new = check_minmax(handle_new)
193         swivelling_new = check_minmax(swivelling_new)
194
195         if np.abs(rotation_new - rotation) < 20:
196             pass
197         else:
198             command_pos(svc_rot,int(rotation_new),cnt)
199
200         if np.abs(articulation_new - articulation) < 20:
201             pass
202         else:
203             command_pos(svc_arti,int(articulation_new),cnt)
204
205         if np.abs(handle_new - handle) <10:
206             pass
207         else:
208             command_pos(svc_handle,int(handle_new),cnt)
209
210         if np.abs(swivelling_new - swivelling) <10:
211             pass
212         else:
213             command_pos(svc_swiv, int(swivelling_new),cnt)
214
215         cnt = cnt+1
```

Bibliography

[1] Willibald Pschyrembel. *Klinisches Wörterbuch*. de Gruyter, Berlin, 2007.

[2] R. E. Carroll. Surgical Catgut: The Myth of Allergy. *Journal of Hand Surgery*, 14(2):218–220, 1989.

[3] Volker Schumpelick. Chirurgisches Nähen - Geschichte, Innovationen, Optimierungsansätze. *nahdran, Aesculap, Tuttlingen*, February 2008.

[4] Ernst Kern. Die zweite Wende der Chirurgie. *Würzburger medizinhistorische Mitteilungen 12*, pages 363–373, 1994.

[5] B. Bose, A. K. Kalra, S. Thukral, A. Sood, S. K. Guha, and S. Anand. Tremor compensation for robotics assisted microsurgery. In *1992 14th Annual International Conference of the IEEE Engineering in Medicine and Biology Society*, volume 3, pages 1067–1068, Oct 1992.

[6] Gyung Tak Sung and Inderbir Gill. Robotic laparoscopic surgery: a comparison of the da Vinci and Zeus systems. *Urology*, 58(6):893–898, dec 2001.

[7] Barbash and Gabriel. New technology and health care costs–the case of robot-assisted surgery. *The New England journal of medicine*, 363(8):701, 2010.

[8] J. Kirkup. The history and evolution of surgical instruments. I. Introduction. *Annals of the Royal College of Surgeons of England*, 63(4):279, 1981.

[9] Classification of surgical suture needle. `https://cpmedical.com.au/wp-content/uploads/2015/04/Picture2.jpg`. Accessed: 16.10.2019.

[10] Monika Flury. *Die Entwicklung chirurgischen Nahtmaterials als Voraussetzung und Folge operativer Tätigkeiten und wissenschaftlicher Forschung*. doctoralthesis, Universität Würzburg, 2002.

[11] Classification of surgical suture theads. `https://3mg34c37ntii24dmio2yy6o5-wpengine.netdna-ssl.com/wp-content/uploads/2015/02/Sutures.png`. Accessed: 16.10.2019 (edited).

[12] Simple interrupted stitch. http://e-learning.studmed.unibe.ch/chirosurf/htmls/print.html?chirosurf|wound|treatment|wtherapy|13. Accessed: 16.10.2019.

[13] Donati suture. http://www.lexikon-orthopaedie.com/images/cont_img_big/p_00150.jpg. Accessed: 16.10.2019.

[14] Allgöwer suture. http://www.lexikon-orthopaedie.com/images/cont_img_big/p_00022.jpg. Accessed: 16.10.2019.

[15] Simple continuous suture. https://classconnection.s3.amazonaws.com/74/flashcards/824074/jpg/11332110185710.jpg. Accessed: 10.12.2019.

[16] Continous intradermal suture. https://classconnection.s3.amazonaws.com/290/flashcards/1175290/jpg/gi1337401360991-thumb400.jpg. Accessed 10.12.2019.

[17] Cyrus Lawrence Day. *The Art of Knotting and Splicing (4th ed.)*. Annapolis: Naval Institute Press, 1986.

[18] Surgeon's knot. http://img.tfd.com/mk/K/X2604-K-09.png. Accessed: 17.10.2019 (edited).

[19] Maxime sterilization methods. https://www.maximintegrated.com/en/app-notes/index.mvp/id/5068. Accessed: 27.06.2019.

[20] Autoclave. http://image.made-in-china.com/2f0j10sBPEpihdLCkS/-Autoclave-de-la-clase-B-del-En-13060-STE-23L-Z-.jpg. Accessed: 13.12.2019.

[21] Plastic sheathing of a surgical robot. https://www.frontiersin.org/files/Articles/314890/fsurg-05-00022-HTML/image_m/fsurg-05-00022-g001.jpg. Accessed: 13.12.2019.

[22] Minimally invasie surgery. http://miss.com.ng/wp-content/uploads/2018/09/health-image-1-1140x759.jpg. Accessed: 10.12.2019.

[23] M. Hünerbein, S. Gretschel, B. Rau, and P. M. Schlag. Traumareduktion durch minimal invasive Chirurgie. *Der Chirurg*, 74(4):282–289, apr 2003.

[24] Trokar kinematics. From the lecture "Computer- und roboterassistierte Chirurgie", Leibniz Universität Hannover, 2008.

[25] Endo 360°, Endoevolution. https://www.assuteurope.com/en/product/endo-360/. Accessed: 16.10.2019.

[26] Proxisure, Ethicon. https://www.ethicon.com/na/sites/na/files/2018-05/proxisure-hero_1.png. Accessed: 16.10.2019.

[27] Endo Stitch, Medronic. http://www.medgadget.com/wp-content/uploads/2011/12/Covidien-Endo-Stitch-closeup.jpg. Accessed: 16.10.2019.

[28] SILS Stitch, Covidien. https://www.medtronic.com/content/dam/covidien/library/global/en/product/hand-instruments-and-ligation/sils-stitch-suturing-device-f.jpg. Accessed: 16.10.2019.

[29] Switch, Mellon. https://www.sparkdesign.nl/img/Project/101/uitgelichte_afbeelding/Mellon-Switch_Spark-01.jpg. Accessed: 16.10.2019.

[30] Mathias Hoeckelmann, Imre J. Rudas, Paolo Fiorini, Frank Kirchner, and Tamas Haidegger. Current Capabilities and Development Potential in Surgical Robotics. *International Journal of Advanced Robotic Systems*, 2014.

[31] daVinci Xi System, Intuitive Surgical. https://fortune.com/future-50/2017/intuitive-surgical/. Accessed: 16.10.2019.

[32] MiroSurge, DLR. https://www.dlr.de/rm/Portaldata/52/Resources/roboter_und_systeme/medizinrobotik/mirosurge/MIROs_table_head_HiRes.jpg. Accessed: 13.12.2019.

[33] ROBODOC, Think Surgical. https://images.squarespace-cdn.com/content/51c3dd4ce4b05645eb82772b/1372018307289-H71V7K7D9N536IQ1Q7AG/DOC+02+Left+Side+Enhanced+Cropped.jpg?format=1000w&content-type=image%2Fjpeg. Accessed: 16.10.2019.

[34] ARTAS system, Restauration Robotics Inc. http://www.darlingroots.com/wp-content/uploads/2015/10/restoration.jpg. Accessed: 16.10.2019.

[35] Teleoperated systems. From the lecture "Computer- und roboterassistierte Chirurgie", Leibniz Universität Hannover, 2018.

[36] Peter Pott and Markus Schwarz. Robotik, navigation, telechirurgie: stand der technik und marktuebersicht. *Zeitschrift für Orthopädie und ihre Grenzgebiete*, 140(02):218–231, 2002.

[37] Ulrich Hagn, R. Konietschke, A. Tobergte, M. Nickl, S. Jörg, B. Kübler, G. Passing, M. Gröger, F. Fröhlich, U. Seibold, L. Le-Tien, A. Albu-Schäffer, A. Nothhelfer, F. Hacker, M. Grebenstein, and G. Hirzinger. DLR MiroSurge: a versatile system for research in endoscopic telesurgery. *International Journal of Computer Assisted Radiology and Surgery*, 2009.

[38] Alexander Kolb. Integration of a flexible endoscope in the DLR MiroSurge system. Master's thesis, Private Universität für Gesundheitswissenschaften, Medizinische Informatik und Technik, Department für Biomedizinische Informatik und Mechatronik, 2019.

[39] MICA instrument. `https://www.dlr.de/rm/Portaldata/52/Resources/roboter_und_systeme/medizinrobotik/mica/MICA_Complete_HiRes.jpg`. Accessed: 13.12.2019.

[40] Dominik S. Schoeb, Julian Klodmann, Daniel Schlager, Philippe F. Müller, Arkadiusz Miernik, and Thomas Bahls. Robotic waterjet wound debridement – Workflow adaption for clinical application and systematic evaluation of a novel technology. *PLOS ONE*, 13(9):1–14, 09 2018.

[41] C. Schlenk, T. Bahls, T. Tarassenko, J. Klodmann, M. Biehler, and T. Wuesthoff. Robot Integrated User Interface for Physical Interaction with the DLR MIRO in Versatile Medical Procedures. *Journal of Medical Robotics Research*, 2013.

[42] U. Hagn, M. Nickl, S. Jör, G. Passig, T. Bahls, A. Nothhelfer, F. Hacker, L. Le-Tien, A. Albu-Schäffer, R. Konietschke, M. Grebenstein, R. Warpup, R. Haslinger, M. Frommberger, and G. Hirzinger. The DLR MIRO - A versatile lightweight robot for surgical applications. *Industrial Robot*, 2008.

[43] Simon Leonard, Kyle L. Wu, Yonjae Kim, Axel Krieger, and Peter C. W. Kim. Smart Tissue Anastomosis Robot (STAR): A Vision-Guided Robotics System for Laparoscopic Stuturing. *IEEE Transactions on biomedical Engenieering*, 2014.

[44] Azad Shademann, Ryan S. Decker, Justin D. Opfermann, Simon Leonard, Axel Krieger, and Peter C. W. Kim. Supervised autonomous robotic soft tissue surgery. *Science Translational Medicine*, 2016.

[45] Beat Roth, Frederic D. Birkhäuser, George N. Thalmann, and Pascal Zehnder. Novel prototype sewing device, EndoSew®, for minimally invasive surgury: an exracorporeal ileal conduit construction pilot study in 10 patients. *BJU International*, 2013.

[46] Siddarth Sen, Animsh Garg, David V. Gealy, Stephen McKingley, Yiming Jen, and Ken Goldberg. Automating Multi-Throw Multilateral Surgical Suturing with a Mechanicel Needle Guide and Sequential Convex Optimization. *IEEE International Conference on Robotics and Automation (ICRA)*, Stockholm, 2016.

[47] Pharma-zeitung.de. Covidien führt mit SILS™ Stitch ein Nahtinstrument für moderne laparoskopische Chirurgie ein. http://www.pharma-zeitung.de/Covidien-fuehrt-mit-SILS-Stitch-ein-Nahtinstrument-\fuer-moderne-laparoskopische-Chirurgie-ein.1395.php. Accessed: 25.10.2019.

[48] Degrees of freedom of the SILS Stitch. https://images.ua.prom.st/1054582473_w640_h640_perezaryazhaemyj-apparat-endoskopicheskogo.jpg. Accessed: 13.12.2019 (Edited).

[49] Degrees of freedom of the Endo Stitch. https://image.tigermedical.com/Products/LargeImages/COV173016.jpg. Accessed: 13.12.2019 (Edited).

[50] Degrees of freedom of the Endo 360°. http://www.endoevolution.com/files/6413/7477/3795/HEADER_3_Devices.jpg. Accessed: 13.12.2019 (Edited).

[51] sages.org. https://www.sages.org/publications/tavac/proxisure-suturing-system/. Accessed: 13.12.2019.

[52] Degrees of freedom of the Proxisure. https://3.bp.blogspot.com/-quzwqW_99QU/WZ2-EMfhtqI/AAAAAAAA1s0/PXwtxenMei8aN9Bhcp9kaWZt6D3CDpqcQCLcBGAs/s1600/1-Fullscreen%2Bcapture%2B8232017%2B73637%2BAM.jpg. Accessed: 13.12.2019 (Edited).

[53] Ditex 1609S. http://www.ditex-servo.com/wp-content/uploads/1609s-ditex-servo.jpg. Accessed: 13.12.2019.

[54] Eos material center. https://eos.materialdatacenter.com/eo/. Accessed: 12.12.2019.

[55] Properties of PPSU. https://media.mcam.com/fileadmin/quadrant/documents/QEPP/EU/Product_Data_Sheets_PDF/Quadrant_PPSU_E_PDS_2011.pdf?_ga=2.112537540.1162109167.1576186937-46971823.1576186937. Accessed: 12.12.2019.

[56] Autoclavable plastics. https://www.ensingerplastics.com/en-us/shapes/plastic-material-selection/sterilisable-autoclavable. Accessed: 12.12.2019.

[57] Florian Schmidt. links and nodes (ln). RMC seminar, 2018.

[58] Spacemouse compact. https://media.ldlc.com/r1600/ld/products/00/04/91/46/LD0004914606_2.jpg. Accessed: 13.12.2019.

[59] Alexander Kirst. Untersuchung zur Echtzeitfähigkeit der Poseschätzung für Messaufgaben. Bachelor thesis, Leibniz Universität Hannover, 2019.

[60] Tobias Ortmaier, Katrin Nülle, and Jens Kotlarski. *Skript zur Vorlesung Robotik I*. Fakultät für Maschinenbau, Institut für Mechatronische Systeme, 2016.

[61] W. Khalil and E. Dombre. *Modeling, Identification and Control of Robots*. Taylor & Francis, New York, 2002.

[62] T. Yoshikawa. *Foundations of Robotics: Analysis and Control*. The MIT Press, Cambridge, 1990.

[63] J.J. Craig. *Introduction of Robotics: Mechanics and Control*. Addison Weslay Longman Publishing Co, Upper Saddle River, 1986.

[64] ditex servo.com. Ditex specifications. http://www.ditex-servo.com/portfolio-produkt/ditex-td1609s/?portfolioCats=8. Accessed: 04.12.2019.

[65] docs.opencv.org. HSV representation. https://www.docs.opencv.org/trunk/de/d25/imgproc_color_conversions.html. Accessed: 07.12.2019.